



EUROPEAN
COMMISSION

Community research

SEARCH

Safety ExploitAtion Related CHEMistry for HLM reactors

(Contract Number: **295736**)

DELIVERABLE D5.7

Characterisation of the fission gas and other species release dispersion in the coolant with CFD modelling

Author: **V. Moreau (CRS4)**

Reporting period: e.g. **01/05/13 – 31/01/15**

Date of issue of this report: **31/01/15**

Start date of project: **01/11/2011**

Duration: **42** Months

Project co-funded by the European Commission under the Seventh Euratom Framework Programme for Nuclear Research & Training		
Dissemination Level		
PU	Public	X
RE	Restricted to a group specified by the partners of the SEARCH	
CO	Confidential, only for partners of the SEARCH project	

[SEARCH]



DISTRIBUTION LIST

Name	Institute	Comments
Bandini Giacomino	ENEA	
Buchlin Jean-Marie	VKI	
Bykov Denis	JRC	
Chen Xue-Nong	KIT	
Class Andreas	KIT	
Cottenier Stefaan	UGENT	
Delville Rémi	SCK•CEN	
Di Piazza Ivan	ENEA	
Eichler Robert	PSI	
Fazio Concetta	KIT	
Flad Michael	KIT	
Forgione Nicola	UNIPI	
Gessi Alessandro	ENEA	
Hania Ralph	NRG	
Heinitz Stephan	PSI	
Jayaraju Santhosh	NRG	
Koloszar Lilla	VKI	
Konings Rudy	JRC	
Li Rui	KIT	
Litfin Karsten	KIT	
Lucan Dumitra	INR	
Maschek Werner	KIT	
Maugeri Emilio	PSI	
Moreau Vincent	CRS4	
Neuhausen Jörg	PSI	
Pellini Donella	KIT	
Planquart Philippe	VKI	
Raison Philippe	JRC	
Retegan Teodora	CHALMERS	
Rineiski Andrei	KIT	
Rizzi Matthias	PSI	
Rijpstra Kim	UGENT	
Roelofs Ferry	NRG	
Schumann Dorothea	PSI	
Schuurmans Paul	SCK•CEN	
Skarnemark Gunnar	CHALMERS	
Tarantino Mariano	ENEA	
Taufall Simon	KIT	
Van den Bosch Joris	SCK•CEN	
Van Speybroeck Veronique	UGENT	
Van Yperen-De Deyne Andy	UGENT	
Weisenburger Alfons	KIT	
Wetzel Thomas	KIT	
Roger Garbil	EC	
European Comission Services		

[SEARCH]

D5.3: [Two-phase CFD model of the MYRRHA-FASTEF primary coolant loop including all relevant thermal aspects](#)

Dissemination level: PU

Date of issue of this report: 14/05/13

SEARCH – Grant Agreement n° 295736

Safe ExploitAtion Related CHemistry for HLM reactors

EC project officer: Roger Garbil

Workpackage No:	WP5	Task No:	1
SEARCH Identification:	DEL5.7-2012	Revision:	0

Short description of revision:

Summary: We describe the updates of the MYRRHA CFD numerical model. We first look at the behaviour of passive scalars to get information on residence time, stagnation regions and dispersion of dissolved substances or very fine particulate. We investigate the dispersion of Lagrangian particles representative of possible fuel particles depending on their density and size under nominal operation for 1200s. We investigate a ULOF incidental scenario, including some fission gas release and a successive fuel particle emission. We discuss the results, the limitations of the simulations and the possible future improvements.

Title:

Characterisation of the fission gas and other species release dispersion in the coolant with CFD modelling

Dissemination level :	PU
Issued by:	CRS4
Internal reference by editing partner:	
Status:	Final

XXXX-XX-XX				
DATE	<i>Author</i> V. Moreau CRS4	<i>Task leader</i> V. Moreau CRS4	<i>WP leader</i> V. Moreau CRS4	<i>Coordinator</i> P. Schuurmans SCK•CEN

[SEARCH]

DEL5.3: Two-phase CFD model of the MYRRHA-FASTEF primary coolant loop including all relevant thermal aspects

Dissemination level: PU

Date of issue of this report: 15/05/13

3/64

[SEARCH]

DEL5.3: [Two-phase CFD model of the MYRRHA-FASTEF primary coolant loop including all relevant thermal aspects](#)

Dissemination level: [PU](#)

Date of issue of this report: [15/05/13](#)

Abstract

The aim of this report is to describe the work performed to characterise the fission gas and other species release dispersion in the coolant using and improving the CFD representation of the MYRRHA primary loop presented in Del5.3 [1].

After a description of the update of the numerical model, we first look at the behaviour of passive scalars to get information on residence time, stagnation regions and dispersion of dissolved substances or very fine particulate.

Second, we investigate the dispersion of Lagrangian particles representative of possible fuel particles depending on their density and size under nominal operation for 1200s.

Third, we investigate a ULOF accidental scenario, including some fission gas release and a successive fuel particle emission.

Last, we discuss the results, the limitations of the simulations and the possible future improvements.

LIST OF CONTENT

ABSTRACT	5
LIST OF CONTENT	5
NOMENCLATURE	8
1. INTRODUCTION	10
2. MYRRHA CFD MODEL.....	11
2.1 Physical domain.....	11
2.2 Materials.....	11
2.3 Main CFD Fluid regions.....	12
2.4 Momentum and Heat Sources	14
2.4.1 Core.....	14
2.4.2 PHX.....	15
2.4.3 PP	17
2.5 Phase control.....	17
3. PASSIVE SCALARS.....	18
3.1 Volumes and masses	18
3.2 First frozen field simulation.....	19
3.2.1 Residence time	19
3.2.2 Constant junk source	20
3.3 First transient simulation	20
3.3.1 Junk release	21
3.3.2 Outer annulus resilience.....	22

[SEARCH]

DEL5.3: [Two-phase CFD model of the MYRRHA-FASTEF primary coolant loop including all relevant thermal aspects](#)

Dissemination level: PU

Date of issue of this report: 15/05/13

3.4	Second frozen field simulation.....	23
4.	LAGRANGIAN PARTICLES.....	25
4.1	Benchmark case.....	26
4.2	Extended range	32
4.3	Analysis.....	37
5.	ULOF PRELIMINARY TESTS AND CONSIDERATIONS	37
5.1	First simulation (ULOF_1).....	37
5.1.1	Preliminary setting	37
5.1.2	Main limitations.....	37
5.1.3	Results.....	38
5.2	Second group of simulations	39
5.2.1	First equilibrium neutronic feedback (ULOF_2)	39
5.2.2	Weighted mean density for neutronic feedback (ULOF_3)	40
5.2.3	Neutronic relaxation time (ULOF_4)	40
5.2.4	Fission gas emission ULOF_5	42
5.2.5	Single FA fission gas emission ULOF_6	43
6.	FINAL THREE-STEPS ULOF SIMULATION (ULOF_4, ULOF_7 AND ULOF_8).....	45
6.1	Single FA fission gas emission, high pressure (ULOF_7).....	45
6.2	Fuel particle release ULOF_8.....	48
6.2.1	Fuel dispersion characteristics	48
6.2.2	LBE flow characteristics	50
7.	DISCUSSION.....	54
7.1	Numerical model	54
7.2	Passive scalars	54
7.3	Lagrangian particles in nominal condition	54
7.4	ULOF simulations.....	56
7.4.1	Setting and calibration of the neutronic coupling.....	56
7.4.2	Fission gas emission.....	57
7.4.3	Lagrangian particles under natural convection.....	58
7.4.4	Natural convection regime	59
7.5	Possible improvements	59
7.5.1	Route to nominal condition.....	59

[SEARCH]

DEL5.3: [Two-phase CFD model of the MYRRHA-FASTEF primary coolant loop including all relevant thermal aspects](#)

Dissemination level: **PU**

Date of issue of this report: **15/05/13**

7.5.2	Pump improvement.....	60
7.5.3	Core improvement	61
7.5.4	Cover gas improvement	61
8.	CONCLUSION	62
9.	ACKNOWLEDGMENT.....	63
10.	REFERENCES	63

[SEARCH]

DEL5.3: [Two-phase CFD model of the MYRRHA-FASTEF primary coolant loop including all relevant thermal aspects](#)

Dissemination level: PU

Date of issue of this report: [15/05/13](#)

NOMENCLATURE

Roman Letters

C_p	specific heat, heat capacity [J/(kg K)]
d	Diameter [m]
f	Force density [N/m ³]
f_f	Fanning friction factor [adim]
H_s	Heat source [MW]
L	Active Length [m]
m_f	Mass flow rate [kg/s]
M	Mass [kg]
P	Pressure [Pa]
R	Radius [m]
T	Temperature [C or K]
u	Velocity [m/s]
v	Superficial velocity [m/s]

Greek Letters

α	volume fraction [adim]
β	Expansion coefficient [adim]
ε	Friction factor [adim]
ϑ	Angle [degree]
κ	thermal conductivity [W/(m K)]
μ	dynamic viscosity [Pa s]
ρ	density [kg/m ³]
τ	characteristic time [s]

Abbreviations and acronyms

3D	Three Dimensional
ADS	Accelerator Driven System
CDA	Core Disruptive Accident
CFD	Computational Fluid Dynamic
EOC	End Of Cycle
FA	Fuel Assembly
FZK	Forschungszentrum Karlsruhe
H	Heavy (fuel particles with 5% porosity)
HH	Very Heavy (fuel particles with 2.5% porosity)
HX	Heat eXchanger

[SEARCH]

DEL5.3: [Two-phase CFD model of the MYRRHA-FASTEF primary coolant loop including all relevant thermal aspects](#)

Dissemination level: PU

Date of issue of this report: 15/05/13

IKET	Institute for Nuclear and Energy Technologies
IPS	In Pile Section
IVFH(M)	In Vessel Fuel Handling (Machine)
IVFS	In Vessel Fuel Storage
L	Light (fuel particles with 10% porosity)
LBE	Lead Bismuth Eutectic
LFR	Lead Fast Reactor
LL	Very light (fuel particles with 12.5% porosity)
LMFR	Liquid Metal Fast Reactor
MYRRHA	Multi-purpose hYbrid Research Reactor for High-tech Applications
MOX	Mixed OXide
PHX	Primary Heat Exchanger
PP	Primary Pump
Re	Reynolds number
ULOF	Unprotected Loss Of Flow
UniPi	University of Pisa
VF	Volume Fraction
VKI	Von Karman Institute
VOF	Volume Of Fluid

[SEARCH]

DEL5.3: [Two-phase CFD model of the MYRRHA-FASTEF primary coolant loop including all relevant thermal aspects](#)

Dissemination level: PU

Date of issue of this report: [15/05/13](#)

1. Introduction

With the increase of computational power and the progress in numerical modelling, Computational Fluid Dynamics (CFD) becomes a tool usable in more and more situations. In the framework of the MYRRHA project [2], through a series of initiatives co-funded by the European Commission, CFD has been already extensively used for the dimensioning and the control of several subsystems and of hypothesis of their variants: spallation target [3], primary heat exchanger [5] , decay heat removal system [4] and so on.

The CFD simulations have been usually restricted to relatively small subsystems, while the global system was investigated by use of nodalized system codes such as RELAP [6] and SIMMER [7]. If we make a crude confrontation in terms of degrees of freedom or in number of control volumes, system codes scale typically from 10^3 up to 10^4 , while CFD 3D codes use on a regular basis 10^5 to 10^6 control volumes for basic applications. In this work, we will reach about 10^7 control volumes. The great improvement in precision given by 3D CFD is however dampened when time enters strongly in consideration. For non-stationary configurations, the time step must scale like the inverse of the control volume size. This means that for a given time laps of simulation, the required computational power scales like the fourth power of the inverse of the control volume size. Thus long transients are much more easily investigated using system codes, even if the information obtained is not very detailed in space.

Unlike time resolution, space resolution can be parallelized and 3D codes strongly use this feature. To fix the ideas, the entice primary loop of MYRRHA (with some necessary simplification) can be modelled with 10^7 control volumes using a base size of 7.2 cm and some refined region at half the base size. Running the simulation with a time step of 0.01 second on a cluster of 256 cores (the maximum we could temporarily afford) allows to compute about 25 s of physical time by day. With these numbers in mind, we can infer that 3D CFD MYRRHA transient simulations are affordable for events lasting no more than a few minutes.

The final objective of this work inside the SEARCH project is to understand the characteristics of fuel dispersion in case of accident leading to the loss of integrity of one or more fuel pin, labelled as Core Disruptive Accident (CDA). By this, we mean investigate if and where the dispersed fuel products will settle and accumulate depending on their size, specific weight and porosity. To reach this objective, we have first already constructed a full 3D CFD model of the primary system of MYRRHA. We then have made the model reach its nominal condition to be in condition to start the incidental initial event leading to the pin failure. This work has been reported in a previous document (Del5.3 [1]).

The base CFD models, is based on version 1.4 of the design [8]. The software starccm+ from CD-Adapco [13] has been used for all the simulations presented here. The model, built with starccm+ version 8.02, includes the solid part and the dead volume, taking into account the conjugate heat transfer.

The models has been upgraded to version 8.04 and then from version to version up to version 9.04. The ultimate simulations have been performed using version 9.06 after re-meshing, taking profit of the imbedded mesher improvements.

In the framework of this work-package [15], the fuel dispersion has also been studied in parallel by VKI using single phase CFD [12]. Also in parallel, three institutes, IKET, ENEA and UNIPI, have performed similar studies, however using the SIMMER-III and SIMMER-IV coarse grid codes [9][11]. Many considerations and data are taken or inspired from their work, often without citing.

The document is organized as follows. We first review the CFD model main features and their improvement since Del5.3. Then, we investigate the behaviour of passive scalars only transported by the fluid velocity. This gives useful information about residence time, stagnation

[SEARCH]

DEL5.3: [Two-phase CFD model of the MYRRHA-FASTEF primary coolant loop including all relevant thermal aspects](#)

Dissemination level: PU

Date of issue of this report: 15/05/13

regions and dispersion for arbitrarily small particulate or dissolved material. Third, we study the evolution of Lagrangian Particles emitted from the core, representative of expected fuel debris, under the assumption of a stationary carrier flow, that is, freezing its related transport equations. This technique saves a great deal of computational time, thus allowing to follow more types of particles for a longer time than formerly foreseen, that is up to 1200s.

The last part of the document is dedicated to the simulation of a ULOF accidental scenario. We first simulate the transient without neutronic feedback. It is an important first step as it allows to define clearly the characteristic time of the simulation, and, by confront with the SIMMER-III simulations performed in CDT [17], put in evidence the large impact of such neutronic feedback. Then, we perform a series of simulations aimed at taking the neutronic feedback into account in a crude but articulated way. In practice, we relate the core power to the mean LBE core density, first under an equilibrium assumption then under a non-equilibrium assumption with a characteristic relaxation time. Moreover, we take into account the strong reactivity feedback radial dependence on the density by computing a specific weighted mean value of the LBE density. The reactivity feedback is tailored to essentially reproduce the SIMMER-III results.

Once the initial ULOF transient has reached its intermediary asymptotic behaviour, that is shortly after the core LBE temperature has reached its maximum value and the mass flow rate has reached the natural convection regime, we emit from the core first some fission gas and then a bunch of Lagrangian particles as in the former part. The simulation being fully transient, the particles and the carrier flow are followed for only 500s. However, this duration is enough to infer strong differences in the particle dispersion/aggregation between the nominal and the natural convection conditions. The fission gas quickly evacuates through the LBE free-surface.

2. MYRRHA CFD model

The MYRRHA CFD model has been built and operated inside the starccm+ framework. Any setting or feature not precised means that the default setting has been used. For a precise description of the geometry, refer to Del5.3.

2.1 Physical domain

The physical domain simulated is essentially the reactor external vessel and all what lies inside. However, the anchoring system of the vessel is not contemplated, as well as most of the features (instrumentation, pipes) located in the cover gas part of the vessel volume. The secondary coolant is also not directly simulated.

2.2 Materials

The materials are fluid LBE, “pseudo-solid” LBE, cover gas and steel. By “pseudo-solid” LBE, we mean a solid with the same physical properties as the fluid LBE. It is used to model a fluid volume unconnected to the main fluid volume and closed around the core region. A simulation as an incompressible temperature dependent density would have been inconsistent due to the volume constraint.

For the LBE, the physical properties are directly taken from the LBE handbook [14] and reported here for commodity.

[SEARCH]

DEL5.3: [Two-phase CFD model of the MYRRHA-FASTEF primary coolant loop including all relevant thermal aspects](#)

Dissemination level: PU

Date of issue of this report: 15/05/13

11/64

Parameter (symbol)[units]	Formula (temperature in K)	Value at 300 C	Value at 350 C	Value at 400 C
Molecular Weight [kg/kmol]	207.2			
Melting Point [K;C]	397.7 124.5			
Density[kg/m ³]	11096 – 1.3236 T	10337.4	10271.2	10205.0
Dynamic viscosity (μ) [kg/m/s]	0.494*10 ⁻³ exp(754.1/T) approximate polynomial form 10 ⁻⁵ *[605-1.078 T + 0.0006 T ²]	1.84 10 ⁻³	1.66 10 ⁻³	1.51 10 ⁻³
Thermal conductivity (k) [W/m/K]	3.61 + 1.517E-2 T -1.741E-6 T ²	11.73	12.28	13.03
Specific heat (C _p) [J/kg/K]	159-2.72E-2T + 7.12E-6 T ²	145.7	144.8	143.9

Table 1: LBE physical properties

Most of the structure, and seemingly all the resolved structure parts are made of AISI 316L steel. The FA wrappers and the core support plate are made of T91. However, these components are geometrically poorly resolved.

In practice, the structure is considered of only one material: AISI 316L. From the Atlas technical handbook [16], we find:

- **Density:** $\rho=8000 \text{ kg/m}^3$
- **Thermal conductivity:** 16.3 W/K/m at 100C and 21.5 W/K/m at 500C (thus linear interpolation $\kappa=11.45 + 0.013 T$)
- **Heat capacity:** $C_p= 500 \text{ J/K/kg}$

The cover gas is an otherwise non specified numerically incompressible fluid with a constant density equal to 11.8 kg/m^3 . This is clearly a non-physical cover gas, but it is a necessary word-around as VOF two phase flows were numerically unstable for density ratio over 1000 at the time when the model was constructed. Tests performed with starccm+ version 9.06 indicate that a much higher density ratio (at least 10,000) is now accessible. This will be however taken into account only in future works.

2.3 Main CFD Fluid regions

The fluid part of the computational domain is divided into several regions which usually differ at least in one way in their numerical treatment. One advantage of this division is that some specific modelling is most easily implemented on a region basis.

[SEARCH]

DEL5.3: Two-phase CFD model of the MYRRHA-FASTEF primary coolant loop including all relevant thermal aspects

Dissemination level: PU

Date of issue of this report: 15/05/13

12/64

The list of CFD fluid domain is given below:

1. Barrel Envelop: region around the core barrel and over the core, requiring a finer mesh definition.
2. Butterfly Fluid: region around the solid Butterfly, requiring a finer mesh definition.
3. Core Bottom: small cylindrical region below the core constrained laterally by the Barrel, which may require a specific mesh size and serves as interface between the core regions and the main fluid region.
4. Core FAs (Fuel Assemblies): array of fuel assemblies connected together at top and bottom by an horizontal layer. Requires a specific heat source and momentum resistance force.
5. Core Inner Dummy: array of Inner FA dummies and CR connected together at top and bottom by a horizontal layer. Requires the same force as the Core FAs, but no heat source in critical configuration. The CR have a smaller section to account for the different foreseen mass flow rate. In under-critical configuration, the heat source in the added FAs is easily differentiated from the CR by a simple geometrical criterion (the radius).
6. Core Outer Dummy: array of Outer FA dummies connected together at top and bottom by a horizontal layer. Requires a different force as the Core FAs, and no (or very small) heat source.
7. Fluid IVFS (In Vessel Fuel Storage): four series of cylinders with the same resistance as in the FAs and a different heat source to represent the fresh replacement cores and the burned ones. The cylinders are connected through a thin horizontal layer in the lower plenum.
8. Fluid Main: all fluid parts that remain to be modelled. Divided into two unconnected parts, a small one trapped between the Core and the Porous ACS (this part is given a specific region in the least CFD model), the other one, the large one, comprising the lower and the upper plenum connected through the top gas region.
9. Fluid Numerical Top: small part at the top of the computational domain with a stagnation inlet and a VF sink (together with the related heat sink). It is added in order to easily comply with the volume and mass conservation constraints.
10. Fluid PP Thrust (Primary Pumps): two horizontal annuli 20cm high where the pumps deliver their head (fitted to get the nominal mass flow rate). This region separates the PPHX assemblies from the lower plenum.
11. Porous ACS (Above Core Structure): two horizontal grids inside the Barrel to fix the various guide tubes. It is treated as a slightly resistive porous material.
12. Porous HXs (Heat eXchangers): the active part of the HXs separating the upper plenum from the PPHX assemblies. It is treated as a porous medium to take into account the secondary coolant (water) tube bundles. Requires a specific porous description and heat source (sink).
13. PPHXs (Primary Pump - Heat eXchanger Assemblies): the two parts region between the HXs and the PPs. May require a specific mesh size.

The regions labelled Main and PPHXs are obtained by subtraction of all the solid structures, of all the other fluid regions and of all the a priori known dead volumes from the volume given by the Outer Vessel envelop. This subtraction gives also an isolated dead volume around the core and a complementary volume inside the core around the FAs. As the structural part is considered, the volume inside the core around the 151 positions is treated as steel while the dead volume around the core is simulated as a fictitious solid LBE.

[SEARCH]

DEL5.3: [Two-phase CFD model of the MYRRHA-FASTEF primary coolant loop including all relevant thermal aspects](#)

Dissemination level: PU

Date of issue of this report: 15/05/13

13/64

2.4 Momentum and Heat Sources

2.4.1 Core

The core is described on a slot/position basis. All slots are hexagonal with the same cross section except the CR which have a cross section reduced to 60%.

	FA	Inner dummy	CR	Outer dummy	Total
Number	69	24	6	42	141
Flow %	100	100	60	65	
Eff. Number	69	24	3.6	27.3	123.9
Flow/Position [kg/s]	76.2	76.2	45.7	49.5	
Flow [kg/s]	5258	1829	274	2079	9440
Mean velocity [m/s]	1.57	1.57	1.57	1.02	
Bulk Friction factor [adim]	12.82	12.82	12.82	31.0	
Distributed pressure loss [kPa]	164.0	164.0	164.0	167.5	
Boundary friction factor [adim]	0.47	0.47	0.47	0.47	
Boundary pressure loss [kPa]	6.0	6.0	6.0	2.5	
Pressure loss [kPa]	170	170	170	170	

Table 2: Foreseen flow, velocity and pressure losses through the core components.

2.4.1.1 HYDRAULIC RESISTANCE (AS A FORCE DENSITY)

The foreseen mass flow rate, velocity and pressure losses through the core components are given in **Table 2**. The rationale to get these numbers are given below.

We take the resistance force density f_r in the form: $f_r = -0.5\varepsilon\rho v^2$, distributed over 1m height, such that the effect is a total pressure loss $\Delta P = 1.7$ Bar. Inlet and outlet pressure drop should naturally be included in the CFD simulation and not accounted for twice. We must evaluate them so as to get the correct total pressure loss.

The inlet is assimilated to a sudden contraction and the outlet to a sudden expansion. The expansion coefficient used is $\beta = 0.49$. The friction factor is: $\varepsilon = 0.45(1 - \beta) + (1 - \beta)^2 = 0.47$, the velocity being always the velocity inside the hexagonal slots.

The total foreseen mass flow rate is $m_f = 9440$ kg/s. The mean density taken is $\rho_{LBE} = 10377$ kg/m³.

2.4.1.2 CORE HEAT SOURCE

The heat source is distributed over 60cm height across the centre height and restricted to the FAs. The heat source H_s follows a parabolic profile in the radial direction in the form:

$$H_s = a [h_0 - (h_0 - h_1)(R/R_1)^2] = 3.57e8(2.15 - 5.25R^2),$$

The parameter a is fitted to get a total of 100 MW from a direct measure in the Starccm+ model.

We take $h_0 = 2.15$, $h_1 = 1$ and $R_1 = 46.8$ cm. To get a distribution close to the one given in Figure 2.

With these parameters, it comes $a = 3.57E8$.

The heat source distribution is shown in **Figure 1**.

[SEARCH]

DEL5.3: Two-phase CFD model of the MYRRHA-FASTEF primary coolant loop including all relevant thermal aspects

Dissemination level: PU

Date of issue of this report: 15/05/13

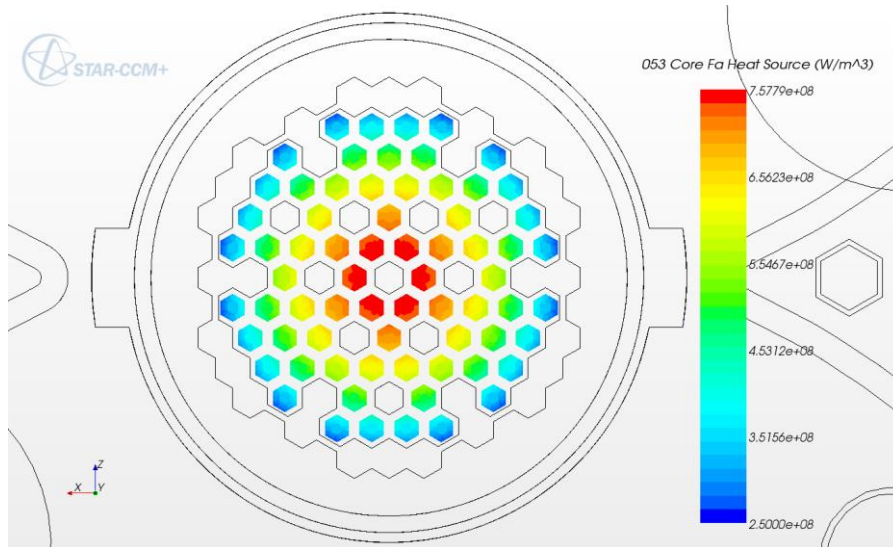


Figure 1: Heat source for a 100 MW critical core.

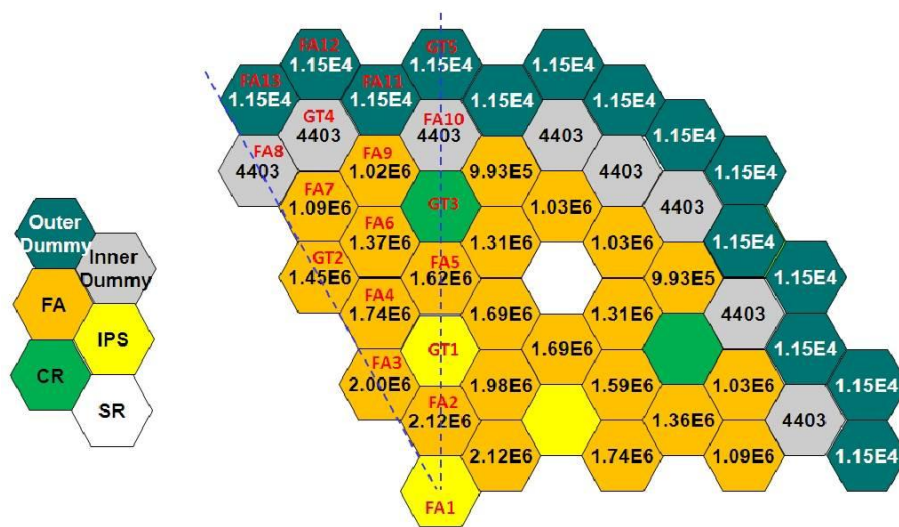


Figure 28 – Radial power distribution in MYRRHA reactor core (Ref. [4])

Figure 2: Foreseen radial power distribution for a 100 MW critical core.

2.4.2 PHX

The PHXs need a specific modelling both to represent the heat exchange with the secondary coolant and to represent its anisotropic hydraulic resistance.

The relevant characteristics of the group of the 4 PHXs are:

- Effective superficial cross section: S
- Nominal flow rate: $m_f = 9440 \text{ kg/s}$.
- Mean LBE density: $\rho_{\text{LBE}} = 10334 \text{ kg/s}$.
- Mean superficial nominal velocity: v .
- Active length: L .
- Characteristic residence time: τ .
- Tubes external diameter: d .
- Number of tubes: N .

[SEARCH]

DEL5.3: Two-phase CFD model of the MYRRHA-FASTEF primary coolant loop including all relevant thermal aspects

Dissemination level: PU

Date of issue of this report: 15/05/13

- Cross section taken by the tubes: $S_t = N \pi d^2/4$.
- Porosity: $\text{Por} = 1 - S_t/S$.
- Real cross section: $S_r = S - S_t$.
- Mean real vertical nominal velocity: $u = v/\text{Por}$.

The PHX specific modelling is given hereafter, splitting between the thermal and the dynamical parts.

2.4.2.1 PHX HEAT SOURCE

The heat source must bring the hot flow from 350C to 270C in a characteristic time τ . This is a conservative assumption for a total heat source in the system of 110 MW. The core power is only 100MW and the power in the IVFS is taken to 2MW. With a diffuse heat release essentially from Polonium decay about 0.5MW, the total heat source amounts to 102.5MW. As we constantly try to keep the cold plenum to 270C, we expect a mean flow temperature of 344C at the PHX inlet. This is however true only for extremely large times. In effect, the decay heat power in the IVFS slowly heats the passing LBE which goes afterward to the cold plenum top lateral annulus and does not participate for a long time to the temperature of the main flow. The expected temperature at the PHX inlet is therefore about 342C for a quite long intermediary asymptotic time.

The heat source is distributed over the entire porous part (representing the surrounding of the tube bundles) of the PHXs. We take the heat source under the form:

$$h_s = -\rho C_p (T - T_0) / \tau,$$

with the adjustable parameter τ which is in fact a characteristic time. This parameter is adjusted during the thermal transient of the simulation so as to keep the PHX outlet flux mean temperature at 270C, this last temperature being monitored.

The cold shut down as well as the water inlet temperature at the PHX secondary side is 200C, while the mean water size wall Temperature is 221C. There are slow flow regions, on top and at the bottom near the central water tube feeder, in which the wall temperature is inadequate. The heat sink formula is therefore quite approximate and we choose $T_0 = 210C$.

2.4.2.2 PHX HYDRAULIC RESISTANCE

The hydraulic resistance is split into two contributions, the vertical one, along the y axis, and the horizontal one (radial). It is given under the form of a distributed force f such that

$$f = -(A + B|v|)v,$$

with A and B two diagonal tensors.

The vertical coefficients are using the following parameters:

- Mean dynamic viscosity: $\mu = 1.80e-3$ Pas/m
- Wetted perimeter: Pe
- Hydraulic diameter: d_h
- Vertical Reynolds Number: $Re = \rho u d_h / \mu$.
- Fanning friction factor: $f_f = 0.046 Re^{-0.2}$.
- Estimated effective length: L
- Vertical pressure loss: $\Delta P = 2\rho f_f u^2 L / d_h$

The next step is to state the equality between the resistance and the pressure drop, that is: $(A_y + B_y|v|)v = \Delta P / L$.

We also force that $B_y|v| = 100 A_y$ for v the mean superficial velocity under nominal condition.

This is to ensure that the quadratic part is dominant when the flow is turbulent but also that the resistance becomes linear when the flow becomes laminar.

[SEARCH]

DEL5.3: Two-phase CFD model of the MYRRHA-FASTEF primary coolant loop including all relevant thermal aspects

Dissemination level: PU

Date of issue of this report: 15/05/13

16/64

To avoid freezing of the cover gas in contact with the HX top, we have set the parameters proportional to the mixture density.

The transverse friction loss coefficients are based on the formula for cross flow over staggered tube banks:

$$\delta P = Eu \rho u^2 / 2.$$

Eu is the Euler number and u is the mean velocity in the smaller cross section. It is related to the mean superficial velocity v by $u = v * a / (a - 1)$, where a is the Pitch to diameter ratio. The pressure drop dP is the one across a single tube row, that is for a distance $\delta l = \text{Pitch} * \sqrt{3} / 2$.

The problem here is that the Euler number depends slightly on the Reynolds number. It is decreasing from 0.3 to 0.2 when the Reynolds number increase from $1e4$ to $1e5$. There is no however a typical HX cross flow Reynolds Number. So, we set $Eu = 0.25$ as a first heuristic guess.

The formula is transformed in starccm+ variables and this pressure loss can be entirely transferred to the quadratic coefficient: $\delta P / \delta l = B_r v^2$, giving:

$$B_r = Eu \rho a^2 / (2 dl (a - 1)^2).$$

The radial quadratic coefficient would be more than 50 times the vertical one.

There is a flaw in this approach, because the flow is essentially not transverse and the radial component of the velocity is generally much lower than the vertical one. It is difficult to understand, seeing the strong anisotropy of the medium, why the vertical velocity would dramatically increase the radial resistance. Making a rapid bibliographic research, we could not find any study of the angle incidence between inline and transverse flows. For this reason, the radial pressure loss is transferred into the linear coefficient, however making it proportional to the horizontal speed: $A_r = B_r (v_x^2 + v_z^2)^{1/2}$. In other terms, the horizontal resistance depends only on the horizontal velocity, with a quadratic dependence.

2.4.3 PP

Only momentum thrust is considered for the primary pump. The pump thrust is localized in an annular section around the PP profiler vertical part. The annulus is 20cm high for an expected pressure thrust about $dP = 2$ Bar giving a force density about $f = 10 \text{ Bar/m} = 1e6 \text{ Pa/m}$. However, the exact value of the force ($1.21e6 \text{ Pa/m}$) is set to equilibrate the flow in nominal condition at the nominal value of 9440 kg/s.

The pump outlet flow is expected to have a swirl component that was under evaluation during the WP activity. The swirl component is given by azimuthal deviation angle of the velocity vector with regards to the vertical axis.

To force this deviation angle to the required value ϑ_0 , we measure the actual deviation angle ϑ , and set the azimuthal force proportional to the lacking part of the azimuthal velocity component. Remembering that the vertical direction is along the y-axis: the two planar component of the force is given by:

- $F_x = -A \sin \vartheta (u_y \text{ Arctg} \vartheta_0 + u_z \cos \vartheta + u_x \sin \vartheta)$
- $F_z = -A \cos \vartheta (u_y \text{ Arctg} \vartheta_0 + u_z \cos \vartheta + u_x \sin \vartheta)$

with $A = 1.E5$, an intensity parameter chosen so as to essentially reach the desired swirl angle without destabilizing the simulation.

In the simulation, the swirl objective has been set to $\vartheta_0 = 10$ degrees. At the time of this report writing, the foreseen value should be about 27 degrees. Anyway, while implemented, the swirl component of the force has not been present for a sufficient time to get its possible global effect on the lower plenum flow configuration.

2.5 Phase control

[SEARCH]

DEL5.3: Two-phase CFD model of the MYRRHA-FASTEF primary coolant loop including all relevant thermal aspects

Dissemination level: PU

Date of issue of this report: 15/05/13

17/64

To avoid unphysical mixing of the two phases, mainly during the filling period, we have to eliminate the light (cover gas) phase at the interface with a source term of the form:

$$S_g = -\text{VolumeFractionPhase1} * \text{VolumeFractionPhase2} / \tau,$$

with the characteristic time taken to $\tau = 2\text{s}$.

This source term has also the advantage to create a natural inflow condition at the top numerical stagnation inlet.

To speed up the start-up transient, we have to use the largest possible time step. We therefore have loss of the overall conservation of the LBE mass. This total LBE mass must be monitored and the eventual discrepancy must be corrected by a LBE volume fraction source term. If the objective mass is M_0 and the measured one is M , we set the LBE volume fraction source term S_{LBE} as

$$S_{\text{LBE}} = (M_0 - M) / (\rho V \tau)$$

Where V is the volume on which the source is applied and $\tau = 10\text{s}$ is the usual characteristic return time. The volume fraction source terms can be completed with a related enthalpy term S_h of the form:

$$S_h = \rho * C_p * S_{\text{LBE}} * T.$$

This would be really necessary only if the mass source is large and would otherwise noticeably alter the temperature. We have chosen to localize the mass source in the PP propeller rings and we have kept it working for all transient simulations.

3. Passive scalars

The first step specifically dedicated to the study of the fuel dispersion consists in evaluating the evolution of some passive scalar which is representative of the evolution of very fine particulate.

3.1 Volumes and masses

The wetted volumes and masses of LBE are obtained by integrating the LBE volume fraction and its product with the LBE density over a volume defined from the simulation regions and/or geometrical constraints. Knowing that the total mass of LBE is $3.83\text{E}6$ kg and the mass flow rate is about 9440 kg/s, this allows to compare the maximum residence time with the mean residence time in outlet of these volumes.

Here are the main LBE masses:

- Upper Plenum: 1210 Ton (excluding HXs), defined as $R < 3.88$ m, and $y > 0.92$ and $\text{ResTime} < 1000$ (on a 1200s test)
- Cold Plenum: 2390 Ton.
- HX: $\text{Porosity} * 65.6$ Ton = 44.0 Ton ($\text{Porosity} * 6.33\text{m}^3 = 4.24\text{m}^3$).
- Casing: 169 Ton (16.3m^3).

The criteria on the residence time was used to count the LBE in the vertical penetrations as part of the cold plenum. More complete information on the repartition of the LBE masses is given in Table 3 and Table 4.

The overall mean residence time for one cycle of the primary loop is therefore 400s of which 130s is taken in the upper plenum and 250s in the lower plenum.

[SEARCH]

DEL5.3: Two-phase CFD model of the MYRRHA-FASTEF primary coolant loop including all relevant thermal aspects

Dissemination level: PU

Date of issue of this report: 15/05/13

Part	Value (kg)
Barrel Envelop	7.747523e+04
Butterfly Fluid	0.000000e+00
Core Bottom	0.000000e+00
Core Fas	0.000000e+00
Core Inner Dummy	0.000000e+00
Core Outer Dummy	0.000000e+00
Fluid Above Core	2.026100e+03
Fluid IVFS	0.000000e+00
Fluid Numerical Top	5.932588e-05
Fluid PP Thrust	0.000000e+00
Main Fluid	1.128680e+06
Porous ACS	1.601902e+03
Porous HX	4.732880e+04
PPHX left	0.000000e+00
PPHX right	0.000000e+00
Total:	1.257112e+06

Table 3: On a region basis, product LBE density per volume fraction restricted to the domain $R < 3.88$ m, $y > 0.92$ m and Residence Time < 1000 (on a 1200s test case).

Part	Value (kg)
Barrel Envelop	7.748166e+04
Butterfly Fluid	8.879180e+04
Core Bottom	3.860179e+03
Core Fas	8.409155e+03
Core Inner Dummy	3.423619e+03
Core Outer Dummy	6.123631e+03
Fluid Above Core	2.313878e+03
Fluid IVFS	2.952656e+04
Fluid Numerical Top	3.425797e-05
Fluid PP Thrust	1.169606e+03
Main Fluid	3.374375e+06
Porous ACS	1.601966e+03
Porous HX	6.562937e+04
PPHX left	8.449793e+04
PPHX right	8.449563e+04
Total:	3.831700e+06

Table 4: LBE inventory on a region basis.

3.2 First frozen field simulation

A simulation of 1200s is performed, freezing all calculated fields except the passive scalar described hereafter.

3.2.1 Residence time

We measure the residence time. It is represented by a passive scalar transported by the flow, increasing as time everywhere outside the core, where it is returned to zero. The residence time allows to locate the completely stagnant and almost stagnant zones. We can see in Figure 3 that only the LBE inside the small vertical penetrations is really stagnant while the LBE in the annulus is slightly renewed indicating a probable maximum residence time of only a few hours. Moreover, there are no stagnant or quasi-stagnant zones in the hot and cold plena.

[SEARCH]

DEL5.3: Two-phase CFD model of the MYRRHA-FASTEF primary coolant loop including all relevant thermal aspects

Dissemination level: PU

Date of issue of this report: 15/05/13

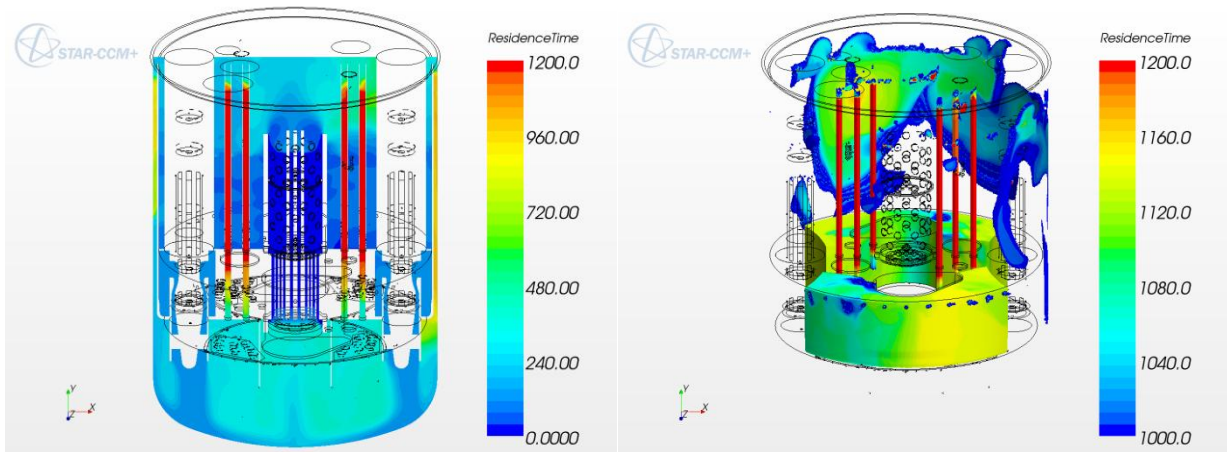


Figure 3: residence time in otherwise frozen field simulation. Left, PP plane. Right, restriction to the fluid domain with residence time higher than 1000s.

3.2.2 Constant junk source

A constant source of junk is emitted from one of the central FAs during all the 1200s time of the simulation. It is destroyed while re-entering the core. We can see that the junk do not completely mix in the upper plenum and that most of it pass through one of the PP, the right one in Figure 4. However, mixing proceeds in the lower plenum, and the junk concentration is almost completely homogeneous while reaching back the core. One can also see a quite intense mixing with the cover gas. This is in fact quite an artefact as the quantity represented is a mass fraction. In the later representations, we will filter this diffusion in the cover gas by plotting instead the mass concentration.

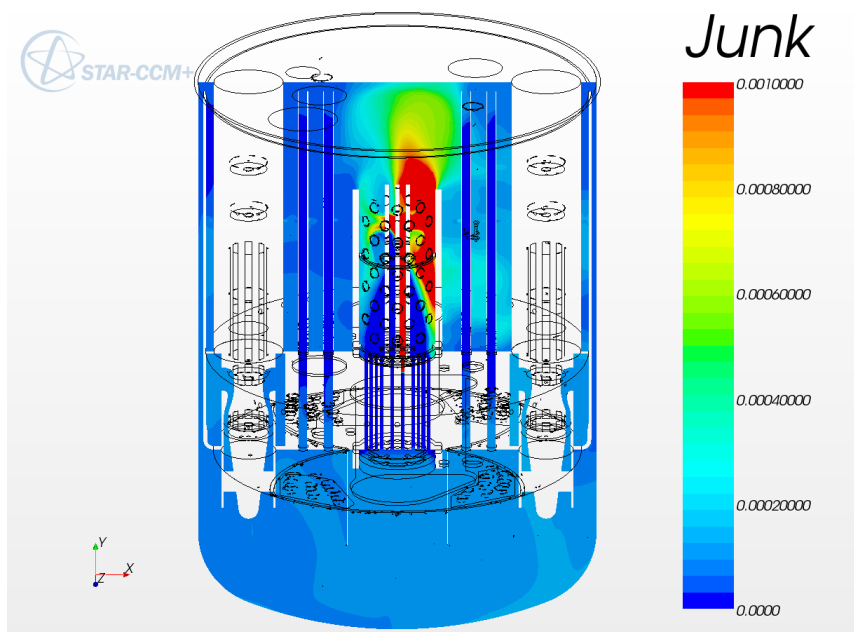


Figure 4: junk mass fraction after 1200s of frozen field simulation.

3.3 First transient simulation

[SEARCH]

DEL5.3: Two-phase CFD model of the MYRRHA-FASTEF primary coolant loop including all relevant thermal aspects

Dissemination level: PU

Date of issue of this report: 15/05/13

Gaining insight from the precedent simulation, we turn to a transient simulation for 60s following some new passive scalars.

3.3.1 Junk release

Passive Junk is released in specific positions in the core, and we monitor its temporal trace in different passage section:

- HX plane horizontal section at height $y=1\text{m}$.
- PP
- Core bottom

The scalar release is done during the first second of the transient, for a total release of 1 (arbitrary) unit.

The junk is released in three different FAs, as indicated on Figure 5. To differentiate their respective trace, they are modelled by three different passive scalars. The hexagonal pipes representing the FAs are distant enough, so that the source term localization can be done on a simple Cartesian constraint:

- JunkA: $0.065 < x < 0.145$, $0.5 < y < 0.6$, $-0.041 < z < 0.041$
- JunkB: $-0.220 > x > -0.300$, $0.5 < y < 0.6$, $0.040 < z < 0.134$
- JunkC: $0.012 < x < 0.092$, $0.5 < y < 0.6$, $-0.410 > z > -0.500$

The source terms are only set in the FA region.

The mass fraction of the three scalars after 60s is shown on Figure 7. We can see that, on this time scale, the original position of the source has a decisive influence on the path followed after leaving the core barrel. The history of various mass flow rates is plotted on Figure 6. One can see that the first signal appears in the HXs after 15 to 20s and back to the core after about 50s.

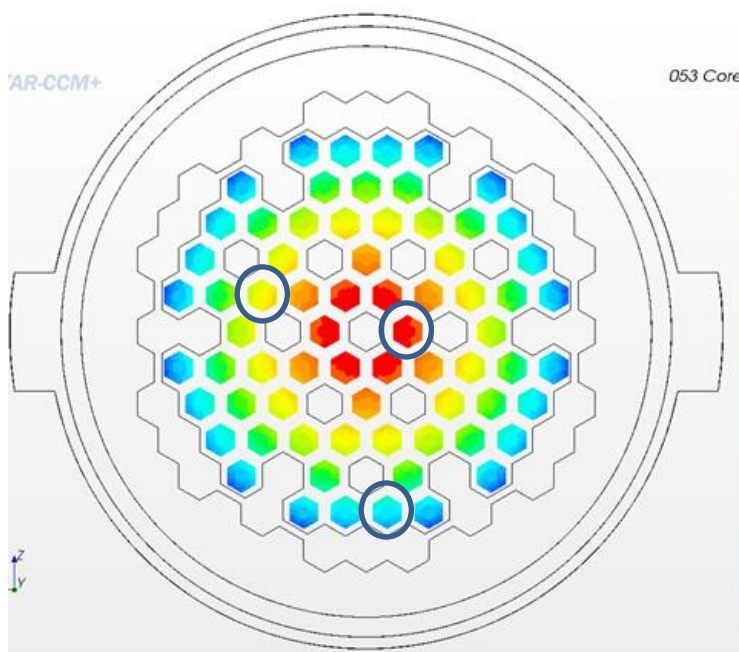


Figure 5: position of the three FAs chosen for the three pulse Junk release.

[SEARCH]

DEL5.3: Two-phase CFD model of the MYRRHA-FASTEF primary coolant loop including all relevant thermal aspects

Dissemination level: PU

Date of issue of this report: 15/05/13

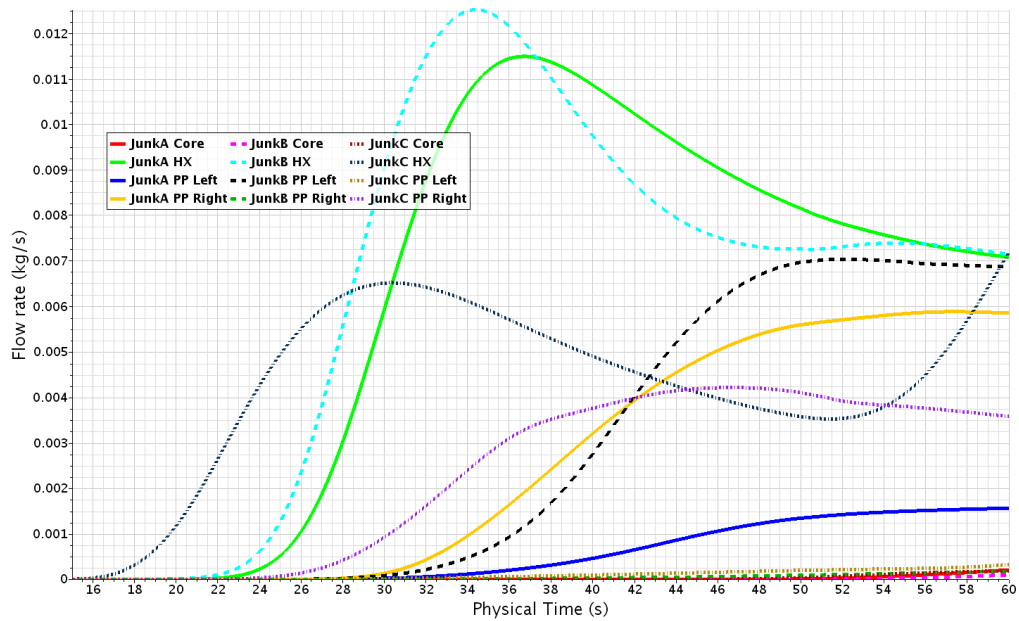


Figure 6: history of the junk passage through the HXs, each PP and back to the core.

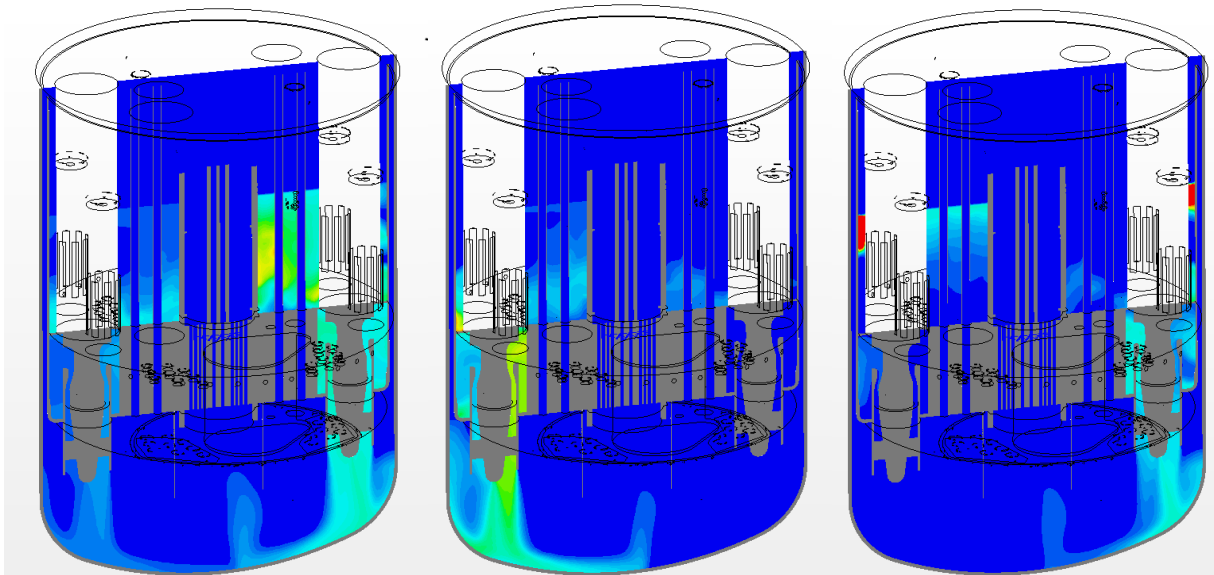


Figure 7: from left to right, repartition of the mass concentration of JunkA, JunkB and JunkC after 60s for an initial pulse of 1s.

3.3.2 Outer annulus resilience

To get further insight on the LBE residence time between the inner and the outer vessels, we set another passive scalar, simply initialized in this hollow cylinder at the LBE volume fraction over 1m from the active core centre height. This is to better evaluate how fast the LBE in the region is renewed. The initial condition and the result after 60s are both shown on Figure 8. Note that the scale enhances small deviations from the initial unit value. The very slight deviations arising from the top come from an imprecise initialization of the scalar to unit where the LBE volume fraction is greater than 0.5. It is a limitation of the numerical implementation and has no physical meaning. The deviations arising from the bottom, instead, come from the turbulent diffusion and from some residual convection. It can be inferred from the picture that twenty replications of the

[SEARCH]

mixing undertaken at the bottom part (for a total of 1200s) would lead to an overall not negligible renewing of the LBE in the annulus. It confirms therefore the previous simulation result obtained with frozen fields on the residence time.

We cannot however conclude to the absence of a completely stagnant region, because the thermal field here is not yet fully stabilized. One can fear that a quite strong thermal stratification here is likely to dampen the residual convection. The existence or not of a thermal stratification depends on the heat transfer to the walls and on details of the bottom flow likely to be influenced by the pump swirl. To be numerically determined, it would require very large times and a much finer mesh, allowing thermal convection patterns between the two walls.

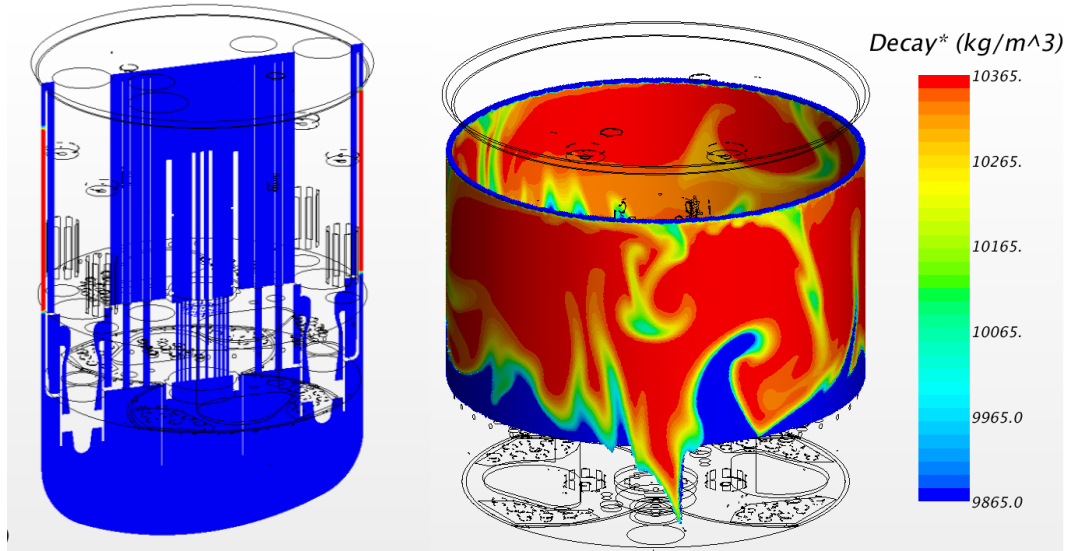


Figure 8: from the 60s transient simulation. Left in red, initial position of the “Decay” scalar. Right, Decay value after 60s.

3.4 Second frozen field simulation

The addition of several additional scalar field increases largely the required computational power. As the flow is in a reasonably stationary configuration, the added value given by a transient approach to the carrier field appears not worth the computational cost. That is why we proceed with additional simulation freezing the carrier fluid.

This simulation is run for 800s of physical time, which is roughly twice the loop characteristic return time. One unit of scalar is created at five different locations: the first three locations are identical to the former transient case. The last two locations are the two pumps annuli. All scalars are eliminated when they reach back the core. The objective is to evaluate the signals of the original pulses when they arrive at the core bottom. The three core pulses are also monitored when they arrive in the HXs and in the pumps, as shown in Figure 9.

The curves show clearly that the original FA position of the pulse largely determines its flow path and that the maximum intensity arrives at different times in the two PP/HX casings. The peak signal while returning to the core is not very pronounced and is between 200 and 250s depending on the pulse. The following decay curve is however very similar for all three pulses after the characteristic return time of 400s.

The signal emitted from the pumps and monitored at the core entrance is shown on Figure 10. The signals differs largely in amplitude during up to 250s which is the lower plenum characteristic time. After what, the decay tail is very similar for both signals. It is worth noting that each curve presents two distinct maxima, indicating a non-trivial flow pattern with two different privileged routes between the PP exit and the core entrance.

[SEARCH]

Looking at the flux accumulated in time, see Figure 11, we observe that all the signal has been transported through the HXs after 500s, while about 7% is still lacking at the core bottom at the end of the simulation after 800s. It can also be seen that the flux is not evenly distributed between the PPs.

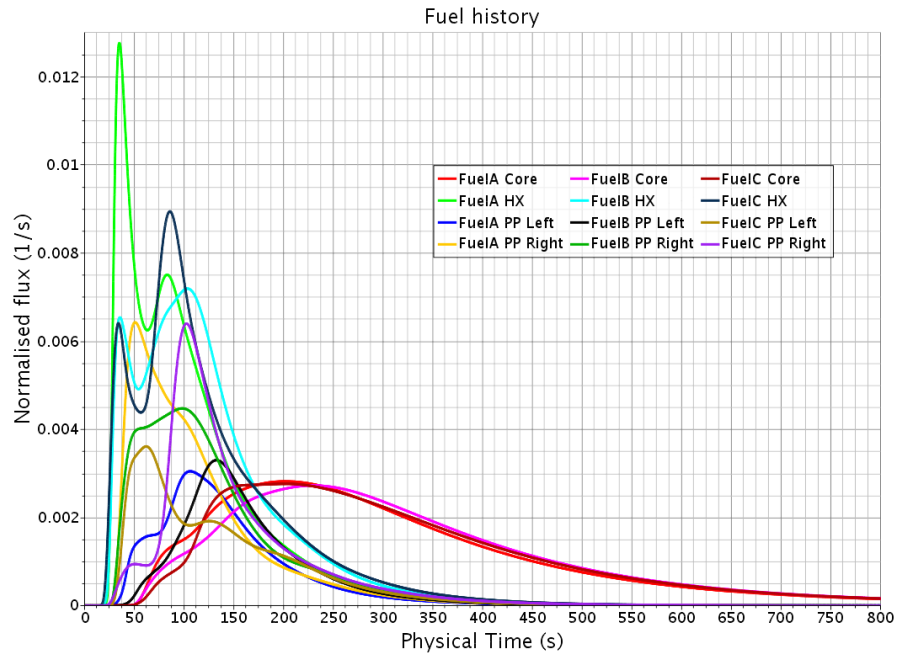


Figure 9: from the 800s frozen fields simulation. Signal of 3 pulses from the core while passing through the HXs, the PPs and back to the core bottom.

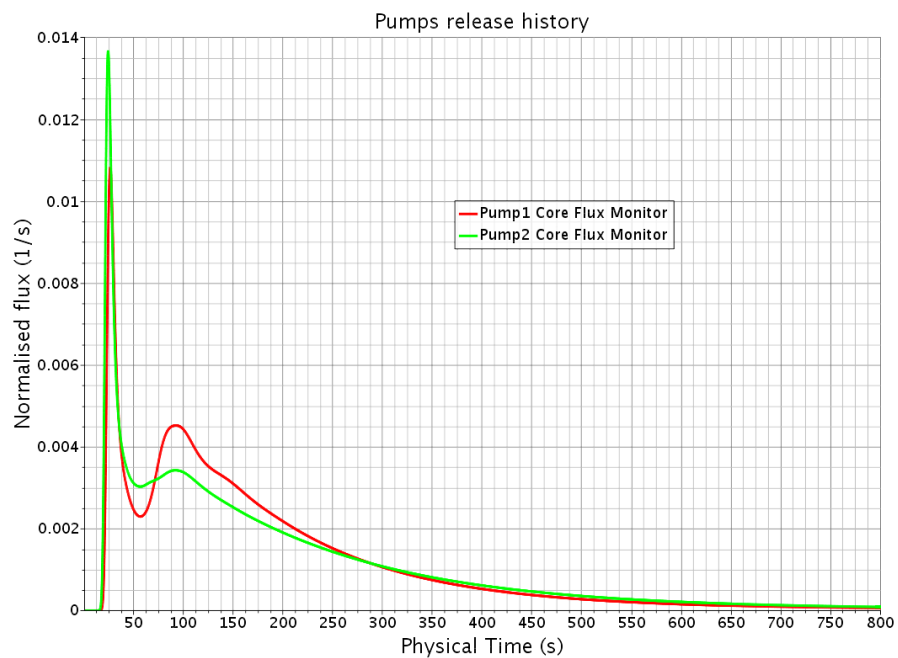


Figure 10: from the 800s frozen fields simulation. Signal of one pulse from each pump measured at the core entrance.

[SEARCH]

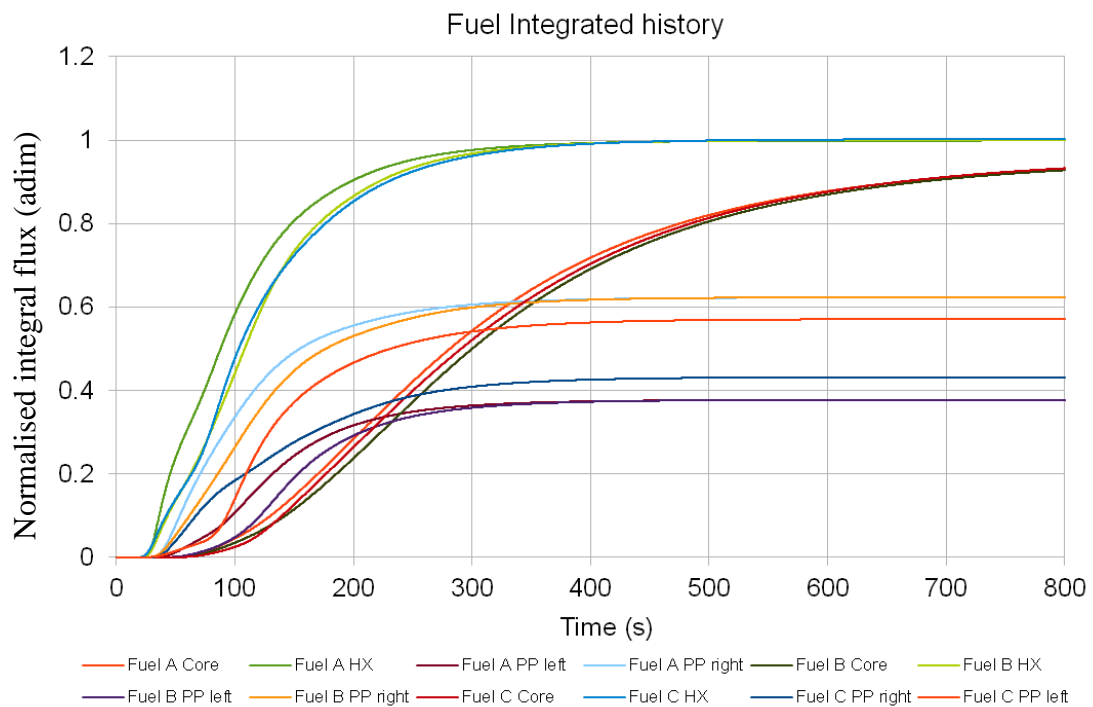


Figure 11: from the 800s frozen field simulation. Integrated signal of Figure 9 (different colours).

4. Lagrangian particles

The passive scalar approach does not allow to investigate the behaviour of a dispersed phase having a drift velocity with the main flow due to buoyancy. For this, we are obliged either to consider a complete Eulerian two-phase flow (with 2 momentum equations) or to switch to a Lagrangian particles approach.

The complete Eulerian two phase flow is however extremely computational intensive. Besides, it is not yet compatible with a quite large cover gas region and a good control of the interface sharpness. Some trial in this direction (with versions up to V902, not reported here), ended in complete failure.

The only practical solution is therefore to use Lagrangian particles. For the same reason given for the passive scalar simulations, we kept the frozen background field policy for all the Lagrangian simulations of this part.

Particles of different diameter and density will be used. The fuel particle density is based on the theoretical fuel density and a porosity factor [9][11][12]. The fuel matrix is sintered with a grain size of order $10\mu\text{m}$ [18], slightly growing in time. The initial fuel porosity is about 5%, the pores are supposedly mainly filled with trapped gas. With such a low porosity, the pores of the fuel matrix are expected to be poorly connected and fuel fragments larger than 0.1 mm should keep the same effective porosity even in case the LBE would strongly wet the fuel. On the other side, fuel fragments are not expected to be very regular, and fission gas can remain stuck into some concavity of the fragment surface. Taking into account that an event leading to the disintegration of the fuel matrix is likely to be very intense with different competing effects, we investigate fuel particles with an effective porosity range from 2.5 to 12.5%, with emphasis on 5 an 10% porosity, corresponding to particles slightly heavier and slightly lighter than the LBE carrier fluid.

The formula used for the particle density is reported in Table 5. In principle, the apparent particle porosity should vary dramatically with the pressure for the part consisting of surface bubble

[SEARCH]

DEL5.3: Two-phase CFD model of the MYRRHA-FASTEF primary coolant loop including all relevant thermal aspects

Dissemination level: PU

Date of issue of this report: 15/05/13

inclusions. In effect, the cover gas is foreseen about atmospheric pressure at 1 Bar, that is also the LBE surface pressure, while the pressure at the bottom of the vessel is about 8 Bars higher. The effect is rather difficult to quantify and its implementation would damage the readability of the results. The effect is therefore ignored.

Material	Porosity [%]	Density [kg/m ³] (T in K)	Density at 270C (kg/m ³)	Density at 350C (kg/m ³)
Liquid LBE	NA	11096-1.3236 T	10377	10271
Fuel	0	11139.1-0.3275 T	10961	10935
Fuel	2.5	10860.6-0.3193 T	10687	10662
Fuel	5	10582.1-0.3111 T	10413	10388
Fuel	10	10025.2-0.29475 T	9865	9842
Fuel	12.5	9746.7-0.28656 T	9591	9568

Table 5: LBE and Fuel density for different values of porosity

4.1 Benchmark case

A first simulation of Lagrangian particles in the MYRRHA numerical model is performed based on conditions from a test case by UNIPI with SIMMER-IV [10].

It considers an almost instantaneous release of one unit of fuel in the primary coolant loop from one of the most central FA in the core. The particles trajectory is then followed for 500s for a benchmark activity, and then up to 1200s.

The fuel density is taken as a linear approximation between 270 and 350C from UNIPI data. Below we give the particle main physical properties, together with the codification of the cases:

- Fuel theoretical density: $\rho_0 = 11050.7 - 26.2 \cdot (T - 270 - 273.15) / 80$
- Fuel porosity: 5% Heavy (H) and 10% Light (L)
- Relative density difference: with $D\rho = \rho_{\text{Fuel}} - \rho_{\text{LBE}}$
 - At 5%: $D\rho / \rho_{\text{LBE}}(270\text{C}) = 0.35\%$, $D\rho / \rho_{\text{LBE}}(350\text{C}) = 1.14\%$
 - At 10%: $D\rho / \rho_{\text{LBE}}(270\text{C}) = -4.9\%$, $D\rho / \rho_{\text{LBE}}(350\text{C}) = -5.2\%$.
- Particles diameter: $d = 0.8\text{mm}$ (080) and $d = 0.15\text{mm}$ (015).
- Heat capacity: $C_p = 250\text{ J/kg/K}$.

The fuel density as a function of temperature for different porosities compared to the LBE density plotted in Figure 12 reproduced from DEL5.6 [12].

d (mm)	0.95 %	0.9 %	0.85 %	0.6 %
0.125	3.4	3.1	5.6	12
0.25	4.9	4.4	7.9	17
0.5	13	12	22	46
1	19	17	31	65
2	41	37	67	140
3.155	52	47	84	180

Table 6: fuel particles terminal velocity in LBE at 310C for different porosities.

[SEARCH]

DEL5.3: Two-phase CFD model of the MYRRHA-FASTEF primary coolant loop including all relevant thermal aspects

Dissemination level: PU

Date of issue of this report: 15/05/13

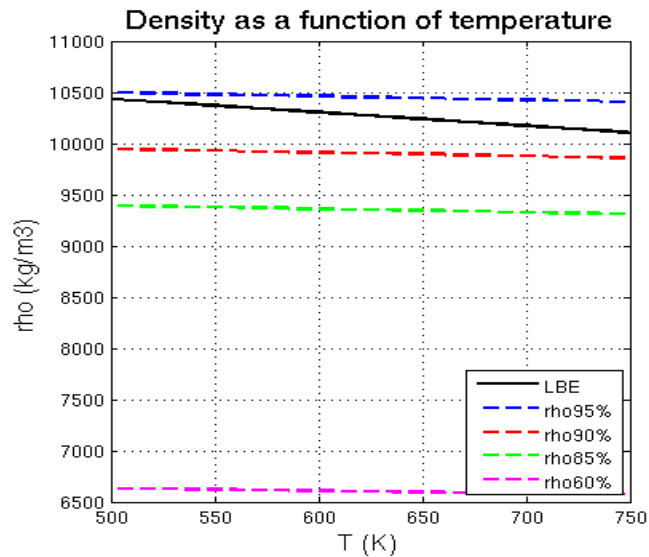


Figure 12: Fuel density compared with LBE density depending on temperature for different porosities.

The very small particle diameter and density difference leads to a quite small drift velocity in confront with the turbulent dispersion speed. This is shown on Table 6 also taken from DEL5.6[12]. Note that the fuel particle conductivity is not required by the model and thus a thermal equilibrium is implicit.

One thousands particles are individually followed, allowing a straightforward conversion between particle counts and particles percentiles. Both porosities 5 and 10% and both diameters 0.15 and 0.80mm give four independent groups of one thousands particles. For each group, the particles were released 20 by 20, each time step (of 0.02s) during the first second of simulation on a vertical segment located in the first ring FA shown on Figure 13.

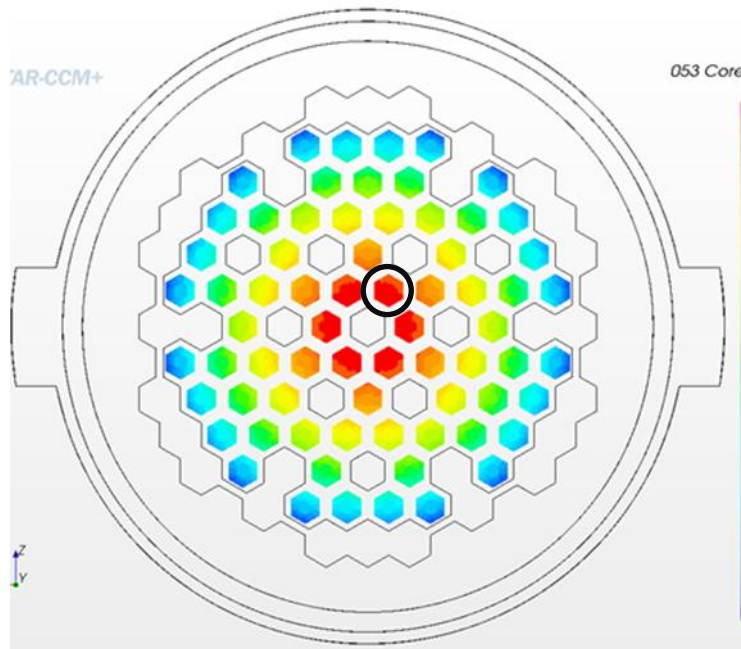


Figure 13: FA position for the benchmark fuel release case.

The benchmark case was set for a time laps of 500s. However, the characteristic return time of the flow being 400s, we felt necessary to perform the simulations up to three characteristic times, that is up to 1200s. The number of particles in the different regions, depending on their porosity

[SEARCH]

and diameter, at benchmark time 500s and final time 1200s, are shown on Table 7.

Operatively, the H80 particles were simulated first, for 1200s. In a second step, we noticed that, while the numerical setup becomes quite cumbersome, the computational burden was not particularly increased by simulating several particle types within the same simulation. Thus we run all four cases together and we also pursued the H80 simulation for another 1200s. The H80 particles are therefore also monitored at 1700 and 2400s given a better insight o the larger time behaviour.

At the bottom of the table, it can be seen that a few particles have been lost during the simulation. This is probably due to some imperfection of the computational grid. The sum of the particles in the different parts also does not equates the total number of particles by a small number. This is due to the fact that the parts do not always correspond to precise numerical entities and there can be some gaps and partial overlap, mainly between the cold plenum and the inter-plate region.

The time history of the particle number for the same diameter and porosity as in Table 7 is shown from Figure 17 to Figure 18, while the final position of the particles is shown on Figure 19 and Figure 20.

Region\Case	L15		L80		H15		H80		H80 + 1200s	
	500	1200	500	1200	500	1200	500	1200	500	1200
Time (s)	500	1200	500	1200	500	1200	500	1200	500	1200
HX2PP	82	89	131	175	83	101	71	57	54	65
Inter-plate	64	104	74	120	64	109	22	47	36	36
Cold plenum FS	13	28	43	116	9	27	6	3	5	3
Annulus	33	47	43	81	41	42	32	25	15	20
Core	9	14	4	3	12	10	9	14	12	16
Hot plenum FS	18	11	77	34	10	9	2	0	2	3
Cold Plenum	456	388	369	371	490	409	452	354	288	230
Hot Plenum	262	226	254	134	194	172	167	142	119	117
Upper Plate	56	94	9	12	81	110	228	343	452	492
Sum	993	1001	1004	1046	984	989	989	985	983	982
Particle number		993		986		985		985		984

Table 7: number of particles in each region after 500 and 1200s for particles of diameter 0.15 and 0.80mm and of porosity 5 and 10%. The last column is for heavy (5% porosity) particles and 0.8mm diameter after an additional 1200s time.

[SEARCH]

DEL5.3: Two-phase CFD model of the MYRRHA-FASTEF primary coolant loop including all relevant thermal aspects

Dissemination level: PU

Date of issue of this report: 15/05/13

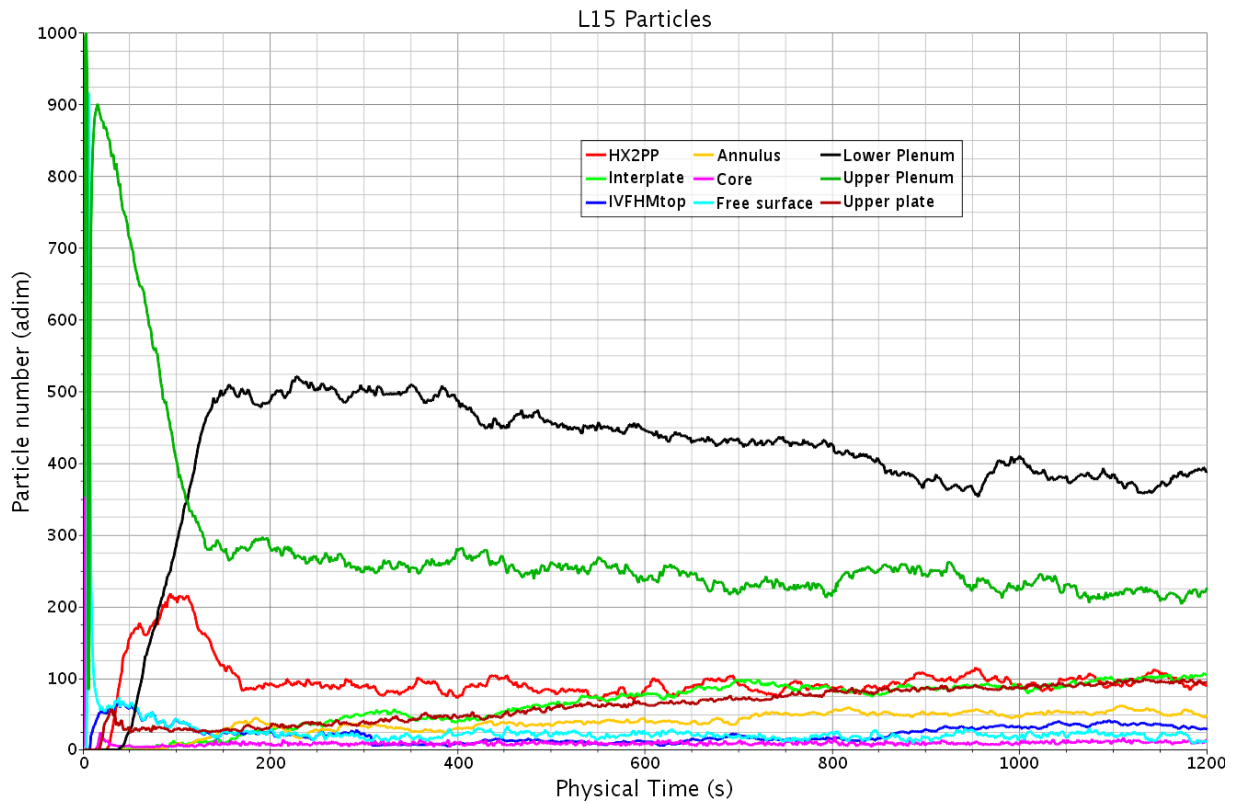


Figure 14: Case L15, porosity 10%, diameter 0.15mm. Time history of the number of particles lying in the different regions.

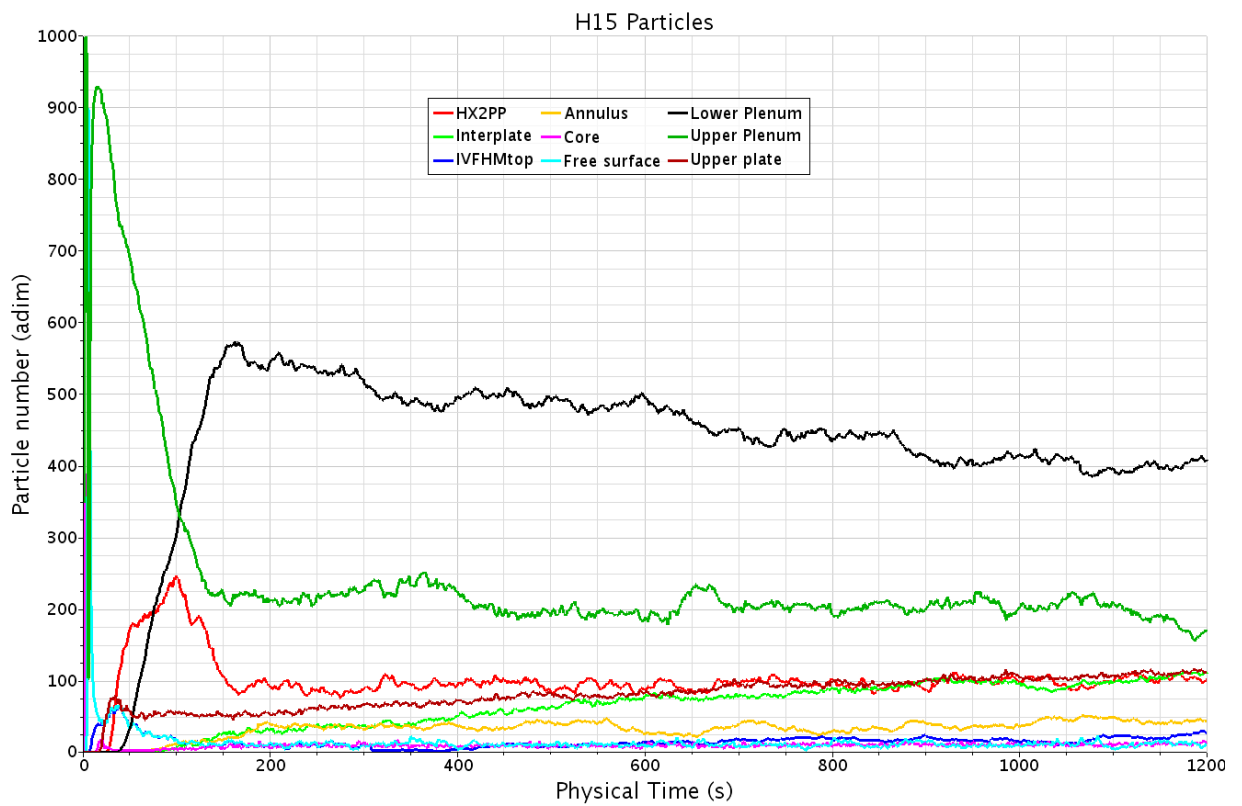


Figure 15: Case H15, porosity 5%, diameter 0.15mm. Time history of the number of particles lying in the different regions.

[SEARCH]

DEL5.3: Two-phase CFD model of the MYRRHA-FASTEF primary coolant loop including all relevant thermal aspects

Dissemination level: PU

Date of issue of this report: 15/05/13

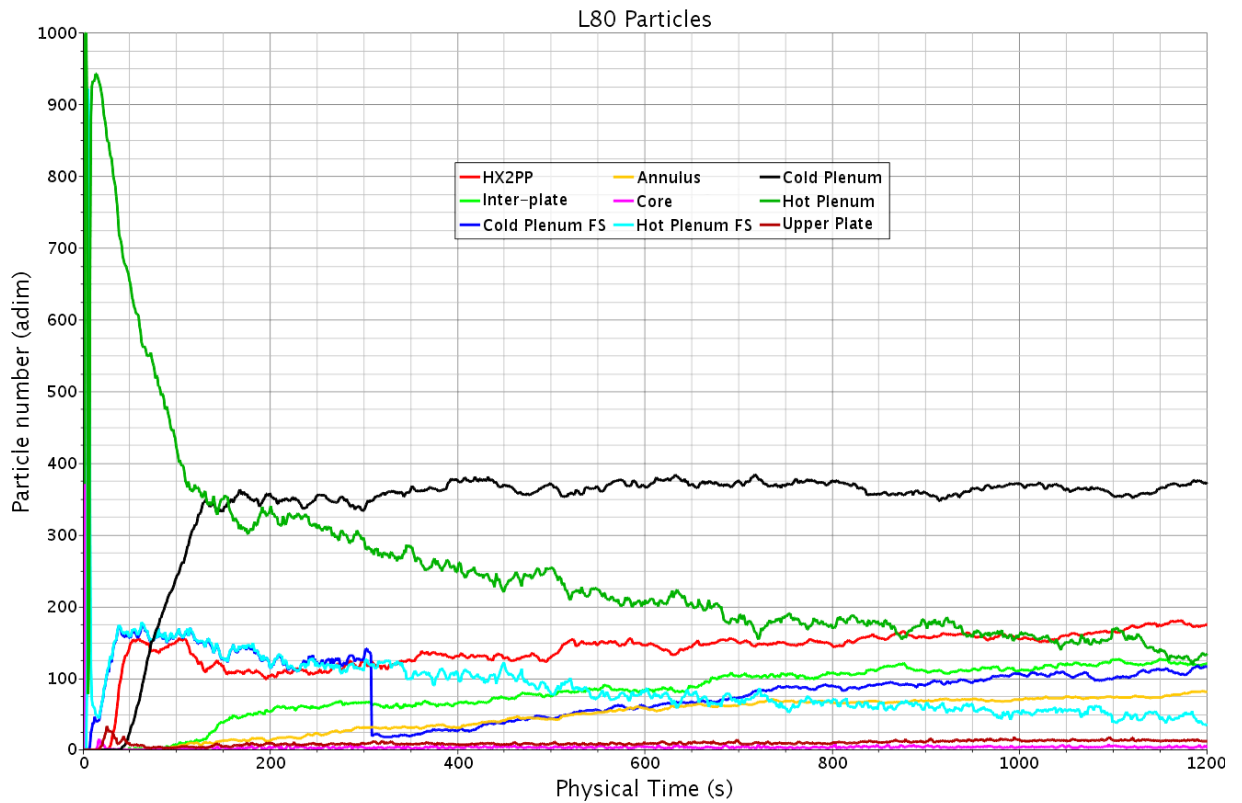


Figure 16: Case L80, porosity 10%, diameter 0.8mm. Time history of the number of particles lying in the different regions (cold plenum free surface value correct only after 300s).

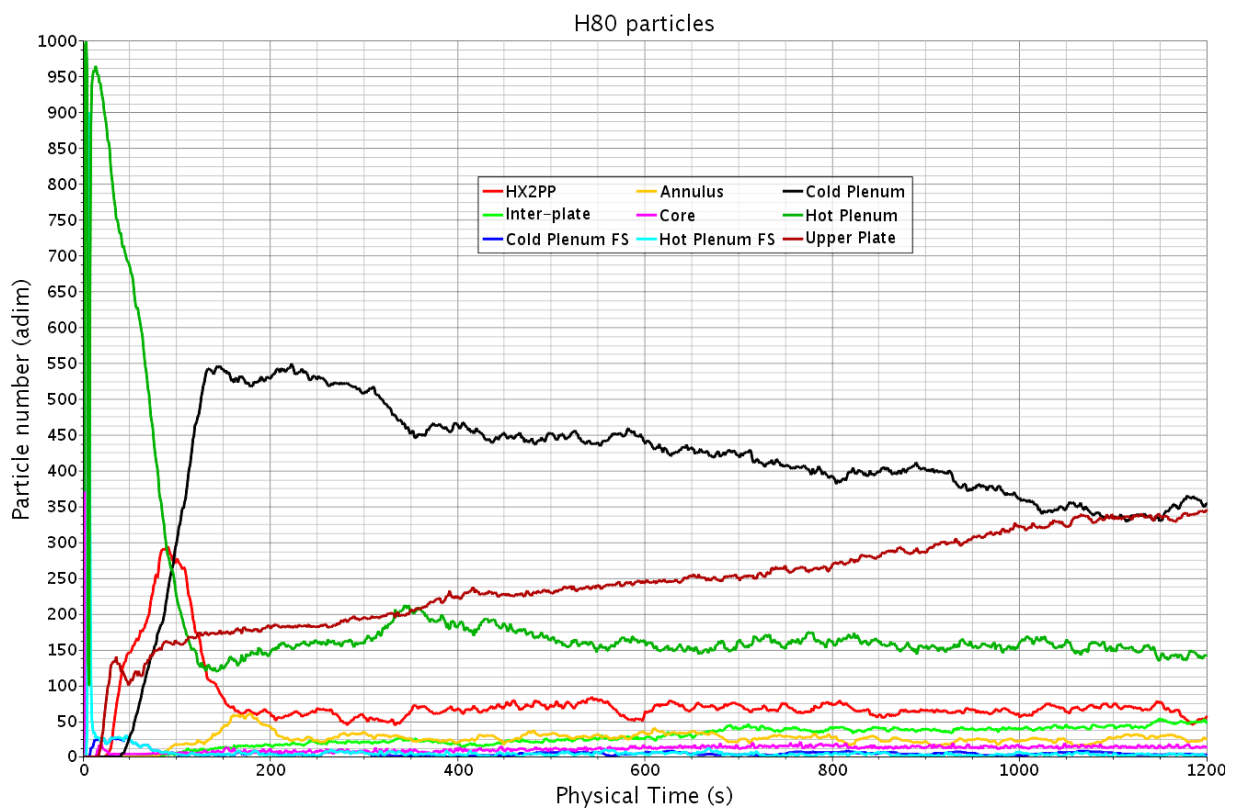


Figure 17: Case H80, porosity 5%, diameter 0.8mm. Time history of the number of particles lying in the different regions.

[SEARCH]

DEL5.3: Two-phase CFD model of the MYRRHA-FASTEF primary coolant loop including all relevant thermal aspects

Dissemination level: PU

Date of issue of this report: 15/05/13

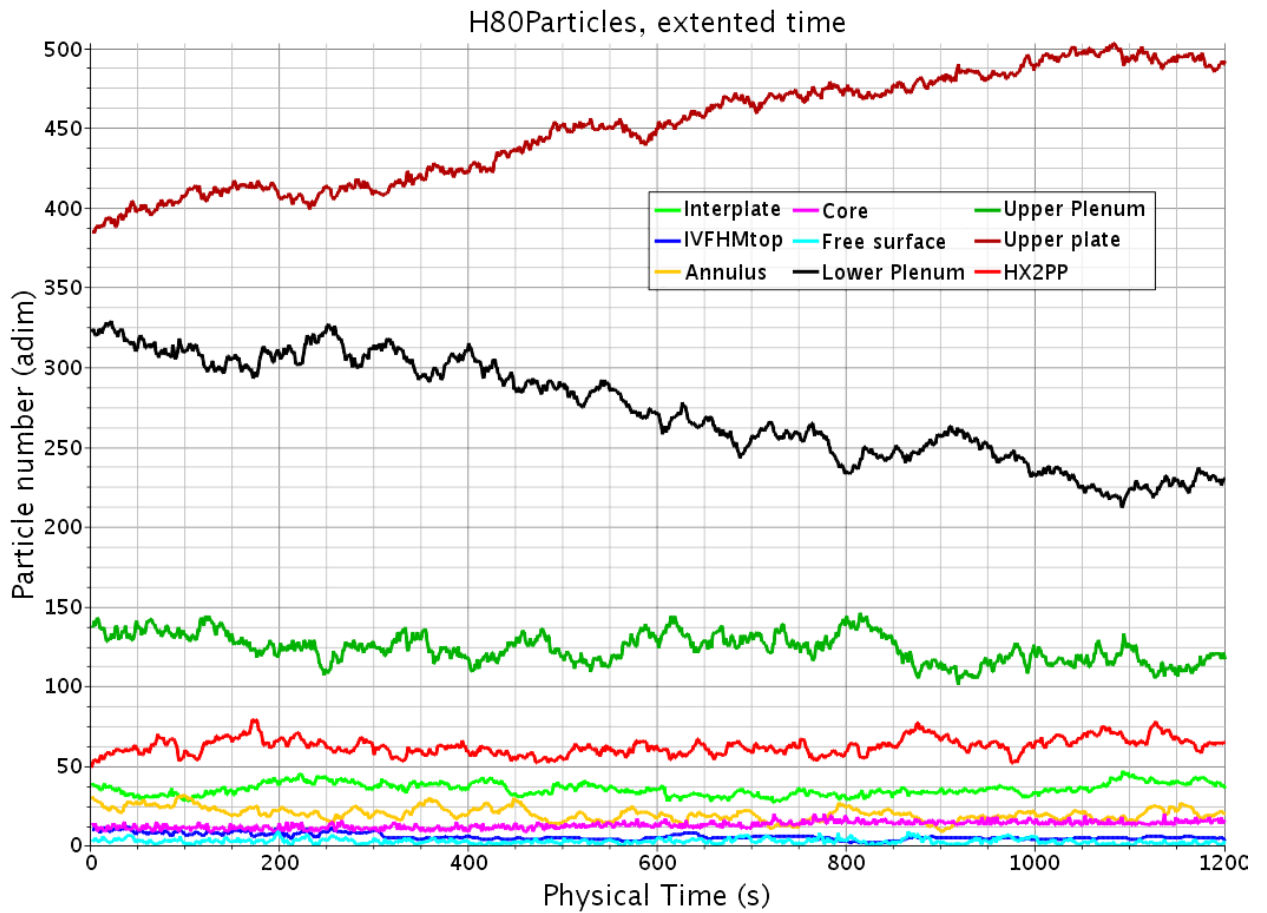


Figure 18: Case H80+1200s, porosity 5%, diameter 0.8mm. Time history of the number of particles lying in the different regions during the second time laps of 1200s.

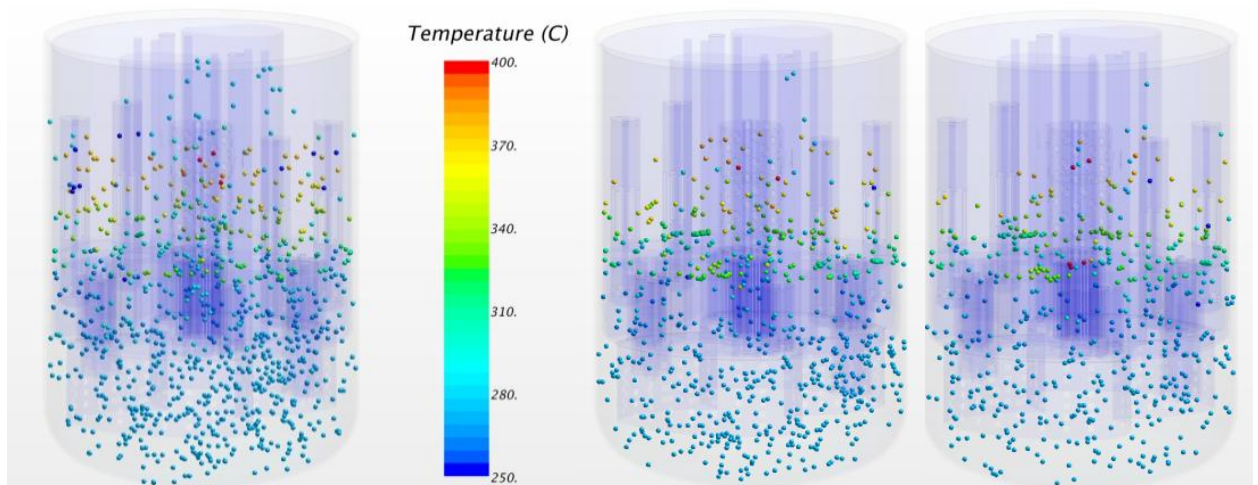


Figure 19: Position of the particles after 1200s, coloured by temperature. Left, case H015. Centre, case H080. Right, case H080+1200s.

[SEARCH]

DEL5.3: Two-phase CFD model of the MYRRHA-FASTEF primary coolant loop including all relevant thermal aspects

Dissemination level: PU

Date of issue of this report: 15/05/13

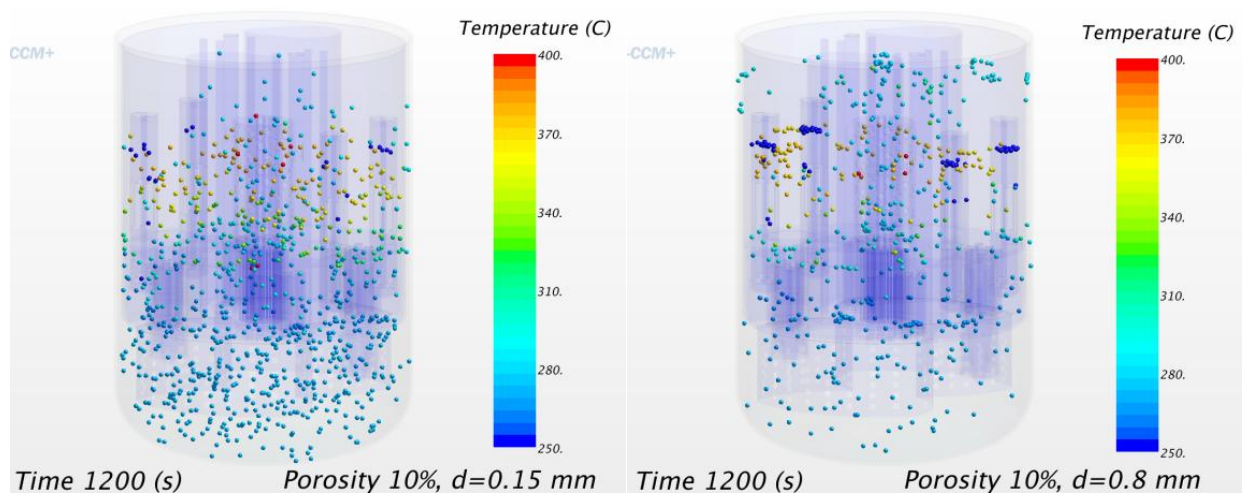


Figure 20: Position of the particles after 1200s, coloured by temperature. Left, case L015. Right, case L080.

4.2 Extended range

The former simulations have taken into account quite small particles with an effective density very close to the LBE one. A wide variety of cause could alter the effective particle density, from change in the fuel composition and fabrication, to wetting of the fuel particles with partial filling by LBE of the holes, or to bubble capture for highly non spherical particles. The size of the particles is also quite likely to depend on the strength of the event that caused the cladding failure with larger particles more likely to appear for stronger disruptive events. It is therefore interesting to extend somewhat the range of porosity and diameter up to values that lead to straightforward extrapolations.

First, we simulated particles with increased diameter, with value 1.2, 2.0 and 3.0mm, still for 5 and 10% porosities. Then, we simulated particles with the same diameter as for the benchmark case, but with porosity values extended to 2.5 (case LL) and 12.5% (case HH).

The repartition of particle after 1200s is given in Table 8 and in Table 9. Its time history is shown on Figure 21 and on Figure 22 (data for the lower plenum in case H120 and case HH120 are missing). The final particle position is shown on Figure 23 and on Figure 24.

Region\Case	H120	H200	H300	L120	L200	L300
HX2PP	31	18	7	173	50	38
Inter-plate	8	2	0	99	21	7
IVFHM top	3	0	0	98	41	10
Annulus	12	1	4	60	16	1
Core	9	11	1	3	0	0
Hot FS	1	0	0	106	769	889
Lower plenum	211	65	50	408	99	53
Upper plenum	61	18	21	99	16	2
Upper plate	650	878	913	3	0	0
Total	987	998	996	1049	1012	1000

Table 8: Localisation of the particles after 1200s for porosity 5 and 10%, diameter 1.2, 2.0 and 3.0mm.

[SEARCH]

DEL5.3: Two-phase CFD model of the MYRRHA-FASTEF primary coolant loop including all relevant thermal aspects

Dissemination level: PU

Date of issue of this report: 15/05/13

32/64

Region\Case	HH015	HH080	HH120	LL015	LL080	LL120
HX2PP	109	13	40	80	159	146
Inter-plate	88	1	0	173	101	41
IVFHM top	14	1	0	33	101	50
Annulus	41	2	2	56	57	20
Core	12	14	8	3	1	2
Hot FS	15	0	0	26	75	442
Lower plenum	375	102	80	349	444	229
Upper plenum	200	45	21	216	101	87
Upper plate	138	813	939	64	2	1
Total	992	991	990	1000	1041	1018

Table 9: Localisation of the particles at 1200s for porosity 2.5 and 12.5%, diameter 0.15, 0.8 and 1.2mm.

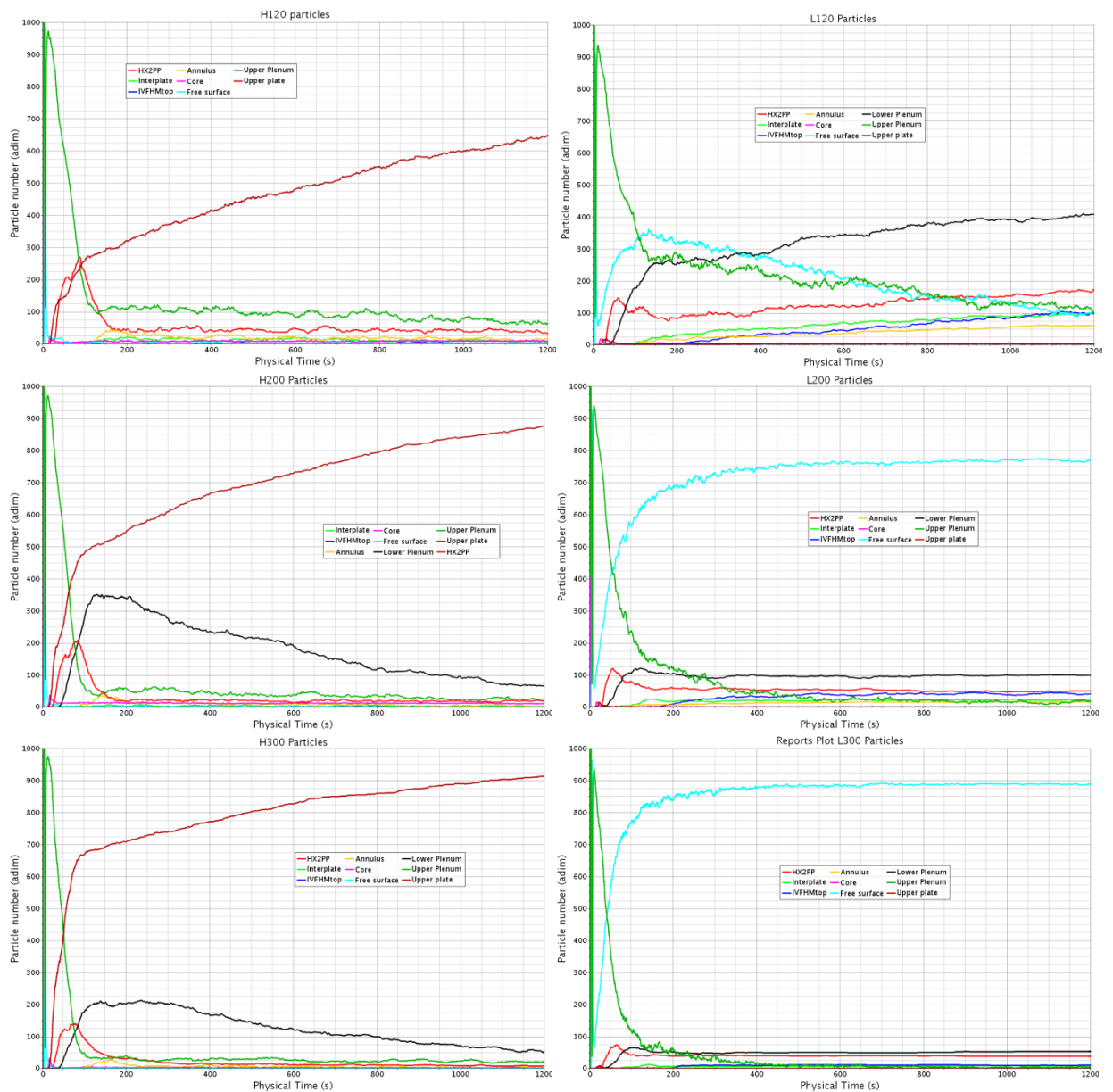


Figure 21: time history of the particle repartition for diameters 1.2mm (top), 2.0mm (middle), 3.0mm (bottom), porosity 5% (left) and 10% (right).

[SEARCH]

DEL5.3: Two-phase CFD model of the MYRRHA-FASTEF primary coolant loop including all relevant thermal aspects

Dissemination level: PU

Date of issue of this report: 15/05/13

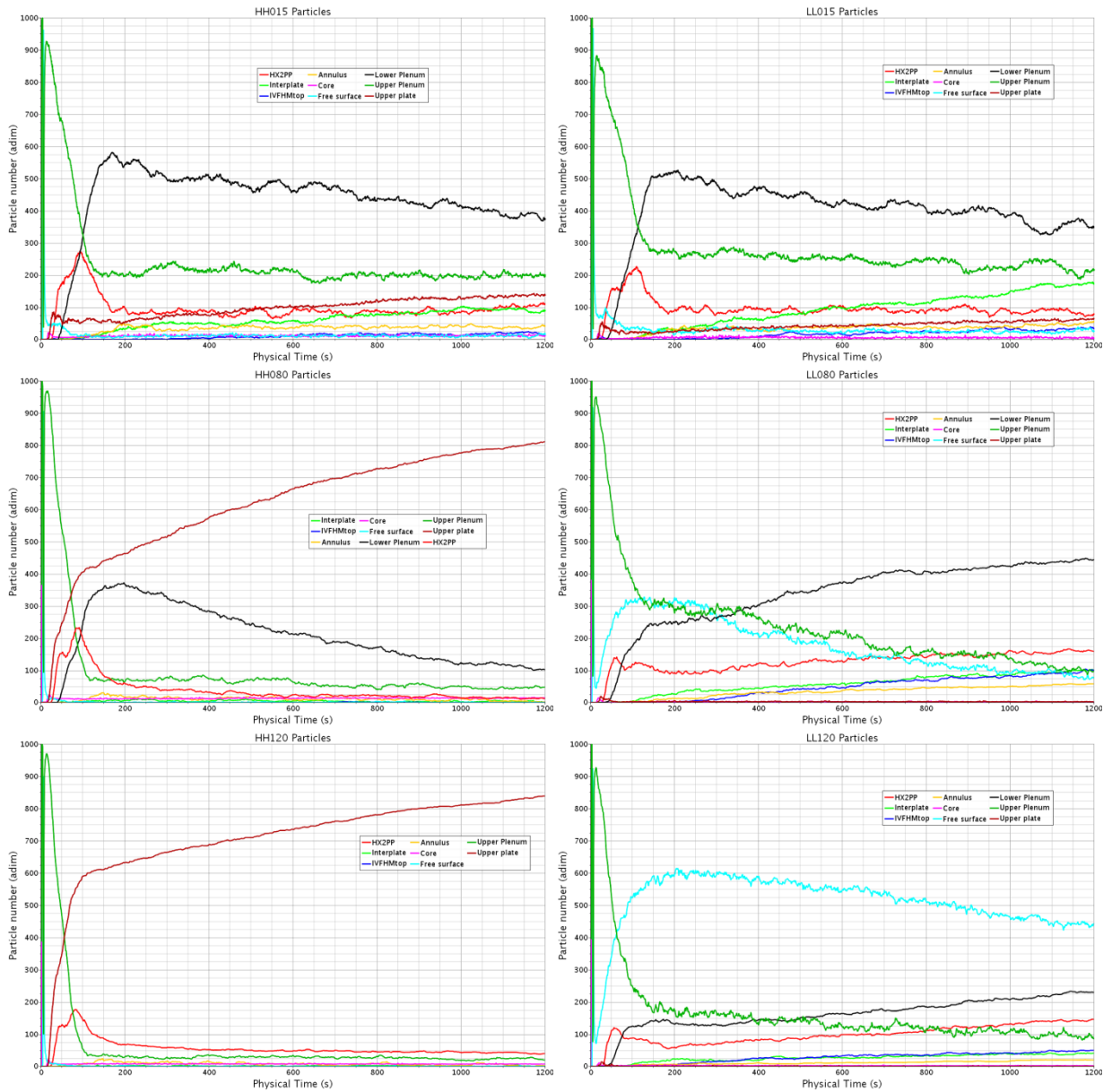
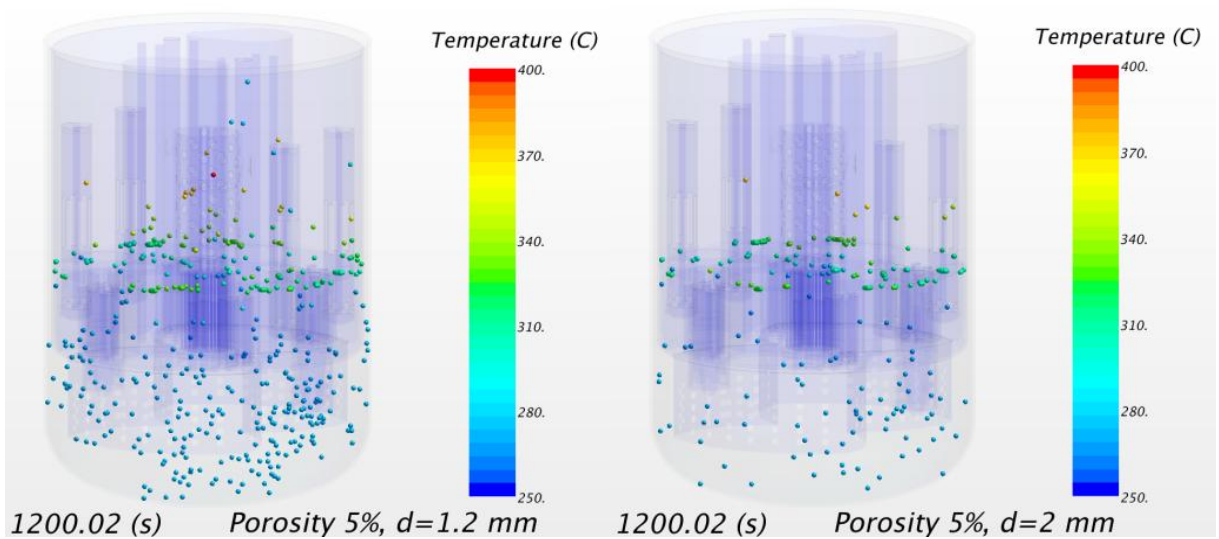


Figure 22: time history of the particle repartition for diameters 0.15mm (top), 0.8mm (middle), 1.2mm (bottom), porosity 2.5% (left) and 12.5% (right).



[SEARCH]

DEL5.3: Two-phase CFD model of the MYRRHA-FASTEF primary coolant loop including all relevant thermal aspects

Dissemination level: PU

Date of issue of this report: 15/05/13

34/64

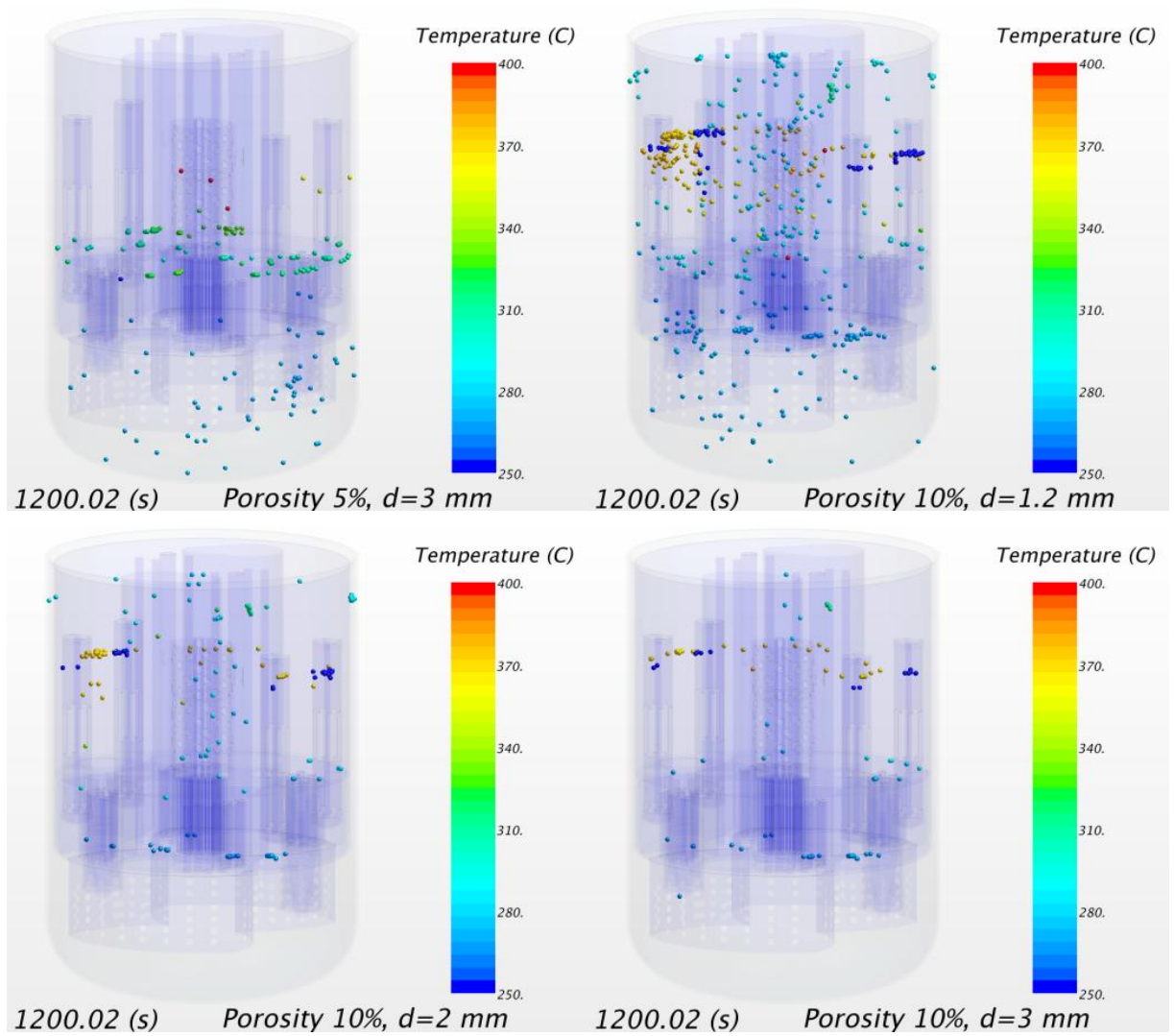


Figure 23: position after 1200s of the particle for diameters 1.2mm (top), 2.0mm (middle), 3.0mm (bottom), porosity 5% (left) and 10% (right).

[SEARCH]

DEL5.3: Two-phase CFD model of the MYRRHA-FASTEF primary coolant loop including all relevant thermal aspects

Dissemination level: PU

Date of issue of this report: 15/05/13

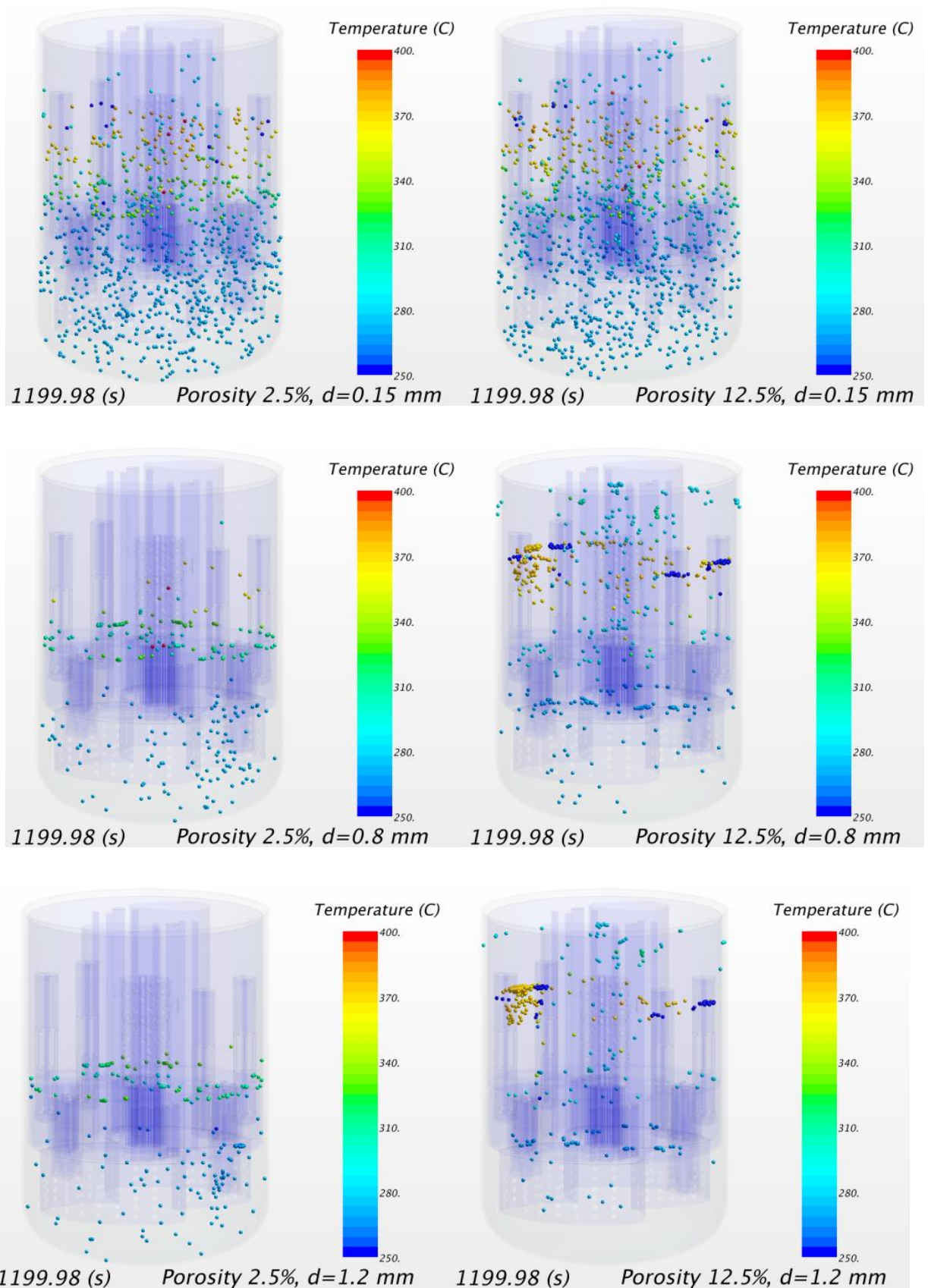


Figure 24: position after 1200s of the particle for diameters 0.15mm (top), 0.8mm (middle), 1.2mm (bottom), porosity 2.5% (left) and 12.5% (right).

[SEARCH]

DEL5.3: Two-phase CFD model of the MYRRHA-FASTEF primary coolant loop including all relevant thermal aspects

Dissemination level: PU

Date of issue of this report: 15/05/13

4.3 Analysis

The former results demonstrate that under nominal operation, fuel particles show a great variety of behaviour depending on their size and porosity. There are several zones of aggregation, mainly the free surfaces, the upper plate top and the lower plate bottom, while the slightly heavier particles tend to be re-circulated for a long time in the lower plenum. Some of these aggregation zones are questionable as they could depend on flow features not taken into account such as several foreseen bypass flows. It should be also noted that the particles have no numerical possibility to be trapped back in the core FAs, while it is probably a preferred relocation in reality and a good part of the particle crosses the core one or more times. However, the diversification of the behaviours by itself is a good indicator that no re-criticalization issue due to a small or medium amount of fuel dispersed in time under nominal operation is to be feared.

A more serious potential issue is the relocation of the fuel and cladding particles in some critical positions limiting in time the effective flow cross section in the core FAs, the HXs or the PPs or increasing the thermal resistance of the fuel pins or the HX tubes. By the very reason that the fuel particles have an effective density very close to the LBE one, they tend to recirculate until they reach a position where they can stick.

5. ULOF preliminary tests and considerations

While it is difficult to foresee potential issues of isolated pin failures under normal operation, the situation may change under some accidental scenario. We now investigate the feasibility to reproduce the Unprotected Loss Of Flow (ULOF) accidental scenario. In this scenario, the pumps fail while all the remnant part of the system continues as is.

5.1 First simulation (ULOF_1)

To take profit of the progress made by the software in its meshing capabilities, considering that the former mesh was built with version 8.02 and that the current version at the time of the simulation is version 9.06, we rebuilt the mesh, keeping exactly the same setting. However, the number of cells reduced from 9.3M to 8.7M. The difference is related to the better mesher behaviour in stiff conditions and its better capability to recognize specific configurations such as tubes and other fine structures. This results in a better mesh quality with a slightly smaller cell number.

After re-meshing, the MYRRHA model was successfully run for 1s of physical time to clean the high frequency/small size interpolation errors and to check its global congruence.

5.1.1 Preliminary setting

To start the preliminary ULOF_1 accident, we only add a multiplier to the pump thrust definition. That is, we set the pump thrust to decay by one half every 5 seconds from the initial time t_0 . More precisely, the multiplier A is set as: $A=0.5^{*((t-t_0)/5)}$, with $t_0=241s$.

5.1.2 Main limitations

The simulation suffers a priori of two main limitations: (i) the pump hydraulic characterization and (ii) the absence of neutronic feedback.

With regards to the pump hydraulic characterization, the main issue is to characterize the hydraulic resistance of the rotor/stator assembly when the pump comes almost to rest and a

[SEARCH]

DEL5.3: Two-phase CFD model of the MYRRHA-FASTEF primary coolant loop including all relevant thermal aspects

Dissemination level: PU

Date of issue of this report: 15/05/13

37/64

strong reverse flow occurs. The absence of related hydraulic resistance can greatly influence the extent of the reverse flow, both in flow rate and duration.

The absence of neutronic feedback is likely to provoke a strong over-estimation of the core power and by turn of the FA LBE temperature.

5.1.3 Results

The mass flow rate through the pumps and the core FAs has been monitored. It has also been monitored separately for one single FA in the first ring, which is the hottest. The maximum temperature in the LBE is also monitored. We must recall that in this version of the model, the heat source is directly provided to the LBE in the FAs.

The core mass flow rate decreases monotonously up to time 295s, see Figure 25, where a very slight minimum is observed about 1200kg/s. In the meantime, the FAs mass flow rate follows a very similar curve but reaching a 1000kg/s asymptotic value at time 282s with no observable local minimum. The former minimum is therefore restricted to the dummies where a residual flow can be induced by buoyancy after some delay caused by the structure thermal resistance. The mass flow curve for the single FA in the first ring, see Figure 26 left, shows the same behaviour as the entire set of FAs, decreasing monotonously from 75kg/s down to 17kg/s (about 23%) the asymptotic value essentially reached at time 285s (i.e. after 45s).

The flow in the pumps exhibits a large inversion for more than 10s with a maximum above 6000kg/s. The buffer fluid inventory coming from the surface level difference between the inner (hot) and outer (cold) plenum is therefore mainly lost uselessly and does not serve to mitigate the core possible initial overheating before the natural convection transition takes place. It is however not unlikely that this behaviour may largely change once a more realistic pump characteristic, valid under a larger range of condition, is implemented.

The maximum temperature in the FA monotonously increases up to an asymptotic value of 1165C essentially reached after 45s. No local maximum is therefore observed. Clearly and as stated before, the absence of neutronic feedback does not allow to draw any conclusion on the real temperature behaviour.

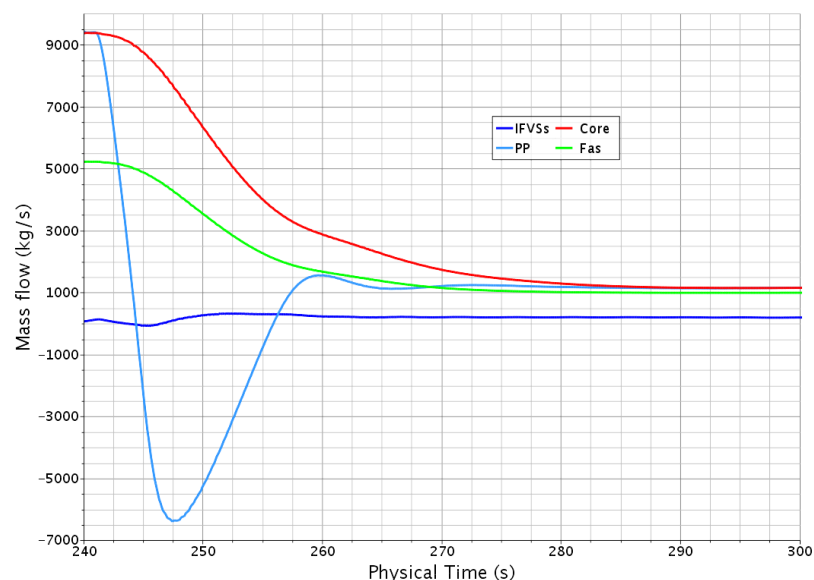


Figure 25: ULOF_1 transient main mass flow rates.

[SEARCH]

DEL5.3: Two-phase CFD model of the MYRRHA-FASTEF primary coolant loop including all relevant thermal aspects

Dissemination level: PU

Date of issue of this report: 15/05/13

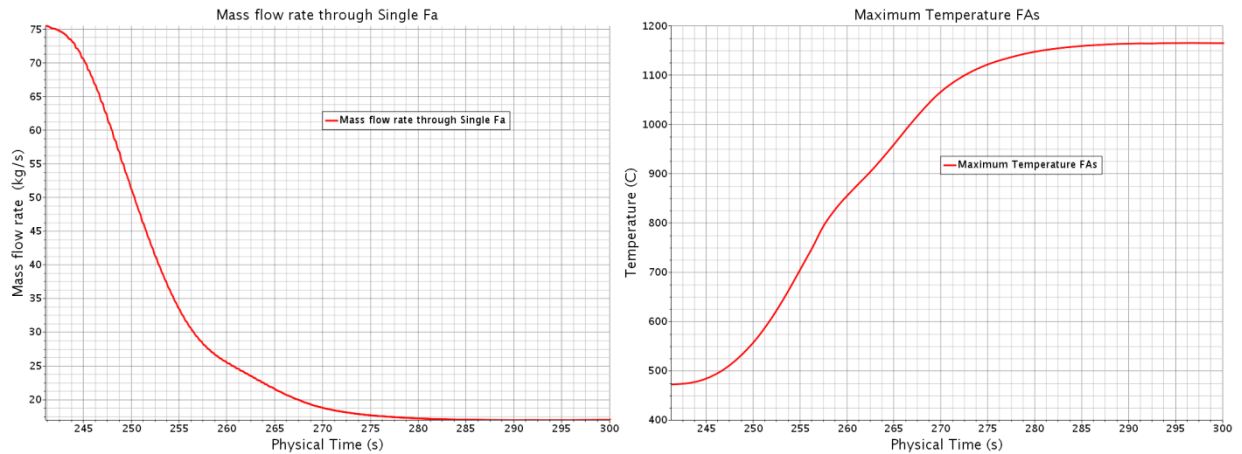


Figure 26: ULOF_1 (left) first ring single FA mass flow rate during (right) Maximum LBE temperature

5.2 Second group of simulations

In the following, we show the simulation improvements and trials that brought us to the final ULOF simulation of this work.

5.2.1 First equilibrium neutronic feedback (ULOF_2)

In this simulation, we begin to take into account in a crude way the neutronic feedback. From the work performed in the EURATOM FP7 CDT project and put in their DEL2.3 [17], we can retrieve the asymptotic power from the FAs mass flow rate. We base our estimation on IKET work as it seems more precise.

In their ULOF simulation with SIMMER-III, they observe asymptotically a halving of the core power in correspondence to a reduction down to 14% of the nominal mass flow rate (about $1/7^{\text{th}}$). This can be roughly transformed in terms of a multiplier (by 3.5) of the LBE temperature increase between inlet and outlet, and also of the difference between the mean and the inlet LBE temperature. In turn, it is also transformed in a change of the mean LBE density (from the inlet one). Then we set the core power linear between these two mean densities. The mean density seems to be a more relevant control parameter than the mean temperature because it could account from changes from the LBE volume fraction (in case of a fission gas emission).

We can set the instantaneous power by having measured the nominal mean inlet and FAs LBE temperature as follows:

- Mean inlet density (nominal): $\rho_0=10375.49 \text{ kg/m}^3$
- Mean density nominal: $\rho_n= 10287.43 \text{ kg/m}^3$, power $\text{Pow}_n= 100\%$
- Mean density IKET asymptotic ULOF $\rho_{\text{IKET}}=\rho_0+3.5(\rho_n-\rho_0)=10067.28\text{kg/m}^3$, power $\text{Pow}_{\text{IKET}}= 50\%$.
- Mean density for 0 power extrapolation: $\rho_z=2\rho_{\text{IKET}}-\rho_n$

By doing this, we consider the core power to be in equilibrium with the LBE inventory, which is a very crude assumption but still an improvement from the precedent modelling.

Some algebra gives the current core power Pow in function of the nominal core Power Pow_n and the current mean density ρ as: $\text{Pow}=\text{Pow}_n*[1+(\rho-\rho_n)/(\rho_n-\rho_z)]$.

In practice, as ρ_{IKET} is only a guess and we do not take into account non-linear effects, only the shape of the power function has to be kept. The simulation serves mainly to get a second point on the power/density curve. With $\text{Pow}=\text{Pow}_n*[1+(\rho-\rho_n)/396.27]$, we find asymptotically:

[SEARCH]

DEL5.3: Two-phase CFD model of the MYRRHA-FASTEF primary coolant loop including all relevant thermal aspects

Dissemination level: PU

Date of issue of this report: 15/05/13

- $Pow_2 = 51.29 \text{ MW}$
- $\rho_2 = 10095 \text{ kg/m}^3$.
- Maximum temperature: $T_{Max} = 829 \text{ C}$ (reached asymptotically)
- Single FA mass flow rate: 13.5 kg/s (asymptote)

5.2.2 Weighted mean density for neutronic feedback (ULOF_3)

From IKET work, it turns out that the coolant feedback reactivity coefficient is strongly space dependent with a value going to almost zero on the core axis. This means that the power will almost not decrease if the LBE becomes hotter only at the core centre. To take into account this feature, the measured mean density must be weighted to reduce the influence of the central part. We take the simple weight function f to be radial in the form: $f(r) = \text{Min}[(r/R)^2, 1]$ with $R = 25 \text{ cm}$, see Figure 27.

The instantaneous core power calculation requires the following inputs:

- Mean inlet density (nominal): $\rho_0 = 10375.49 \text{ kg/m}^3$
- Mean weighted density nominal: $\rho_n^* = 10292.09 \text{ kg/m}^3$, power $Pow_n = 100 \text{ MW}$
- Mean weighted density ULOF_2: $\rho_2^* = 10103.88 \text{ kg/m}^3$, power $Pow_2 = 51.3 \text{ MW}$.
- Mean density for 0 power extrapolation:
 $\rho_z^* = (Pow_n - Pow_2)^{-1} (Pow_n \rho_2^* - Pow_2 \rho_n) = 9905.62 \text{ kg/m}^3$.

The core power is then calculated essentially with the same formula as before:

$$Pow = Pow_n^* [1 + (\rho^* - \rho_n^*) / (\rho_n^* - \rho_z^*)]$$

This formula however still resents of the non-linearity of the problem. To get a more precise asymptotic core power, we prolong the precedent simulation, using a core power formula with a slightly stiffer curve ($1/368$ instead of $1/386.5$): $Pow = Pow_n^* [1 + (\rho^* - \rho_n^*) / 368]$

After performing the simulation, we find:

- $Pow_3 = 50.0 \text{ MW}$
- $\rho_3^* = 10108.1 \text{ kg/m}^3$.
- Maximum temperature: $T_{Max} = 819.6 \text{ C}$ (reached asymptotically)
- Single FA mass flow rate: 13.7 kg/s (asymptote)

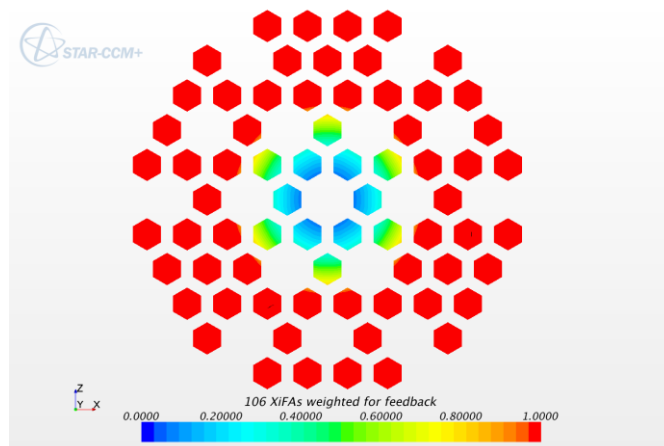


Figure 27: FAs cross section coloured by the weight used to determine the mean weighted LBE density.

5.2.3 Neutronic relaxation time (ULOF_4)

[SEARCH]

DEL5.3: Two-phase CFD model of the MYRRHA-FASTEF primary coolant loop including all relevant thermal aspects

Dissemination level: PU

Date of issue of this report: 15/05/13

In the two precedent simulations, we related the core power to the mean LBE density through an equilibrium assumption. However, there is a delay between the LBE density change and the core power variation. This simulation is similar to the ULOF_3 simulation except that we introduce such a delay with a characteristic time of $\tau_d=5s$.

In other terms, if the equilibrium hypothesis reads: $Pow=f(\rho^*)$, then the transient governing equation becomes: $\partial_t Pow + [Pow - f(\rho^*)]/\tau_d = 0$.

We use the equilibrium function of ULOF_3. The asymptotic values do not change but the transient behaviour might do. The main interrogation relies in whether or not the transient maximum temperature is higher than the asymptotic maximum temperature. It turns out that there is a very slight local temperature maximum at 825C at time $T=275s$ while the asymptotic values stabilizes 5 degrees below, Figure 28 top right. There is also a local minimum mass flow rate in the single central FA at 13.63kg/s, but at time $T=296$, Figure 28 top left, quite later than the temperature maximum. The mass flow rate slightly increases further up to 13.86kg/s at the end of the simulation at time $T=318s$. The core power decreases very close to 50% as expected, as shown in Figure 28 bottom left, where we can also see that the reactivity feedback introduced effectively slows down and slightly delays the power decrease.

We find:

- $Pow_4 = 49.9 \text{ MW}$ (minimum at $T=302s$)
- $\rho_4^* = 10098 \text{ kg/m}^3$ (Minimum at $T=295s$)
- Maximum temperature: $T_{Max} = 825C$ (plateau between 274 and 282s)
- Single FA mass flow rate: 13.63kg/s (minimum at $T=296s$)

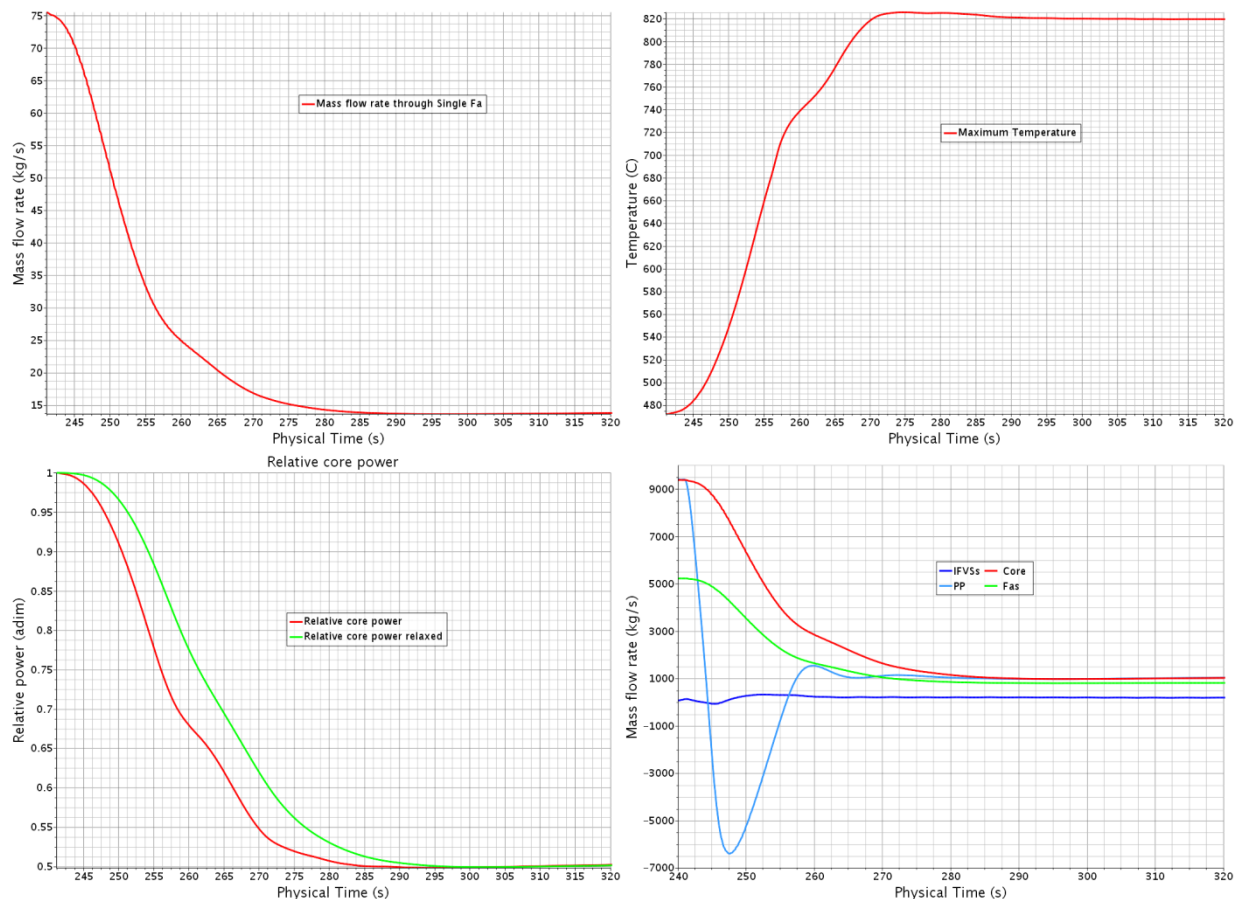


Figure 28: ULOF_4. Top left, mass flow rate in one central FA. Top right, maximum LBE temperature in the core. Bottom left, core power: in green, effective; in red equilibrium. Bottom right, mass flow rates.

[SEARCH]

5.2.4 Fission gas emission ULOF_5

Fission gas blowout is expected to occur when the cladding exceed 1040C. The cladding temperature is expected to be about 50K above the LBE bulk temperature (which is the temperature that we are actually simulating). Clad melting is however reached at about 1480C. Therefore, in the condition of the previous simulation, gas blowout, which would have surely occurred without coolant reactivity feedback, is not so likely even if it cannot be excluded. In effect, the maximum temperature is measured on a size scale that cannot take into account possible large local variations on the inter fuel pin scale.

Under the assumption that the maximum temperature can locally lead to fission gas release and that the phenomena propagates inside the faulty FA, we can try to evaluate the effect, mainly the thermal effect, of the fission gas release and its path in the hot plenum. This is what we are going to investigate here.

Considering a single fuel pin, the fission gas gather into two distinct cylindrical volumes. The larger one is at the pin bottom while the smaller one is at its top. To retrieve the volume occupied by the fission gas in one FA, we need the following numbers:

- Lower gas plenum height: 58cm,
- Upper gas plenum height: 6cm
- Gas plena internal diameter: 5.65mm,
- Pin number per FA: 127.

This gives us a fission gas volume per FA about $V_{fg}=2dm^3$. In case of pin failure, we expect the fission gas to exit the pin until its pressure equilibrate with the LBE one. The pressure in the LBE at the active core level is about 5 Bar. Two values are given for the fission gas pressure at EOC, a conservative one at 50 Bars and a more realistic one at 25 Bars.

Taking into account that the current MYRRHA CFD model, the VOF treatment leads to incorporate the fission gas released in the gas phase used for the cover gas. Moreover, the cover gas is treated as incompressible with no density dependence on temperature. Under these conditions, the fission gas inventory accessible for release in one FA amounts to $v_{tot}=18dm^3$ in the conservative case and to $v_{tot}=8dm^3$ in the more realistic case. As we release the fission gas in all the 6 Fas of the first ring, the total inventory amounts respectively to $V_{tot}=108dm^3$ and to $V_{tot}=48dm^3$.

The simulation starts from the ULOF_4 simulation taken at time $T_0=280s$, that is 5 seconds after the maximum LBE temperature has been reached

The fission gas inventory is then released homogeneously on a slab 20cm high above the core centre in the first FA ring, in 10s with a hat shaped time release profile.

We first have to measure the volume in which the gas will be released by integration in starccm+ of its characteristic function χ . We find $V_0=5.4568dm^3$.

The formula to define the volumetric volume gas source S_{Gas} is:

- If $T_0 < t < T_0 + 5$, then $S_{Gas} = (t - T_0) * V_{tot} / 25V_0$
- Else if $t < T_0 + 10$, then $S_{Gas} = [2 - (t - T_0)] / 5 * V_{tot} / 5V_0$.

The corresponding enthalpy source of the gas, $H_{Gas} = \rho_{Gas} * C_{p_{gas}} * T * S_{Gas}$, must also be implemented.

The current implementation of the interface sharpening algorithm enters in conflict with the implementation of the fission gas emission. To resolve the conflict, some corrective actions are taken. The strength of the user-defined sharpening algorithm is reduced by two orders of magnitude while the sharpening factor is raised from 0.1 to 0.2 and the condition set to switch to the second order scheme is relaxed above $CFL=2$. The reduction of the light phase sink is such

[SEARCH]

DEL5.3: [Two-phase CFD model of the MYRRHA-FASTEF primary coolant loop including all relevant thermal aspects](#)

Dissemination level: PU

Date of issue of this report: 15/05/13

that the sink becomes irrelevant on the time scale of the fission gas release and its evacuation in the cover gas, while it is still effective on the 400s global return time scale to clean some undue light phase numerical entrainment. The two last actions aim at strongly reducing the intensity of this numerical light phase entrainment.

In the realistic case ($V_{tot}=48 \text{ dm}^3$), there is a small peak of temperature $T= 829\text{C}$ at time $t=294\text{s}$ in correspondence with a slight minimum of the mass flow rate in the central FAs, see Figure 29. The core power shows a small minimum at time $t=288\text{s}$, about 3s after the minimum equilibrium power has been reached, while the global mass flow rates remain largely undisturbed, see Figure 30.

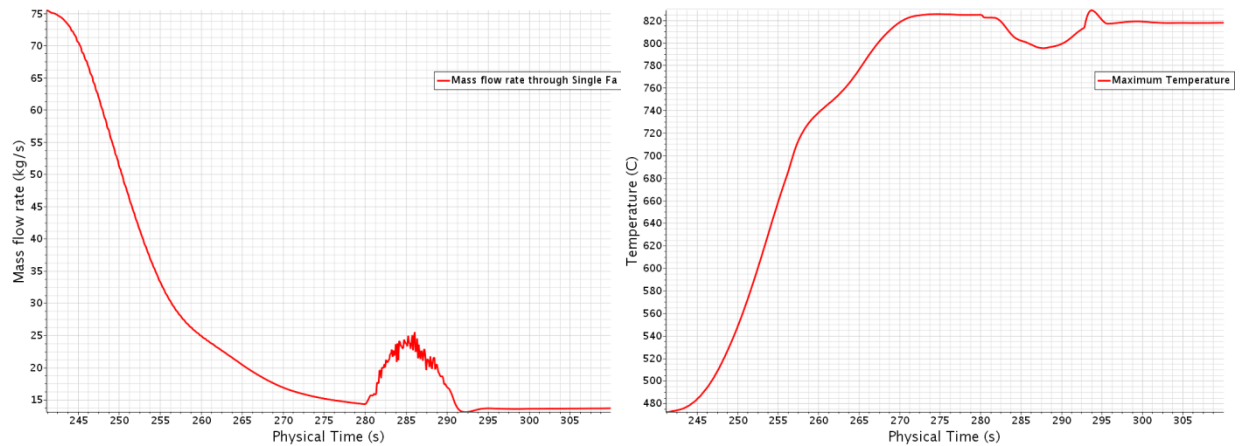


Figure 29: ULOF5. Left, mass flow rate through a single FA. Right, maximum temperature.

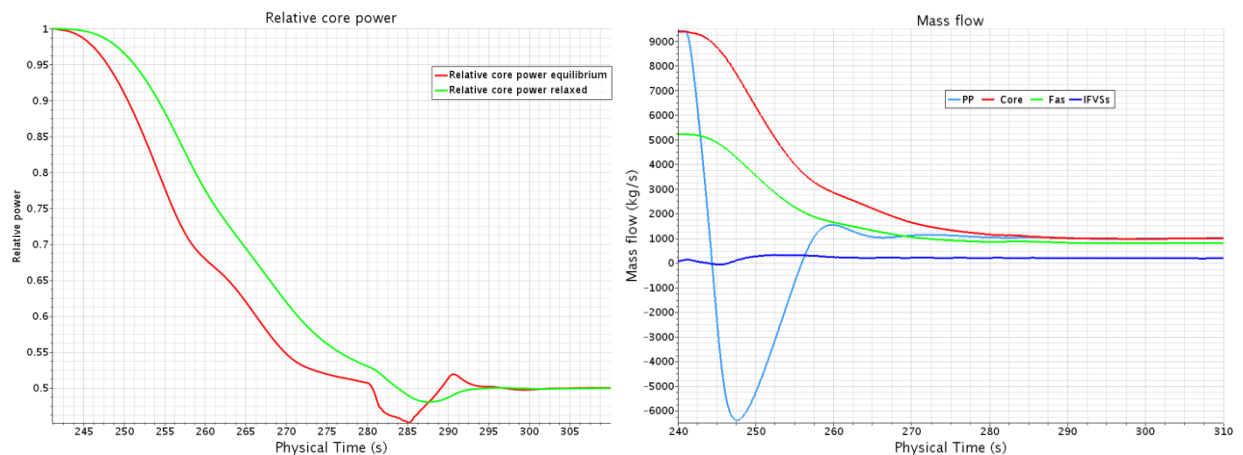


Figure 30: ULOF5. Left, relative core power. Right, principal mass flow rates.

5.2.5 Single FA fission gas emission ULOF_6

This simulation is identical to the previous one except that the fission gas is released in only one FA. The corresponding reactivity insertion should have an intensity about six times lower and we expect a slightly higher temperature peak.

In confront with ULOF_5, the mass flow rate and the maximum temperature are almost identical (829.4C at $t=293.5\text{s}$), see Figure 32. In fact, the maximum temperature is only related to the local minimum of the mass flow rate, because the core power has already reached the equilibrium value. However, before reaching this value, the core power decreases monotonously in ULOF_6, see Figure 33 left, while it shows a neat local minimum in ULOF_5. As a security check, we also plot the time evolution of the volume integral (in space) of the fission gas source and the fission

[SEARCH]

DEL5.3: Two-phase CFD model of the MYRRHA-FASTEF primary coolant loop including all relevant thermal aspects

Dissemination level: PU

Date of issue of this report: 15/05/13

gas flow rate measured at height $y=0.3\text{m}$ (top of the heat source region).
 Between ULOF_5 and ULOF_6, we have also reduced the final time of the simulation from 310 to 300s as we noticed that all the perturbations induced by the fission gas release had disappeared 10s after the end of the release.

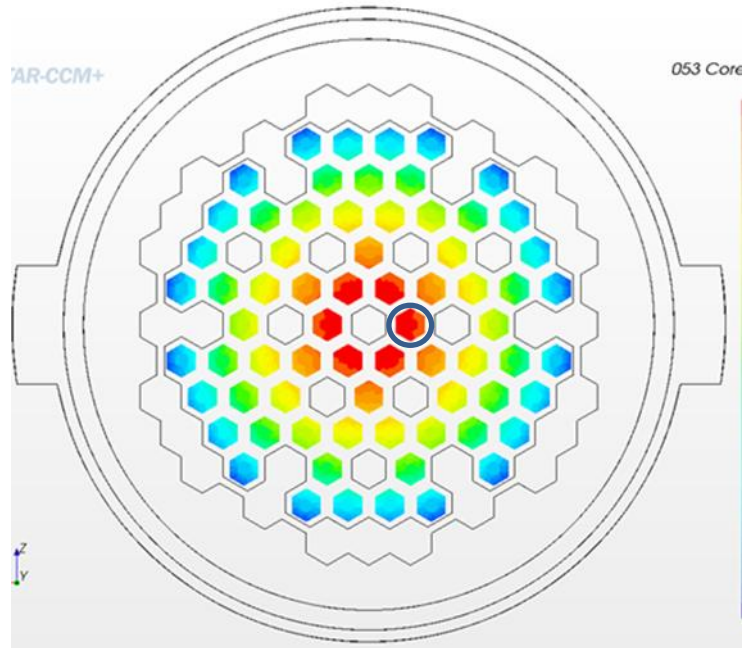


Figure 31: ULOF_6 to ULOF_8. Position of the fission gas release, followed by the particles release.

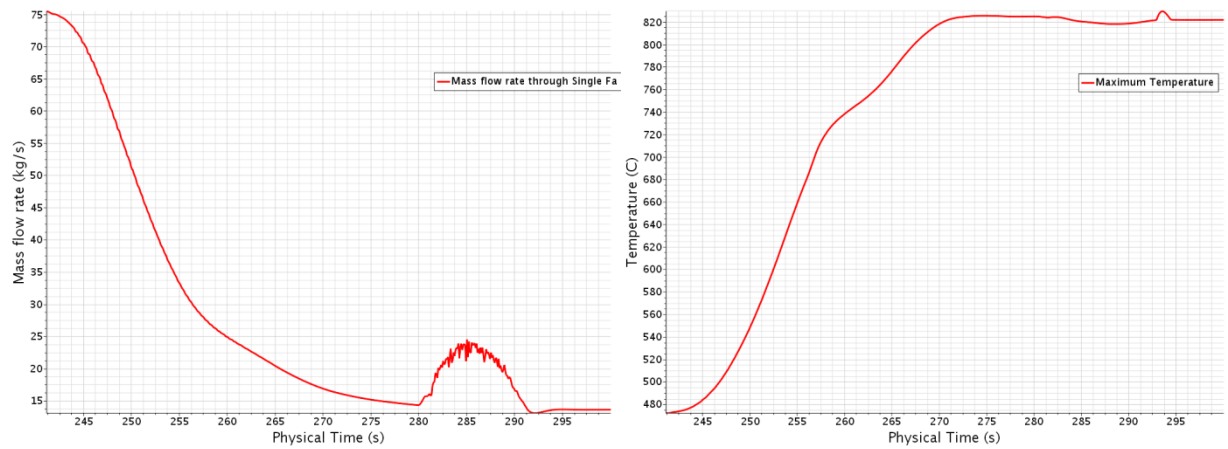


Figure 32: ULOF_6. Left, mass flow rate through the damaged FA. Right, maximum temperature.

[SEARCH]

DEL5.3: Two-phase CFD model of the MYRRHA-FASTEF primary coolant loop including all relevant thermal aspects

Dissemination level: PU

Date of issue of this report: 15/05/13

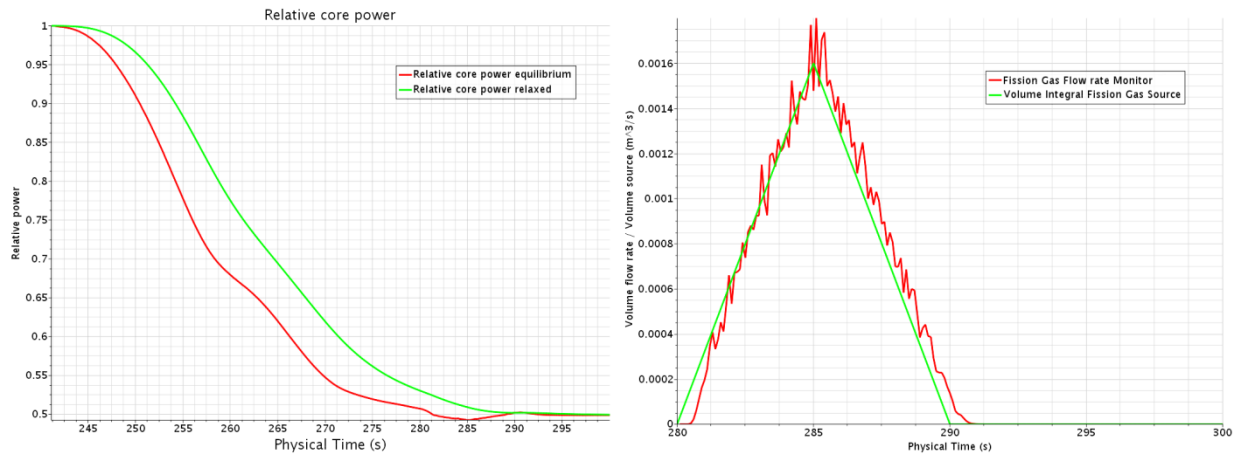


Figure 33: ULOF_6. Left, relative core power. Right, fission gas volume source (green) and volume flow rate at height $y=0.3\text{m}$.

6. Final three-steps ULOF simulation (ULOF_4, ULOF_7 and ULOF_8)

In the context of this work, the former simulations allow us to propose and perform a quite complete and articulated ULOF scenario. This scenario is organised in three steps, the first one involving the ULOF_4 simulation up to time $t=280\text{s}$ (already treated previously). Then, for 10s, up to time $t=290\text{s}$, we release 18dm^3 in the single “faulty” FA. Finally, at time $t=300\text{s}$, the damaged FA pins begin to release fuel particles of different size and porosity. The release also lasts for 10s and the particles are followed for 500s until time $t=800\text{s}$.

6.1 Single FA fission gas emission, high pressure (ULOF_7)

This simulation is identical to the previous one except that the fission gas pressure is supposed to be 50Bars and the total volume released amounts to 18dm^3 .

The more than doubled gas release induces some amount of added mass flow rate but only a marginal increase of the maximal temperature at the end of the event: $T_{\text{Max}}=832.3\text{C}$ at $t=293.7\text{s}$, see Figure 34.

Some plots of the 5% gas volume iso-surface between times 281 and 295s are shown on Figure 35. The corresponding effect on the velocity field is shown on Figure 36.

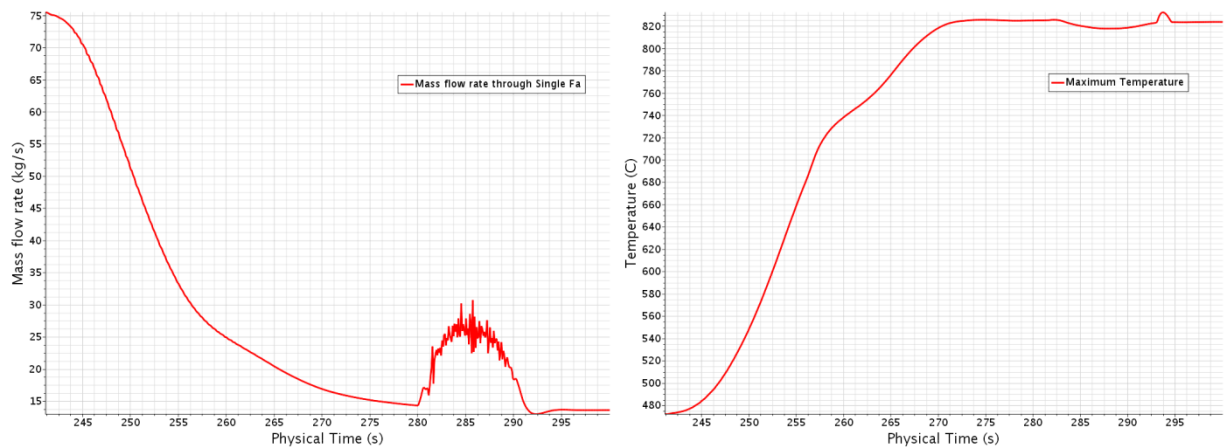


Figure 34: ULOF_7. Left, mas flow rate in the damaged FA. Right, maximum temperature.

[SEARCH]

DEL5.3: Two-phase CFD model of the MYRRHA-FASTEF primary coolant loop including all relevant thermal aspects

Dissemination level: PU

Date of issue of this report: 15/05/13

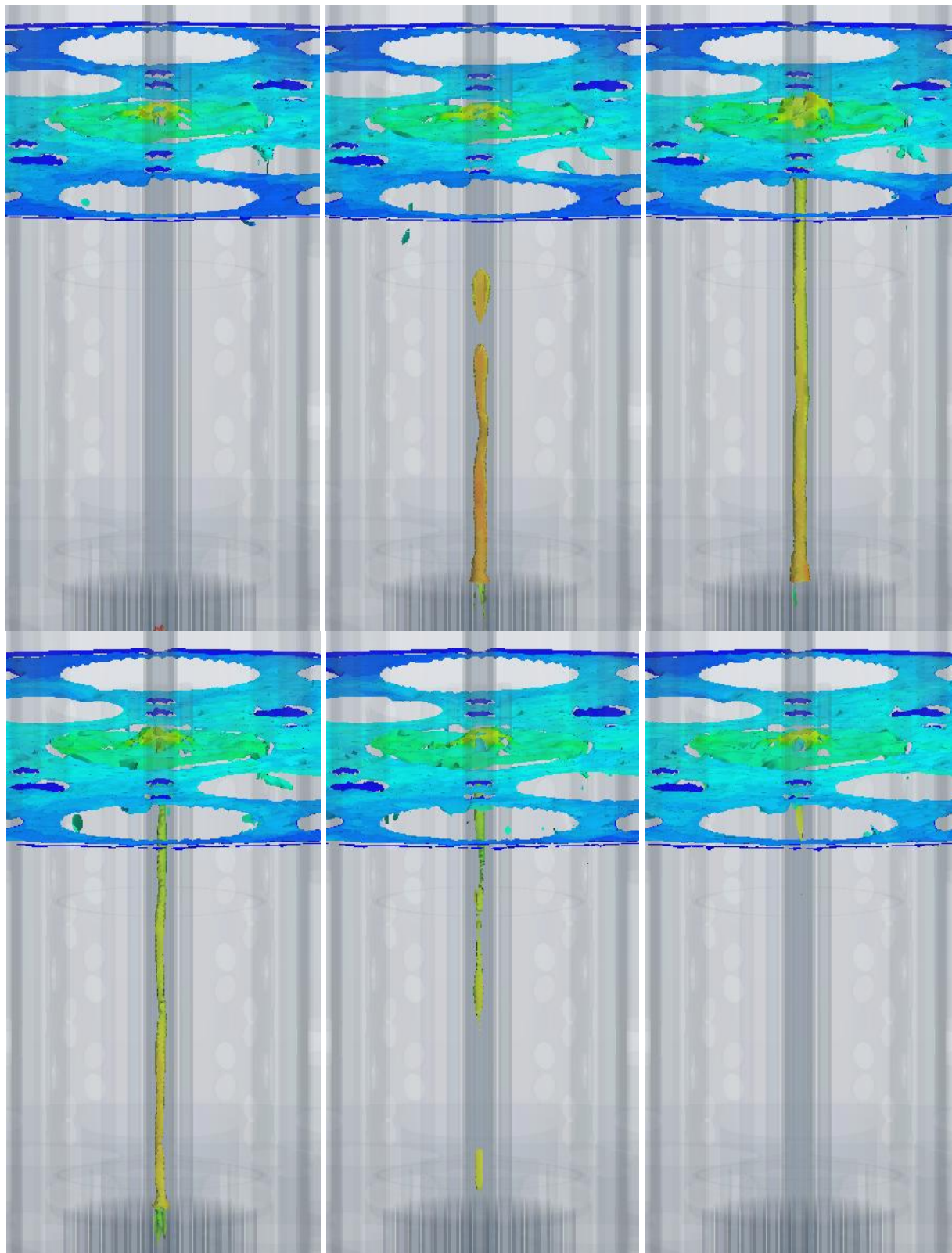


Figure 35: ULOF_7. Iso-surface of 5% gas volume. From left to right, from top to bottom time 281, 283, 285, 290, 292, 295s. Coloured by temperature (red=800C).

[SEARCH]

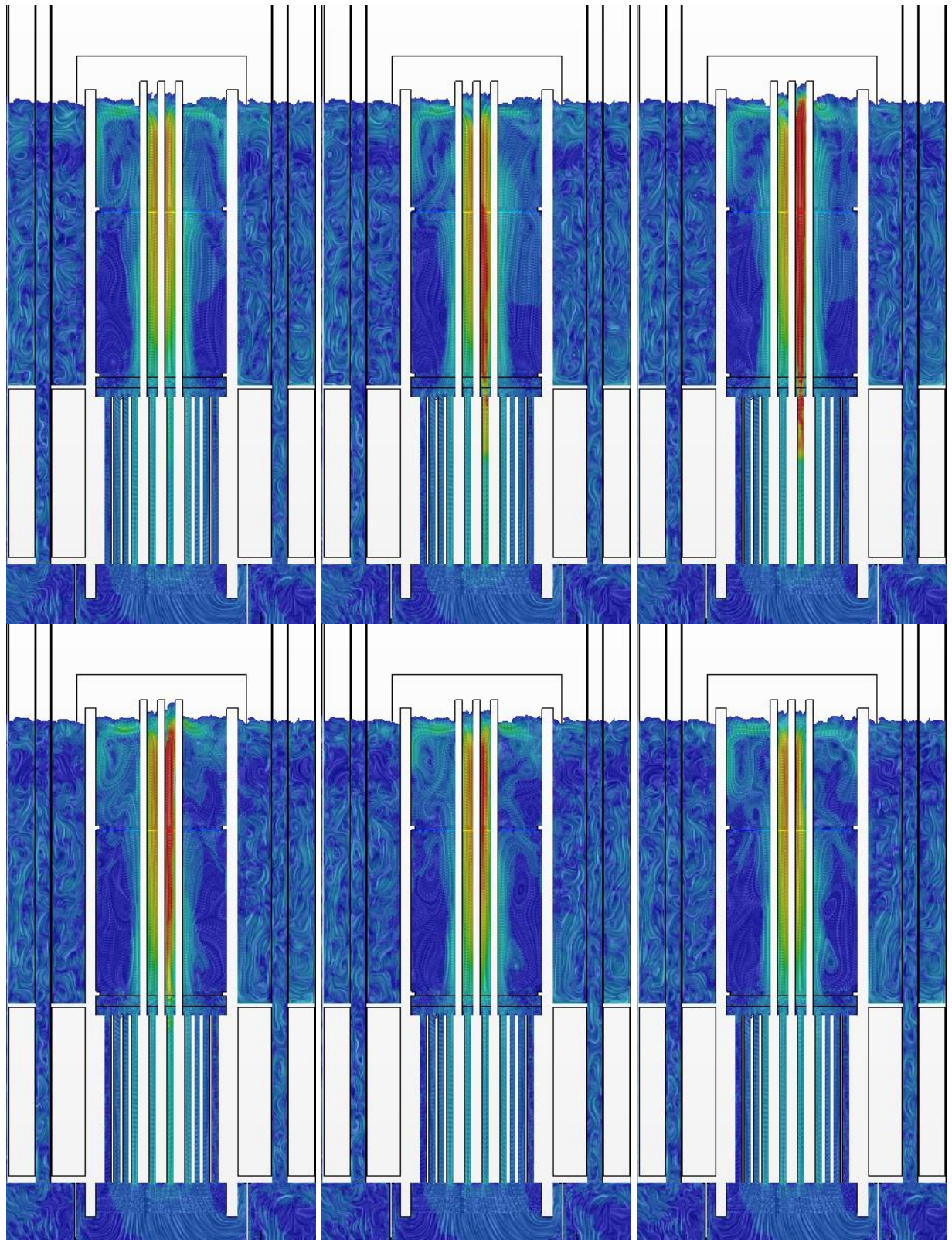


Figure 36: ULOF_7. Velocity field. From left to right, from top to bottom time 281, 283, 285, 290, 292, 295s. Coloured by velocity magnitude (scale 0, 1.5m/s).

[SEARCH]

DEL5.3: Two-phase CFD model of the MYRRHA-FASTEF primary coolant loop including all relevant thermal aspects

Dissemination level: PU

Date of issue of this report: 15/05/13

6.2 Fuel particle release ULOF_8

This simulation starts 10s from the end of the fission gas release in ULOF_6 at time $t=300s$. Six types of particle are released from the FA, one for each type every time step (0.01s) for 10s. A total of 6000 particles are thus released. The six types span 3 different diameters: 0.15, 0.8 and 1.2 mm and on two different porosities: 5 and 10%.

The main difference with the former particle release is that we are no more in nominal operation condition but at the beginning of the natural circulation regime under ULOF condition. The simulation is therefore fully transient and last for 500s until time $t=800s$.

6.2.1 Fuel dispersion characteristics

The particle number per region and per type at simulation end and at time $t=800s$ is shown on Table 10. The corresponding time history of the particle numbers is shown on Figure 37 and the position of all the particles, on a type basis, at the end of the simulation, is plotted on Figure 38.

It can be seen that the re-meshing between version 8.04 and 9.06 of starccm+ has improved the quality of the Lagrangian particle simulation as we did not lose any more even a single particle.

While quite long, time and computational power consuming, 500s of transient is far for enough to get the asymptotical behaviour of all types of particles. In effect, due to the dramatic drop of mass flow rate, it is only a fraction of the characteristic return time of the primary loop. In fact, it is roughly half the upper plenum characteristic residence time.

On the other hand, the flow velocity dramatically decreases everywhere except at the plume centre and the turbulence intensity has to follow the same trend. The effect of the Lagrangian particle proper drift velocity is consequently much less perturbed.

The heavy particles with 0.8 and 1.2m diameter have already largely settled on the upper plate, and even on the periphery of the core top. The light particles with 0.8 and 1.2m diameter, on the contrary, largely stay put on the free surface or close to it in the upper plenum.

The small particles, light and heavy, show a quite different trend. They are both highly diffused in the upper plenum and convected by the carrier flow to the HX and PP casing, a few of them already reaching the lower plenum. In this case, the global time scale argument stands and it is difficult to know where will be the main settling locations. In particular, the light particles having reached the free surface may or may not stay put in place. Correspondingly, the heavy particles deposited on the upper plate also may or may not remain there.

Region\Case	H015	H080	H120	L015	L080	L120
HX2PP	195	42	14	184	14	3
Inter-plate	0	0	0	2	0	2
IVFHM top	0	0	2	4	0	0
Annulus	0	0	0	0	0	0
Core	0	26	56	1	0	0
Hot FS	13	3	6	103	716	797
Lower plenum	165	36	12	87	3	1
Upper plenum	575	559	444	599	265	197
Upper plate	52	334	466	20	2	0
Total	1000	1000	1000	1000	1000	1000

Table 10: ULOF_8. Particle number per region and per type at end simulation at time $t=800s$.

[SEARCH]

DEL5.3: Two-phase CFD model of the MYRRHA-FASTEF primary coolant loop including all relevant thermal aspects

Dissemination level: PU

Date of issue of this report: 15/05/13

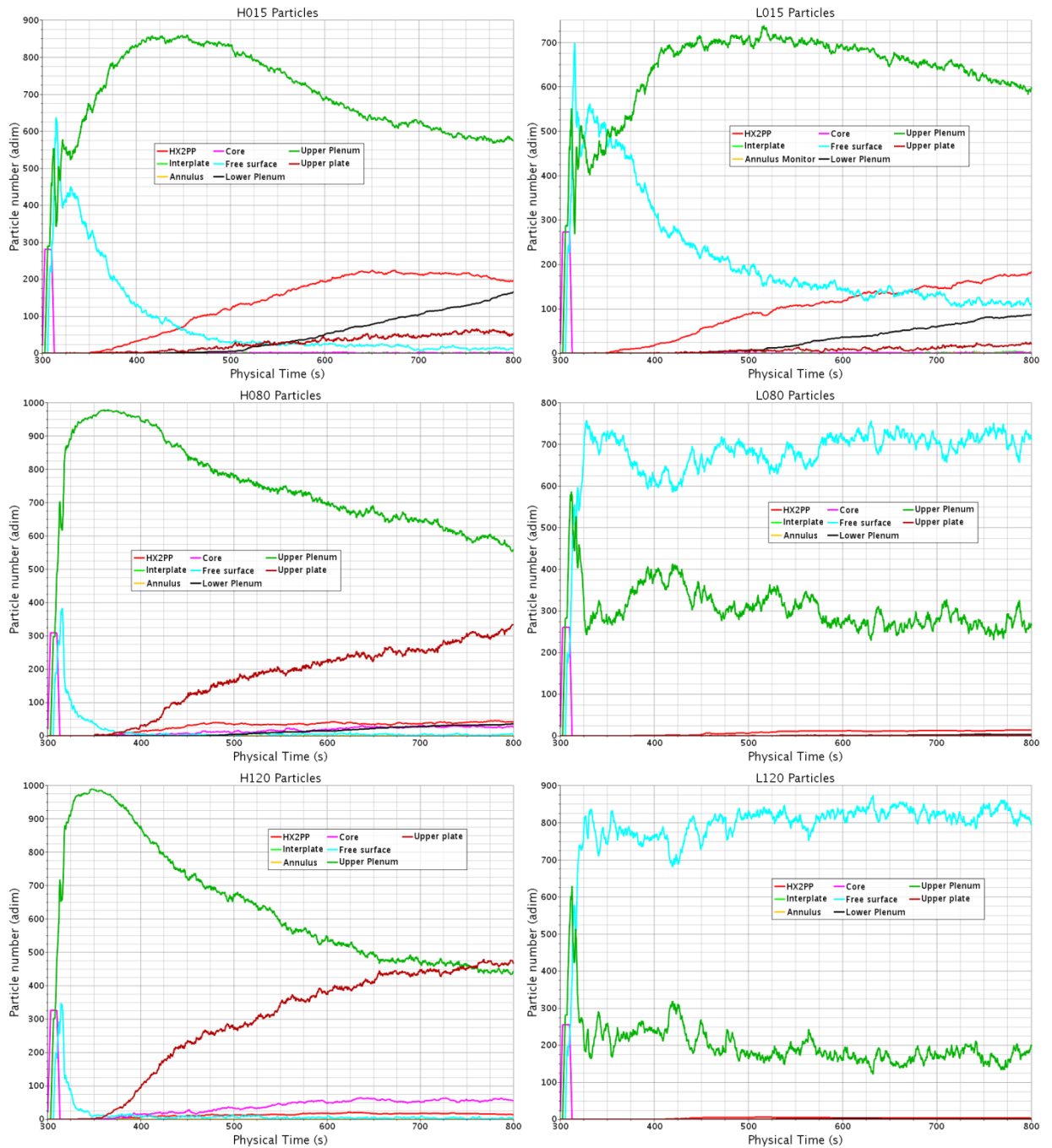


Figure 37: ULOF_8. Time history of the particle repartition for diameters 0.15mm (top), 0.8mm (middle), 1.2mm (bottom), porosity 5% (left) and 10% (right).

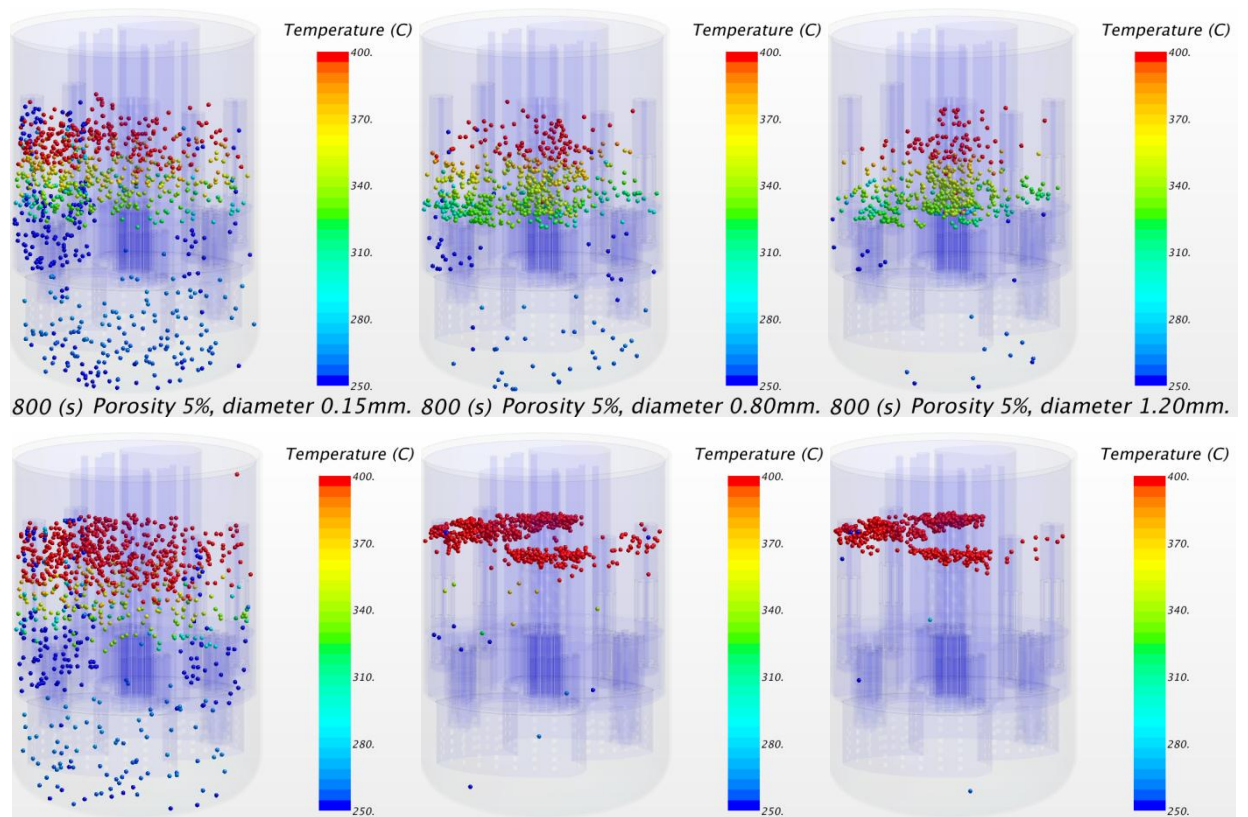
[SEARCH]

DEL5.3: Two-phase CFD model of the MYRRHA-FASTEF primary coolant loop including all relevant thermal aspects

Dissemination level: PU

Date of issue of this report: 15/05/13

49/64



800 (s) Porosity 5%, diameter 0.15mm 800 (s) Porosity 5%, diameter 0.80mm 800 (s) Porosity 5%, diameter 1.20mm
 800 (s) Porosity 10%, diameter 0.15mm 800 (s) Porosity 10%, diameter 0.80mm 800 (s) Porosity 10%, diameter 1.20mm
 Figure 38: ULOF_8. Position at t=800s of the particle for diameters 0.15mm (left), 0.80mm (centre), 1.20mm (right), porosity 5% (top) and 10% (bottom).

6.2.2 LBE flow characteristics

Although this document should be more focused on the particle release dispersion, we also refer on the simulation results for the carrier flow characteristics.

Starting with the graphics of the time evolution of specific data, the HXs power is indicated in Figure 39 right, while the temperature is indicated in inlet and outlet of the HXs in Figure 39 left. The mass flow rate through the “faulty” FA is monitored in Figure 40 left. The mean density history (both effective and weighted) of the LBE in the core is shown on Figure 40 right. The relative core power is followed on Figure 41 left, while the core maximum temperature is shown on Figure 41 right.

The temperature field is analysed in more details. It is indicated at the end of the simulation in Figure 42 for the surface on the left, for the main vertical plane at the centre and on the PP plane on the right. The corresponding time history, with a plot every 100s, is shown on Figure 43 and on Figure 44.

The velocity field on two planes, passing respectively through the two PPs and through 2 HXs are shown on Figure 45.

While the maximum temperature is almost constant in time and stays slightly below the small initial peak, during the simulation, the upper plenum becomes hotter and the lower plenum becomes colder. The over-heating of the upper plenum is driven by the free-surface temperature increase and then slowly propagates downwards. The mean temperature of the flow entering the HXs initially dropped due to the backward flow and global mixing of the plenum. Then it slowly

[SEARCH]

DEL5.3: Two-phase CFD model of the MYRRHA-FASTEF primary coolant loop including all relevant thermal aspects

Dissemination level: PU

Date of issue of this report: 15/05/13

50/64

risers again to overcome the nominal temperature only 50s before the end of the simulation. The temperature in outlet of the HXs, due to the dramatic decrease of mass flow rate, quickly reaches the hypothetical temperature of the secondary coolant (here slightly over-estimated at 210C), and stays put at this value. The effect is to slowly decrease the lower plenum temperature, with the 265C isotherm about to reach the core at the end of the simulation. As the core inlet temperature slightly rises, it induces a slight increase of the core power, during the 500s of the simulation from 50 to about 52 % of the nominal power. The effect on the maximum temperature is quite mitigated as the increased power is essentially used to compensate the inlet temperature decrease.

The velocity field is dominated by the buoyancy induced plume at the core centre with a maximum magnitude about 1.5m/s. With regard to the cold plenum, the tendency of the PP outlet flow to be decentred towards the core, due to the proximity of the nearby vessel, is quite enhanced.

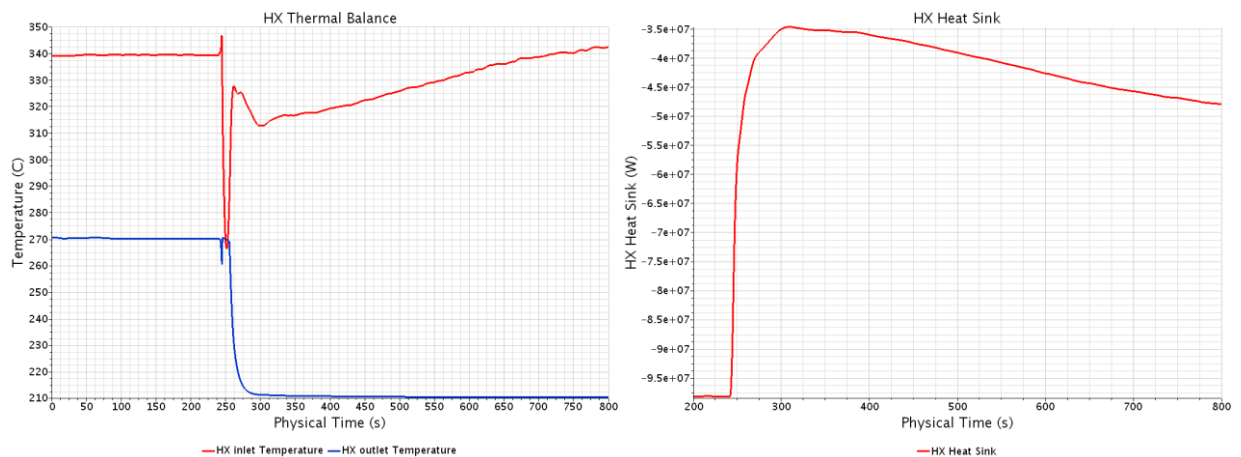


Figure 39: ULOF_8, time history. Left, HX thermal balance with inlet and outlet temperature. Right, HXs thermal power.

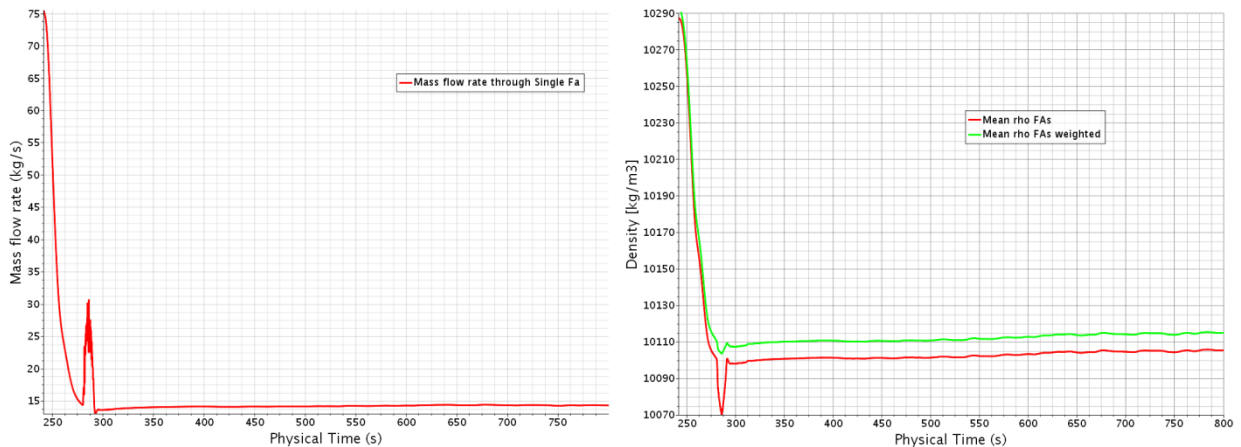


Figure 40: ULOF_8, time history. Left, mass flow rate through the "faulty" FA. Right, mean density (real and weighted) for the same FA.

[SEARCH]

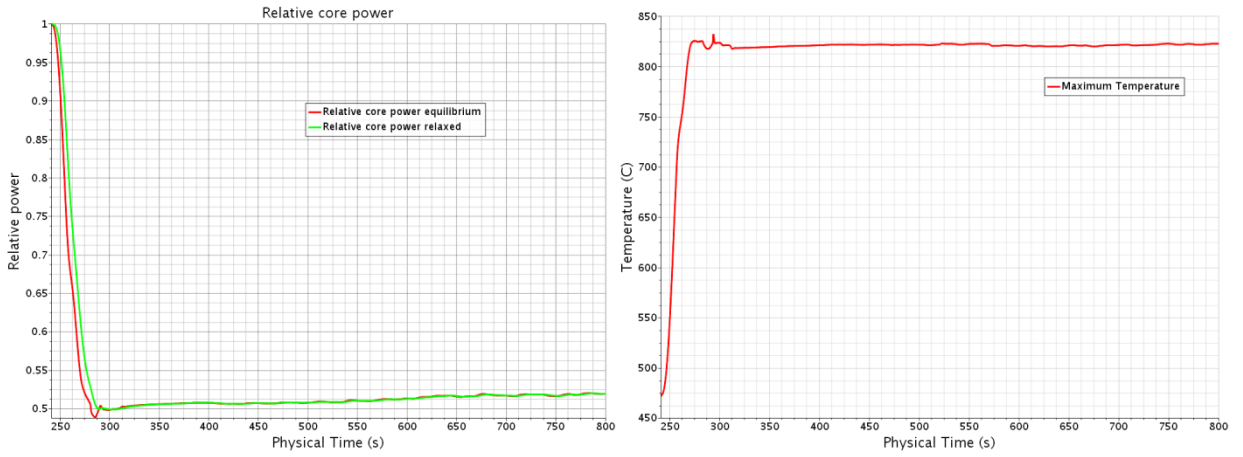


Figure 41: ULOF_8, time history. Left, relative core power. Right, core maximal temperature.

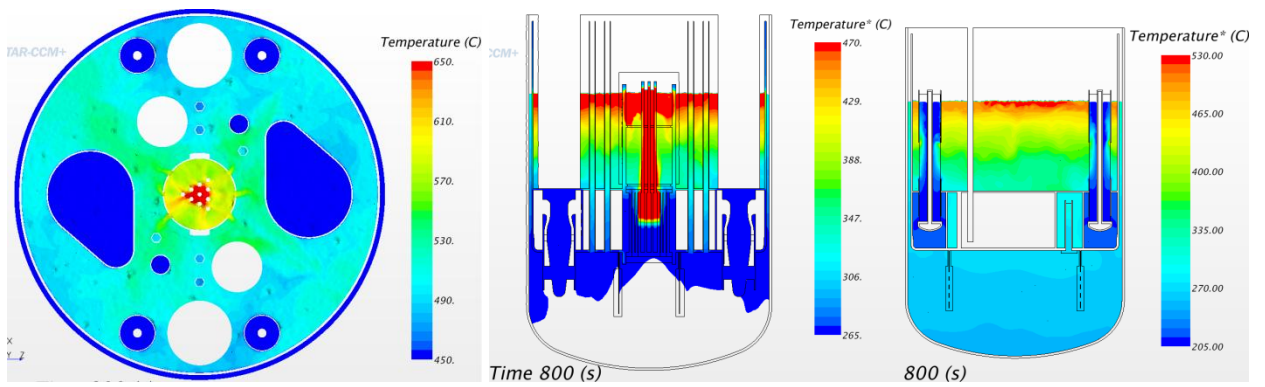


Figure 42: ULOF_8, time t=800s, end of simulation. Left, surface temperature on scale 450-650C. Centre, cropped temperature on main vertical plane on scale 265-470C. Right, HX plane temperature on scale 205-530C.

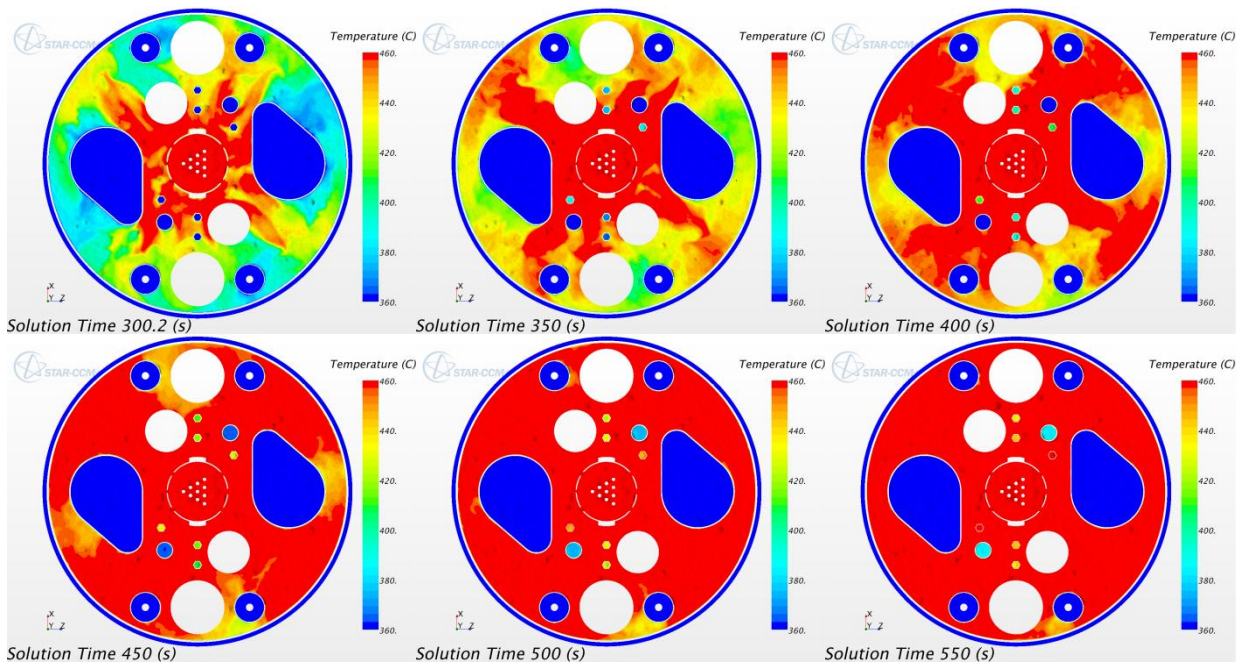


Figure 43: ULOF_8. Surface temperature on scale 360-460C from time t=300sto time t=550s.

[SEARCH]

DEL5.3: Two-phase CFD model of the MYRRHA-FASTEF primary coolant loop including all relevant thermal aspects

Dissemination level: PU

Date of issue of this report: 15/05/13

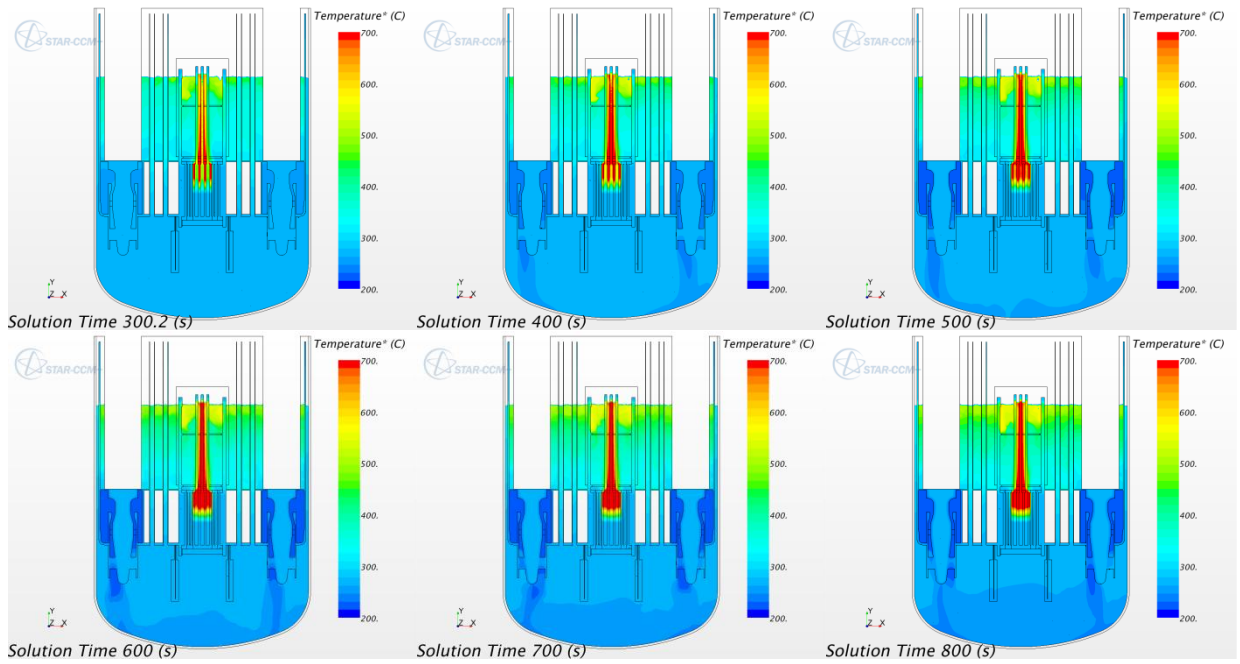


Figure 44: ULOF_8. Temperature profile on scale 200-700C, from time t=300s to time t=800s, step 100s.

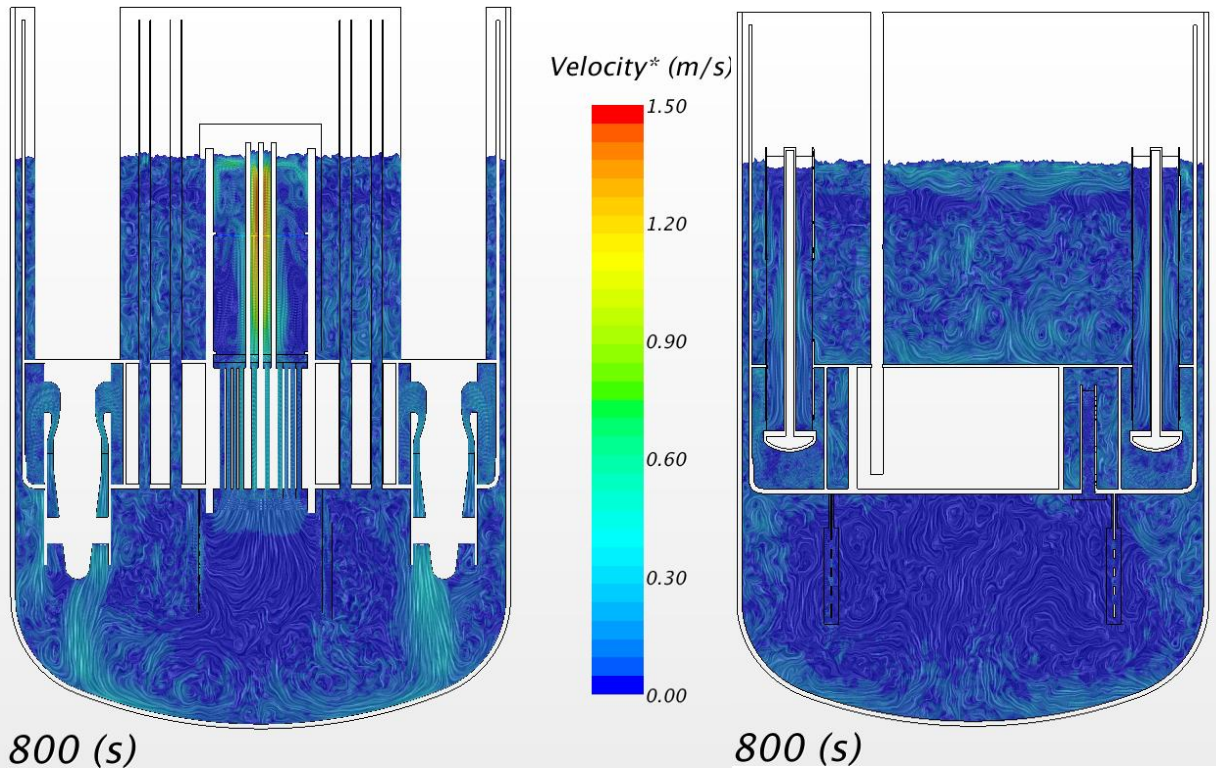


Figure 45: ULOF_8, time t=800s. Velocity field on the two vertical planes passing through the PP and the HXs.

[SEARCH]

DEL5.3: Two-phase CFD model of the MYRRHA-FASTEF primary coolant loop including all relevant thermal aspects

Dissemination level: PU

Date of issue of this report: 15/05/13

53/64

7. Discussion

7.1 Numerical model

A CFD representation of MYRRHA primary system with 9.3 million control volumes has been built and described in Del5.3. This representation includes the conjugate heat transfer with the structural part, dealt with 1 million control volumes. This model however is subject to the time scale of the temperature diffusion through the solid structure. The consequence is a greater thermal inertia and a strong increase of the time necessary to reach a reasonably stabilized thermal profile. The thermal profile is thus only partially stabilized in the peripheral regions while it is essentially steady state in the main flow circulation path.

This model is therefore adequate for the current study, the flow and thermal fields being used as reasonably suitable initial conditions.

7.2 Passive scalars

The use of passive scalar has allowed us to better understand the complexity of the flow path and of the various time scales involved while dealing with arbitrary small convected particles. While the global time scale of the primary loop under nominal condition is order 400s, a signal emitted from the core can be felt back after only 50s, while the return time peak occurs between 150 and 250s, depending of the specific FA position of the initial signal. While the temporal signal depends quite a lot on the initial release position, it is spatially homogeneous when reaching the core bottom.

7.3 Lagrangian particles in nominal condition

Convected Lagrangian sets of particles show a variety of behaviours, depending essentially on their size and their specific weight relatively to the carrier flow density. In fact, in a preliminary approximation, the only relevant parameter is the terminal velocity under the buoyancy force. Arbitrarily small particles that do not stick to the walls or to the free surface are diffused by the turbulence until they reach a homogeneous concentration. Large heavy particles quickly fall back to the nearby bottom while large light particles quickly reach the free-surface and stay put there. The difficulty is to quantify the terms “small, large, light and heavy” and to characterise the particle dispersion/aggregation in the intermediary range.

From the simulations performed particles of 0.15mm with porosity 5 and 10% can be considered as small. For porosities 2.5 and 12.5%, they enter the intermediary range where some trend can be observed but the time scale and the mesh resolution does allow to draw definitive conclusions. This is also true for 0.8mm particles with porosity 5 or 10%. The other investigated cases clearly enter the large light and large heavy behaviour.

Some consideration should be done about the strong assumptions made to perform the simulations.

- The carrier flow is not stationary: small particles (light or heavy) can be trapped by the specific flow configuration at the time of the freezing. This has seemingly lead, for example, to small light particles trapped non physically at the hot plenum bottom.
- The particles are spherical and their density is supposed independent from the pressure while a particle with a tiny bubble attached could be lighter than LBE

[SEARCH]

DEL5.3: [Two-phase CFD model of the MYRRHA-FASTEF primary coolant loop including all relevant thermal aspects](#)

Dissemination level: PU

Date of issue of this report: 15/05/13

close to the free-surface and heavier under the core level.

- There is no specific interaction of the particles with the walls or the free-surface taken into account. The particles bounce back from the wall and are not trapped by surface tension effects. Results could be dramatically affected for particles that tend to stick to the wall or are non-wetting for the LBE.

The particles simulated are therefore only illustrative of the behaviour of some typical real fuel particles. Precise evaluation makes little sense and we will make only general comments on the general behaviour of the particles.

Due to the configuration of the primary loop, the behaviour of the heavier particles is the more simple to understand. Heavier particles tend to fall down to the bottom. In the hot plenum, the bottom is almost stagnant and the particles can settle there. In the cold plenum, on the contrary, the bottom is disturbed by the flow directly coming from the pumps and the heavy particles are continuously re-entrained by the flow until they eventually are driven through the core back to the hot plenum. The cold plenum acts thus as a temporally buffer while the hot plenum bottom is the principal privileged aggregation region of the heavier particles.

The behaviour of the lighter particles is more tricky. In the hot plenum, they should tend to reach the free surface. But once there, they are convected to the areas (close to walls or where down-coming vortices form) where the surface flow re-enters the bulk flow. An depending on their size and lightness, they are also re-entrained in the bulk flow. The problem here is that the spatial mesh resolution (a few centimetres) at the free surface is absolutely not adequate to investigate such phenomenology.

The particles small and light enough to be re-entrained in the cold plenum are likely to occasionally reach the cold plenum top where they can slowly shift until they find an upward opening such as the annulus, the IVFS entrance, the IVFH opening, the various vertical penetrations and the core. Clearly, this may depend on tiny details of the geometry. The LBE in the vertical penetrations is almost fully stagnant. Light particles entering them should quickly reach their free surface and stay trapped there. This is also probably true to some extent if the particles enter the annulus or the IVFH opening. However, their larger size and interface with the cold plenum leave room for large turbulence or residual flow structures to enter deeply these volumes. The situation in the annulus can be complicated by buoyancy induced flow structures.

There is a small vertical gap between the IVFS top and its outlet towards the annulus. Due to the small mass flow rate, it is thus quite likely that entering particles get trapped at the IVFS top. A last interesting position is the free surface inside the HXs where there is a gathering of light particles. The mesh resolution here is also not sufficient to understand if it is a temporary buffer or an aggregation region.

To resume the general tendency, the particles not sufficiently large and light enough to stay put at the hot free surface where the surface flow re-enters the bulk flow will end after some complete cycles into one of the cold plenum stagnant free surface or at the IVFS top. This can however takes a much longer time that the 1200s of the simulation.

In this work, we did not investigate the dispersion of fission gas “particles”, which in fact would simply be bubbles. While the argument is clearly present in the document title, much can be inferred from the fuel particle dispersion results. In effect, gas bubbles have a much lower density than the LBE, to the point that their terminal velocity under the buoyancy force is independent of their own density. In practice, a bubble is not independent but is “attached” to its added mass for a volume roughly half the bubble one. The bubble tendency to reach the free surface, at parity of size, will be much greater than the fuel particles with 12.5% porosity. Moreover, the particle will grow while rising because of the pressure change, increasing their

[SEARCH]

DEL5.3: [Two-phase CFD model of the MYRRHA-FASTEF primary coolant loop including all relevant thermal aspects](#)

Dissemination level: PU

Date of issue of this report: 15/05/13

55/64

drift velocity in the upper plenum. The effect is that many more bubbles will effectively reach the free-surface. Once arriving on the free-surface, the bubbles will either explode and mix with the cover gas, or remain trapped under the effect of the surface tension precisely on the free-surface with a much lower tendency than solid (passive) particles to be re-absorbed into the bulk flow.

Thus, we expect almost no bubble in the 1mm diameter range to close the primary coolant loop, and only few in the 0.1mm range. Much smaller bubbles, in the micrometre range will obviously behave almost like passive particles, but the mechanism by which they could reach and accumulate in the core is quite difficult to imagine and would require in any case much longer times.

7.4 ULOF simulations

The ULOF simulations presented here represent the meeting of an important milestone with success. Indeed, it is only with transient simulations involving noticeable variations of the free surfaces level that the VOF approach really makes sense. Being a first-of-a-kind in the framework of the MYRRHA CFD models, these simulations must be considered as a proof of feasibility and a good material for discussion and improvement. The principal reference material is the similar work performed in CDT with SIMMER-III [17]. In this work, a benchmark exercise demonstrated that the quality of the neutronic coupling had a strong influence on the most important parameter, namely the core power. Because the apparently most articulated coupling was performed by IKET, our primary objective was to mimic IKET results, still implementing a dynamical coupling. By this, we mean that we did not want to force arbitrarily a power curve in time, instead we want to dynamically link the core power to the evolution of the most relevant available physical parameters, the results by IKET serving to calibrate the linking.

7.4.1 Setting and calibration of the neutronic coupling

The first simulation (ULOF_1) had two main objectives: (i) check the simulation global setting and measurement, (ii) establish the relevant time scale and (iii) obtain a reference result in the naïve configuration without neutronic coupling, to be compared with IKET results. It showed without ambiguity, seeing the great differences in the output, that some kind of neutronic coupling must absolutely be implemented for this transient in order to get any usable results.

The next simulations (ULOF_2 to ULOF_6) show an attempt to reach progressively a rough but sensate coupling. For homogeneity and consistency with the HX modelling, and also by analogy, we wanted to implement a two-parameters coupling. To enforce readability, the two parameters must be clearly related to the coupling properties.

Given a correct initial core power value, the first parameter objective is to get a correct asymptotic value. The form in which the parameter is used serves to get also reasonable intermediary transition values under the assumption of constant quasi-equilibrium (in the same spirit that thermo-dynamical calculations are performed for reversible processes). If the first parameter is a simple physical quantity, we can expect in first approximation and in absence of other data a linear behaviour between the initial and asymptotic core value.

A convenient way to describe a nuclear core with a neutronic code is to give its power in nominal operation and its reactivity feedback parameters under perturbation assumption (with linear dependence). These parameters are related to: (i) movement of parts (control/scram rods), (ii) thermal dilatation (both displacement and density change), (iii) thermal (Doppler) effect and (iv) void effects. We do not investigate any scram rod nor control rod behaviour. For the rest, type (i) and (ii) parameters can be expressed in terms of temperature, while type (i), (ii) and (iii) parameters can be expressed in terms of (effective) densities. Temperatures under steady state

[SEARCH]

DEL5.3: [Two-phase CFD model of the MYRRHA-FASTEF primary coolant loop including all relevant thermal aspects](#)

Dissemination level: PU

Date of issue of this report: 15/05/13

56/64

(equilibrium) condition are strongly correlated, especially those that are not or badly represented in the CFD model, such as the fuel, the cladding and the wrapper temperatures, and so are their corresponding densities. Because we want to include the fission gas release in our simulations, the density of the coolant mixture seems a better suited parameter than its temperature.

For a non-specialist, a surprising property of the nuclear core is that, while its power strongly (linearly) depends on perturbations, the power spatial distribution does not. This means that the effects of small perturbations is highly non-local and only the total power needs to be re-evaluated. It would be interesting to understand up to what level of perturbation one can consider the core power profile constant. On the contrary, and as IKET found out in their benchmark exercise, the intensity of the perturbation (in terms of temperature or density) is highly dependent on the localisation of the perturbation. They put in evidence that a perturbation near the core centre has much less influence than the “same” perturbation at an intermediary ring of FAs. They also stated the relative influence of the perturbation on a FA ring basis. In our foreseen case, during the transition from forced to natural convection, the LBE flow initially independent of the FA position will eventually become strongly dependent on the local FA heat release. The change in LBE local density is not expected to be trivially scaled. The mean LBE density in the core, which would have otherwise been a good parameter, is no more so much adapted. To take into account the spatial influence of the perturbation, we have instead weighted the calculation of the mean density to reduce the influence of the central zone. The weight used is highly empirical and has been set mostly to bring this issue in evidence.

The first parameter to set the core power is thus a weighted mean of the coolant mixture density in the core. The core power dependence is linear and is calibrated to reach 50% nominal power under natural convection regime, thus mimicking IKET results.

The second parameter that we wanted to use had the objective to take into account some delay between the LBE density variation and the core power variation. The idea behind it is the following: with the falling of the mass flow rate, the LBE is going slower, and thus gets hotter. But it takes some time for the temperature increase to be propagated to the other core components: the cladding, the fuel, the wrappers and the support grid. Some delay may also arise from the heat directly and indirectly generated by the delayed neutrons. The altogether phenomena is quite complex but the results looks like, by empirical comparison of the power and LBE temperature curves by IKET, as a delayed power decrease. The simplest way to take into account a delayed effect with a single parameter is to introduce a relaxation time in the equation relating the time evolution of the core power to the mean weighted density. And that is exactly what we have done.

In practice, we have to solve a simple differential equation in terms of the core power and its time derivative. While in principle not very difficult, as for anything performed for the first time within the software capabilities, only the effective implementation proves the feasibility of the procedure.

7.4.2 Fission gas emission

The fission gas emission suffers from many defects and approximation, similarly to the Lagrangian particle dispersion. In the same spirit as for the neutronic coupling, we wanted to establish a proof of feasibility and a starting point for discussion and future improvement.

In the current implementation, the fission gas is in fact the same as the numerical cover gas and suffers from the same defects, but in a more critical way. The incompressibility issue is maybe the more critical one because the fission gas emitted in the LBE flow path, after a very fast transient, should have a specific volume changing by a factor about 5 between the release in the core and the release through the free-surface.

[SEARCH]

DEL5.3: [Two-phase CFD model of the MYRRHA-FASTEF primary coolant loop including all relevant thermal aspects](#)

Dissemination level: PU

Date of issue of this report: 15/05/13

Another critical issue is that we have no idea how the fission gas is expected to mix with the LBE. In practice, under the VOF setting used, the fission gas is expected to mix intimately with the LBE as if it were made of extremely small bubbles. But at the same time, due to the parameters of the sharpening (starccm+) algorithm, the light phase has a decisive tendency to spontaneously concentrate. In consequence, in the simulation, we see the fission gas plume reach very soon the free surface and get absorbed there, with no apparent diffusion effect.

However, from the neutronic coupling point of view, we have represented a quite sound void insertion. And as stated before, the void insertion modelling is naturally included in the two-parameters core power model.

In order to have a conservative configuration, it is quite common to think that more is better. For the fission gas / void insertion issue, this is not exactly the case. The trick lies in the non-locality of the negative reactivity feedback while the potential damage is local. For several void insertions in different FAs, there will be a greater negative reactivity feedback than for just one void insertion. On the other hand, a very concentrated local void insertion will have a negligible negative reactivity feedback while the capability to evacuate the heat can be greatly damaged. That is why we ended by restricting the fission gas emission to only one FA.

The maximum LBE temperature shows almost no variation due to the fission gas emission. It must be stressed out that it does not mean anything about what would be the cladding and fuel maximum temperature. In case of a gas film enveloping a fuel pin, the heat transfer from the pin to the LBE would be dramatically lowered with a consequential very fast and large increase of the pin temperature. This phenomenology is however completely out of range of the current study.

The idea behind the final ULOF scenario is that a single pin may fail because of the fast transient induced by the pump loss. Then, some fission gas is released and some nearby pin, with its heat transfer hindered also fails, thus initiating a chain reaction in the entire FA. The pin clad can then locally reach the melting temperature letting the fuel enter in contact and begin to be eroded by the LBE, initiating the Lagrangian particle emission phase.

In principle, we could have tried to model the fission gas emission with Lagrangian particles. To capture the collective flow acceleration effect, we would have to use a complete two-way coupling. We have however no clear idea on what could be the typical distribution of the size of the gas bubbles. The added value with regard to the current approach is therefore quite questionable.

7.4.3 Lagrangian particles under natural convection

In the final part of the ULOF scenario, we suppose that a few seconds after the pin failure crisis and related fission gas emission, damaged fuel pins begin to release some particulate in the LBE carrier flow.

When the particle emission starts, the flow has essentially already entered the natural convection regime. The mass flow rate remains almost constant during the 500s of the simulation at about 13% (1200 kg/s) of the nominal value. The temperature field instead continues to slowly evolve, with the free surface getting hotter and the lower plenum slightly colder.

With the much lower mass flow rate, the jets out of the core barrel, the free-surface velocity and the turbulence structures become much weaker. The buoyancy force now dominates for all but the smallest particles. The configuration of the HXs inlet, not crossing the free-surface nor reaching the hot plenum bottom, allows only the bulk flow to recirculate and now acts much more as a physical barrier for the passage of most particles. While we can fear that the flow from the pumps is no more strong enough to re-circulate particles falling at the bottom and gathering there, this is not a point because only very few particles manage to reach the cold plenum.

[SEARCH]

7.4.4 Natural convection regime

The transition from the forced flow in nominal condition to the natural convection regime takes a little less than 60s. The final ULOF simulation thus encompasses a little more than 500s of natural convection regime. As already said, the mass flow rate drops to 13% of the nominal value. On a FA position basis, the mass flow rate profile changes quite a lot. The active FAs now concentrate about 1000kg/s of the 1200kg/s total. The FAs in the central ring stay at about 18% of the original value.

It is clear, from global balances but also from the results shown (see for example Figure 39), that the thermal asymptotic profile is far from being reached. The appearing tendency is however a re-enforcing of the thermal stratification with the free-surface temperature getting close to the hot plume temperature near 800C.

It could be tempting to revert to the frozen field technique to investigate larger times and the asymptotic temperature profile. Unfortunately, much more than in the nominal configuration, the very slow and progressive establishment of the thermal stratification is likely to strongly modify the flow pattern, so that freezing it would be an excessive forcing.

7.5 Possible improvements

The current work as brought to life an articulate CFD model of MYRRHA able to make preliminary investigations on particle dispersions in different flow regimes. As all first-of-a-kind work, there is room for many improvements. There are two main reasons for this: (i) the starccm+ software as improved, gaining many new features and (ii) our understanding of the MYRRHA secondary flow has also improved. In the following, we present some ideas on how future MYRRHA CFD models could be improved.

7.5.1 Route to nominal condition

In this work, the nominal condition was obtained in two steps. First considering only the fluid part and then including the structural part for inclusion of the conjugate heat transfer, in a perspective of progressive increase of complexity. Mainly, the physical time needed to reach a sound flow pattern was unknown and a sensitive issue.

Our experience now gives us two important information. First, the thermal field is the longer to stabilize and second, the lower plenum velocity is strongly controlled by the pump flow swirl. While testing first the fluid phase can be useful, there is no need to prolong too much the simulation time before including the structural part.

There was the hope that the thermal convergence could be reached in a second step using frozen field techniques, letting only the temperature field evolve. Unfortunately, this method is currently incompatible with the VOF setting and the interface temperature quickly diverges. The main reason is the following. Suppose that at freezing time, a column of LBE is very slightly rising. Then, the LBE enthalpy also follows the movement. But, by freezing the movement, the energy is transferred across the interface to the light phase, making it quickly heat due to the very large difference of volumetric enthalpy between the two phases. There are however some other ways to accelerate the route to the nominal configuration. The basic idea is first to establish the large scale features and deal with the smaller scales in a second step.

First, we can largely relax the CFL condition using quite large time steps. To avoid light flow entrainment, the VOF parameters controlling the surface sharpness (both in-house and starccm+ native) must be aggressively strengthened. The use of a large time step can modify the global hydraulic losses of the loop, so that an active control of the mass flow rate, for example, through an active control of the pump thrust must be implemented. Of course, this method will modify

[SEARCH]

DEL5.3: [Two-phase CFD model of the MYRRHA-FASTEF primary coolant loop including all relevant thermal aspects](#)

Dissemination level: PU

Date of issue of this report: 15/05/13

the small scale structure of the flow which will be retrieved in a second step.

A second method serves to speed up the establishment of the thermal profile across the structural parts. It consists in setting the solid specific heat to a very low (clearly unphysical) value. We must recall that the specific heat enters the equation only through the time derivative term and therefore has no influence on the steady state configuration. We are only dealing with an acceleration procedure. The main issue is to get back to the correct value of the specific heat when a reasonable steady state has been reached. In effect, the temperature is a derived quantity as the code effectively considers the enthalpy. Changing the specific heat by a certain ratio effectively induces a change of temperature by the inverse ratio. The trick lies in making just one small time step after the specific restoration with a very specific added source term. More precisely, the source term is the product of the current temperature by a huge term, while its temperature derivative is minus this huge term. The method by which the code splits the source term in implicit and explicit part makes that the temperature is conserved through the time step process.

Combining this two methods, at parity of computational power, we should be able to get closer and faster to the steady state.

7.5.2 Pump improvement

In the current model, the pump is codified “software”, through a localized source term in momentum equation. This is easy to perform for the vertical component. However, during the development of the projects, it turned out that the flow in outlet of the pump stator has a noticeable swirl component. Its value, that was at first thought about 10 degrees has been then fixed to 27 degrees. The swirl component is likely to largely control the flow pattern in the cold plenum. If, as it is quite probable, the two pumps rotate in the same direction, they progressively build a flow rotational momentum about the core axis. This rotational momentum is expected to take several (cold plenum) characteristic times to reach steady state. Therefore it is important to know it from the beginning of the simulation.

Moreover, we have observed that the pump outlet flow stability is not assured and the swirl component will influence this characteristic.

While a correct geometrical description of the rotor/stator part is still out of range and not of current real interest, there is room for some upgrade. We split the possible pump modelling improvement into two parts, the vertical thrust and the swirl component:

- Vertical part: the software coding is very convenient and adapted. A volumetric source term in the momentum equation is doing well. It must however be made more sound and flexible to better capture the dynamic of a pump trip. Taking profit of the experience gained for the modelling of the core power, we can relate the pump thrust to its moment of inertia (and maybe also to the current mass flow rate) and solve a simple differential equation for the change of the pump rotational speed due to the energy transfer to the fluid and to the friction losses. The model must behave correctly for the pump at rest and for reverse flows. It must also forbid the pump to invert the direction of rotation. When the pump is at rest, it must behave as a localized pressure loss.
- Swirl: the current “software” coding of the swirl, is based on the measure of the difference between the current flow angulation and its desired value and a force correcting this difference. The force intensity must be sufficient to bring essentially the correct angulation but not too strong to avoid numerical instabilities. The intensity is based on some characteristic time consideration and trial and error. It is rather empirical. Keeping a priori a sound and stable

[SEARCH]

DEL5.3: [Two-phase CFD model of the MYRRHA-FASTEF primary coolant loop including all relevant thermal aspects](#)

Dissemination level: PU

Date of issue of this report: 15/05/13

intensity under loss of flow incident is quite delicate. A possible improvement is to code “hardware” the swirl component. By this we mean putting in the available space a geometrical device, with slanted baffles or winglets, but not true to the real device. This approach was at first discarded because of CFL consideration as it needs a locally quite finer mesh than desired. However, we know that the turbulence characteristics of the pump outlet flow are completely out of range. In this context, there is no need to reduce the time step only to respect the CFL constraint for this part. Last but not least, the effective modularity of the software has greatly improved, and the possible substitution, during the simulation, of the pump region (say, with a different winglet angulation) is no more a sensitive issue.

7.5.3 Core improvement

Some work has already been performed to take into account some neutronic coupling. With regards to the transients, the main defect of the current core modelling is the non-representation of the fuel pin bundles. The core power is directly furnished to the LBE phase while it should normally be released in the fuel and transit through the cladding to the coolant. The time laps between the fuel overheating and the coolant overheating is a fundamental key for a better neutronic coupling as it allows to assemble the reactivity feedback from two different essential components with different temperatures.

From the geometrical point of view, the strong added value of the current modelling is the specific localisation of each single FA position. This was done at the limit of the mesher capability. In the meantime, the mesher capability has been greatly improved, with a much better recognition of specific structures such as thin sheet or generalized cylinders and their specific treatment for a good mesh quality keeping a reasonable cell size. Moreover, the porous media modelling also has been greatly improved, now allowing to define consistently the solid part of the medium together with its own temperature and a thermal exchange between the two parts based on an embedded used defined source term. This feature can be used to describe the pin bundle. The solid part would represent both the cladding and the fuel with only one temperature. This is not yet totally satisfying but still a decisive modelling improvement. We can also expect in the near future, some further software improvement allowing a porous media with three different components, as is typical for heat exchangers. To complete the core modelling, another porous media could be used for the region around the FA positions, which would be representative of the FA wrappers for the solid part and of the inter-wrapper LBE for the fluid part.

Some geometrical constraint (mainly some cross sections) need not be respected. If needed for meshing purpose, the inter FA medium can be widened. In effect, what must be conserved are the fluid parts cross section and the solid parts global heat capacity. A discrepancy on a solid parts cross section can be compensated by a related artificial change of the solid density.

The addition of two new temperature fields in the core, one for the pin bundle and one for the FA wrapper would give more margin to infer a better neutronic coupling, yet to define.

7.5.4 Cover gas improvement

In the current MYRRHA CFD model there is truly no cover gas modelling. The cover gas is present only to allow the LBE surface to move and its properties are set only to get rid of problems and control issues. Until recently, VOF simulations used to become unstable for phase density ratios above one thousands. In other terms, VOF simulations were stable only for

[SEARCH]

DEL5.3: [Two-phase CFD model of the MYRRHA-FASTEF primary coolant loop including all relevant thermal aspects](#)

Dissemination level: PU

Date of issue of this report: 15/05/13

“cold” air-water flows under atmospheric condition. Therefore, the cover gas has been considered incompressible with a constant density set to 11.8 kg/m^3 .

With the relaxing of the density ratio constraint, we can try to approach the real cover gas physical properties. The foreseen cover gas is Argon, a noble gas with atomic number 18. It is slightly heavier than air, having a density at 273K and 1 Bar of 1.784 kg/m^3 . In contact with the LBE free-surface, the density will range roughly from 0.6 to 0.9 kg/m^3 in nominal condition and down to 0.35 kg/s under ULOF condition. Thus the density ratio can easily reach 3.E4 and the flow stability for such a huge ration must be preventively carefully checked. By prudence, we only contemplate here the possibility to include a temperature dependence of the density, but still keeping the light phase incompressible.

If the cover gas is subject to an external cleaning treatment and is reintroduced in the top plenum at about room temperature, then we will face quite a large gas phase density range and can expect quite strong buoyancy induced currents which can have a non-negligible influence on the temperature of the upper structures.

A consistent cover gas treatment also enters in conflict with the in-house sharpening algorithm. Here again, the progress made by the software largely relax the necessity of its use. Some cleaning of the LBE may still be necessary, especially for the initial transient to the nominal condition but can be suppressed in a second time or restricted to the bulk flow (on a pressure consideration basis).

A better modelling of the cover gas would open the route to the simulation of the dispersion and transfer of pollutants from the coolant.

8. Conclusion

We have completed the construction of a quite complete CFD model of the MYRRHA primary coolant loop. The model is based on the VOF paradigm. The cover gas and the main structures are taken into consideration. The model has shown to be compatible with the use of passive scalar that have allowed to determine some relevant characteristic times. The model has allowed to evaluate the dispersion of Lagrangian particles representative of fuel particles with different size and porosity under nominal operation for up to 1200s. Characteristics of the dispersion and possible re-aggregation of the particles have been established. Definitive conclusions on eventual re-aggregation could be drawn for all but only for the smallest particle investigated are they are globally recirculating for much longer times that the one of the simulation. In particular, there is no re-aggregation of the heavier particles at the vessel bottom, as they are re-entrained by the pump flow. The larger heavy particles soon finish at the bottom of the upper plenum.

The model has also been upgraded to allow the simulation of an articulated ULOF scenario with consequent release of fission gas and fuel particles. It must be stressed that the fission gas and fuel particle release are a priori parts of the scenario and are not implied by the results of the simulation. Anyway, to demonstrate the feasibility of such a scenario, it has been necessary to develop the framework of a preliminary coupling of the core power with the neutronic feedback due to the LBE change of temperature. The necessity of the coupling arises by comparison with a similar simulation performed by IKET in the CDT project and we have presented the different steps that have allowed to finally mimic their results. Under the ULOF scenario, except the smaller ones, most of the heavier particles precipitate at the bottom of the hot plenum while the lighter particles remain trapped by the hot plenum free surface.

The limitations of the current model have been discussed and some future improvement have been proposed.

The main issue address by this document is the eventuality of a re-criticalisation under fuel dispersion events. While no definitive conclusion can be drawn, in the case simulated, we have observed a variety of behaviour, depending on the size and weight of the particles, with a large

[SEARCH]

DEL5.3: [Two-phase CFD model of the MYRRHA-FASTEF primary coolant loop including all relevant thermal aspects](#)

Dissemination level: PU

Date of issue of this report: 15/05/13

62/64

extension of the re-aggregation zones such that it is very unlikely that a high quantity of fuel can gather locally in one of these zones. In consequence, a re-criticalisation seems for now also very unlikely.

9. Acknowledgment

This research has been co-funded by the Autonomous Region of Sardinia.

10. References

- [1] V. Moreau, Two-phase CFD model of the MYRRHA-FASTEF primary coolant loop including all relevant thermal aspects, SEARCH contractual deliverable D5.3 (Contract Number: 295736),05/2013.
- [2] <http://myrrha.sckcen.be>
- [3] F. Bianchi et al., Thermo-hydraulic analysis of the windowless target system, Nuclear Engineering and Design, Volume 238, Number 8, page 2135--2145 - august 2008.
- [4] V. Moreau et al., A case history of CFD support to accelerator driven system plant design, Proceedings of The 17th Int. Conf. On Nucl. Eng num. 75588 ASME – 2009.
- [5] V. Moreau, FASTEF Heat exchanger tube rupture CFD simulation, Nuclear Engineering and Design Elsevier pages 42-51 vol. 252 - 2012 doi: <http://dx.doi.org/10.1016/j.nucengdes.2012.06.030>
- [6]<http://www.inl.gov/relap5/>
- [7] <http://www.iaea.go.jp/jnc/zooarai/ejoarai/simmer/>
- [8] MYRRHA Team, “MYRRHA Technical Description Rev. 1.4”, <http://search.sckcen.be/>, June 2012.
- [9] N. Forgione et al., Operability of the SIMMER-III and SIMMER-IV models for the MYRRHA-FASTEF reactor, SEARCH contractual deliverable D5.1 (Contract Number: 295736),12/2012.
- [10] M. Eboli et al., Report on the 3D SIMMER-IV analysis for the more representative fuel failure conditions, SEARCH contractual deliverable D5.4 (Contract Number: 295736),12/2013.
- [11] R. Li, X.-N. Chen, A. Rineiski, Report on assessment on fuel dispersion after pin failure under blockage conditions, SEARCH contractual deliverable D5.5 (Contract Number: 295736),08/2014.
- [12] S. Buckingham, L. Kolozár (VKI), Ph. Planquart (VKI), Characterisation of long term dispersion of fuel in the coolant with CFD modelling, SEARCH contractual deliverable D5.6 (Contract Number: 295736),10/2014.

- [13] <http://www.cd-adapco.com/>.
- [14] Handbook on Lead-bismuth Eutectic Alloy and Lead Properties, Materials Compatibility, Thermal-hydraulics and Technologies, Nuclear Energy Agency 2007 Edition
<http://www.nea.fr/html/science/reports/2007/nea6195-handbook.html>
- [15] <http://search.sckcen.be/>

[SEARCH]

DEL5.3: Two-phase CFD model of the MYRRHA-FASTEF primary coolant loop including all relevant thermal aspects

Dissemination level: PU

Date of issue of this report: 15/05/13

[16] <http://www.atlassteels.co.nz/site/pages/technical-handbooks-of-stainless-steel.php>

[17] E. Bubelis, M. Schikorr, et al. "FASTEF safety analysis – critical and subcritical mode (Part 1: critical FASTEF safety analysis)", Deliverable D2.3 (2012), CDT, 7th Framework Programme Euratom.

[18] Reinaldo Gonzaga et al., Study of the microstructural variations (average grain size) on UO₂ pellets in relation to the Si and Al contents, in production scale,
http://www.engopt.org/nukleo/pdfs/0614_artigo_engopt.pdf

[SEARCH]

DEL5.3: [Two-phase CFD model of the MYRRHA-FASTEF primary coolant loop including all relevant thermal aspects](#)

Dissemination level: PU

Date of issue of this report: [15/05/13](#)